PHAGE-BASED MAGNETOELASTIC SENSOR FOR THE DETECTION OF

SALMONELLA TYPHIMURIUM

Except where reference is made to the work of others, the work described in this dissertation is my own or was done in collaboration with my advisory committee. This dissertation does not include proprietary, restricted or classified information.

_____

Ramji S. Lakshmanan

Certificate of Approval:

_____	_____
Zhong-Yang Cheng Associate Professor Materials Engineering	Bryan A. Chin, Chair Professor Materials Engineering
_____	_____
Valery A. Petrenko Professor Department of Pathobiology	Dong-Joo Kim Associate Professor Materials Engineering

_____

George T. Flowers
Dean
Graduate School

PHAGE-BASED MAGNETOELASTIC SENSOR FOR THE DETECTION OF *SALMONELLA TYPHIMURIUM*

Ramji S. Lakshmanan

A Dissertation

submitted to

the Graduate Faculty of

Auburn University

in Partial Fulfillment of the

Requirements for the

Degree of

Doctor of Philosophy

Auburn University, Alabama
December 19, 2008

PHAGE-BASED MAGNETOELASTIC SENSOR FOR THE DETECTION OF

SALMONELLA TYPHIMURIUM

Ramji S. Lakshmanan

_____
Signature of Author

_____
Date of Graduation

VITA

Ramji S Lakshmanan, son of Anandhi Sitaraman and G. Sitaraman, was born on March 8th, 1979 in Margao, Goa, India. He graduated from St Johns Senior Secondary School in March 1996. He joined Indian Institute of Technology- Bombay, Mumbai, India in August 1997 and graduated with a Bachelor of Technology in Metallurgical Engineering and Materials Science in May 2002 and a Master of Techonology in Ceramics and Composites in May 2002. He entered doctoral program in Materials Engineering at Auburn University in August 2002. He married Subhadravalli V. Chitti, daughter of Dr. Chitti Bhavanarayana Murthy and Chitti Rohini Annapurna, in May 2006.

DISSERTATION ABSTRACT

PHAGE-BASED MAGNETOELASTIC SENSOR FOR THE DETECTION OF *SALMONELLA TYPHIMURIUM*

Ramji S. Lakshmanan

Doctor of Philosophy, December 19, 2008
(M. Tech, Indian Institute of Technology, Bombay, 2002)
(B. Tech, Indian Institute of Technology, Bombay, 2002)

171 Typed Pages

Directed by Bryan A. Chin

In recent years, food-borne illness have garnered the attention of mainstream America with calls now coming from the media for more inspections to ensure the safety of our food supply. Food borne illness from the ingestion of *S. typhimurium* has been of great concern due to its common occurrence in food products of daily consumption. Annually approximately 80 million cases of food poisoning are reported in the United States alone. The ever growing need for rapid detection of pathogenic microorganisms present in food, environmental and clinical samples has invoked an increased interest in research efforts towards the development of novel diagnostic methodologies. Currently, the detection of bacteria in contaminated food relies on conventional microbiological methods that are time consuming and manpower intensive.

This study presents the results of the characterization of a phage-based magnetoelastic biosensor for the detection of *Salmonella typhimurium*. This affinity-

based biosensensor is comprised of a magnetoelastic material as the transducer and filamentous phage as the bio-recognition element. Magnetoelastic materials are ferromagnetic amorphous alloys that change dimensions in the presence of a magnetic field. This effect in combination with the reverse effect (inverse magnetostriction) is utilized in a typical sensor application. A time varying magnetic field causes these sensors to oscillate at a characteristic resonance frequency. The characteristic resonance frequency is dependent on the initial dimensions and physical properties of the material. These materials are of particular interest owing to their unique capability to perform remote (without direct wire contacts to the sensor) sensing, making *in-vivo* detection and detection in closed containers possible.

The phage-immobilized magnetoelastic biosensor was characterized for specificity; dose response in water, spiked apple juice and in spiked milk; selectivity; and longevity. The sensor's sensitivity is known to be higher for sensors with smaller dimensions. Hence sensors of different dimensions were studied to obtain better detection limits. The sensors' sensitivity increased from 98 Hz/decade to 1150 Hz/decade (decade of *S. typhimurium* concentrations) for a decrease in length from 5 mm to 500 μm. The responses of 2 mm (length) sensors were studied in spiked fat free milk and in mixtures with other bacteria. Binding assays of tests conducted in water showed K_d values of 149±76 cfu/mL with a binding valency of 2.42±0.02, whereas in fat free milk tests showed a K_d value of 136±42 with a binding valency of 2.50±0.03. The similar responses obtained in two dissimilar liquids demonstrates the consistent performance of the sensor even in complex matrices.

The effect of phage aggregation using varying counterion concentrations on the sensor performance was also studied. It was established that the formation of phage aggregates at higher counterion concentrations (>420 mM Na^+) was realizable. Its effect on the binding numbers was, however, contrary to the expectations. A sharp decline in the binding numbers was observed for higher counterion concentrations (>420 mM Na^+) owing to localized accumulation of these aggregates upon immobilization. Visual verification of bacterial binding to the phage-immobilized sensor was achieved through Scanning Electron Microscopy (SEM) studies of the sensor surfaces. High magnification SEM also provided an insight into the distribution characteristics of immobilized phage.

In summary, specific and selective biosensor with a magnetoelastic transducer and filamentous phage was investigated and demonstrated to be suitable for the detection of *S. typhimurium* in liquid foods.

ACKNOWLEDGEMENTS

I would like to express my sincere gratitude to Dr. Bryan A. Chin for his expert guidance, support and persistent encouragement throughout my study period. It is a privilege to work under Dr. Chin with his extensive knowledge and genuine concern for his students. I would like to emphasize that his influence on me was not only in acquiring scientific knowledge but also as a person.

I received utmost support from my committee members Dr. Z-Y. Cheng, Dr. Valery A. Petrenko, and Dr. Dong-Joo Kim and thank them whole heartedly. I would also like to express my thanks and appreciation to Dr. Stuart Wentworth and Dr Vitaly J. Vodyanoy for their thoughtful discussions and suggestions for my defense.

Special thanks to Dr. Ben Fiebor, Dr. Hu Jing, Leslie C. Mathisson, Dr. Hong Yang, Shichu Huang, Michael Johnson Wen Shen and Dr. Jiehui Wan. I would like to thank my friends Dr. Jyoti Kumar Ajitsaria, Prakriti Choudhary and Dr. Rajesh Guntupalli, for their constant motivation and valuable discussions.

I would like to thank my parents and brothers for their constant emotional support and encouragement during the course of my studies. I would like to dedicate this dissertation to my wife Subhadravalli Lakshmanan for supporting me and being patient through the ups and downs of the last 5 years. Without her love, prayers, support and help this work would not have been possible.

Style manual or journal used Sensors and Actuators B

Computer software used Microsoft Office XP and Microcal Origin 6.0

TABLE OF CONTENTS

LIST OF FIGURES

LIST OF TABLES

1. INTRODUCTION

1.1. Background

Food-borne illnesses or "food poisoning," as it is more commonly known is not of recent occurrence. Each year approximately 76 million illnesses, 325,000 hospitalizations and 5000 deaths are reported in the United States alone [1]. Food-borne illnesses are primarily caused by viruses, bacteria and parasites. These illnesses cause mild diarrhea to severe life-threatening neurological ailments. The reason for these large numbers of cases can be attributed to changing human demographics, human behavior, mass transportation of foods and microbial adaptation [2, 3]. Improved medical care has increased the median age of human beings [2, 3], however people of older age are at a higher risk due to weaker immune systems. The changes in human lifestyle and food consumption behavior are also to be blamed. Interest in international cuisine and frozen food products directly lead to longer transportation and storage times. The longer shelf life of foods allow for greater chances of spoilage and the production of foods in foreign countries where health standards vary significantly has lead to a plethora of additional contamination sources. Contamination of food may occur at any stage during processing, production, packaging, transportation or storage. The risks of food contamination can be decreased by the use of existing technologies. The Food and Drug Administration (FDA) and Centers for Disease Control (CDCs) have emphasized the problem of food-borne

illnesses to be one of the most serious, yet avoidable problems. With better awareness and proper hygienic practices, the losses due to food-borne illnesses can be reduced drastically.

In spite of the significant impact of food-borne illnesses on society, it has never been a major issue of concern to the general public. Food supply bio-terrorism has invoked greater interest among researchers and authorities as a result of the looming terrorism threats following the September 11th, 2001 attacks and the Anthrax mailings there after. The food supply system is most vulnerable to a bio-terrorism attack. The first deliberate and largest act of bio-terrorism in modern history of the United States was in 1984. Two members of the Rajneesh cult targeted the voters in Oregon to influence the outcome of the elections in their favor. These members contaminated the local restaurant salad bars with *Salmonella typhimurium* [4] sickening about 800 people.

1.1.1 Bacterial food-borne pathogens

There are more than 250 food-borne pathogens that exist in the environment, including viruses, fungi and bacteria. About 90% of food-borne illnesses caused can be attributed to bacterial contamination of food. Bacterial pathogens such as *Salmonella typhimurium, Salmonella enteritidis, Escherichia coli, Listeria monocytogenes, Staphylococcus aureus, Campylobacter jejuni,* and *Bacillus cereus* are sources of bacterial contamination in the food products. *Salmonella* species are the most frequent and commonly occurring bacterial food-borne pathogens worldwide [5]. There are over 2000 distinct types of serovars of *salmonella* species. Figure 1-1 shows the 5 most reported serotypes isolated from human sources in the United States as indicated by the

CDC annual reports 2000-2005 [7]. *Salmonella enterica* serovar *Enteritidis* followed by serovar *typhimurium* are the most frequently occurring serotypes (shown in Figure 1-1) isolated from human sources in the USA [6]. In the United States the occurrence of *Salmonella typhimurium* is more predominant.

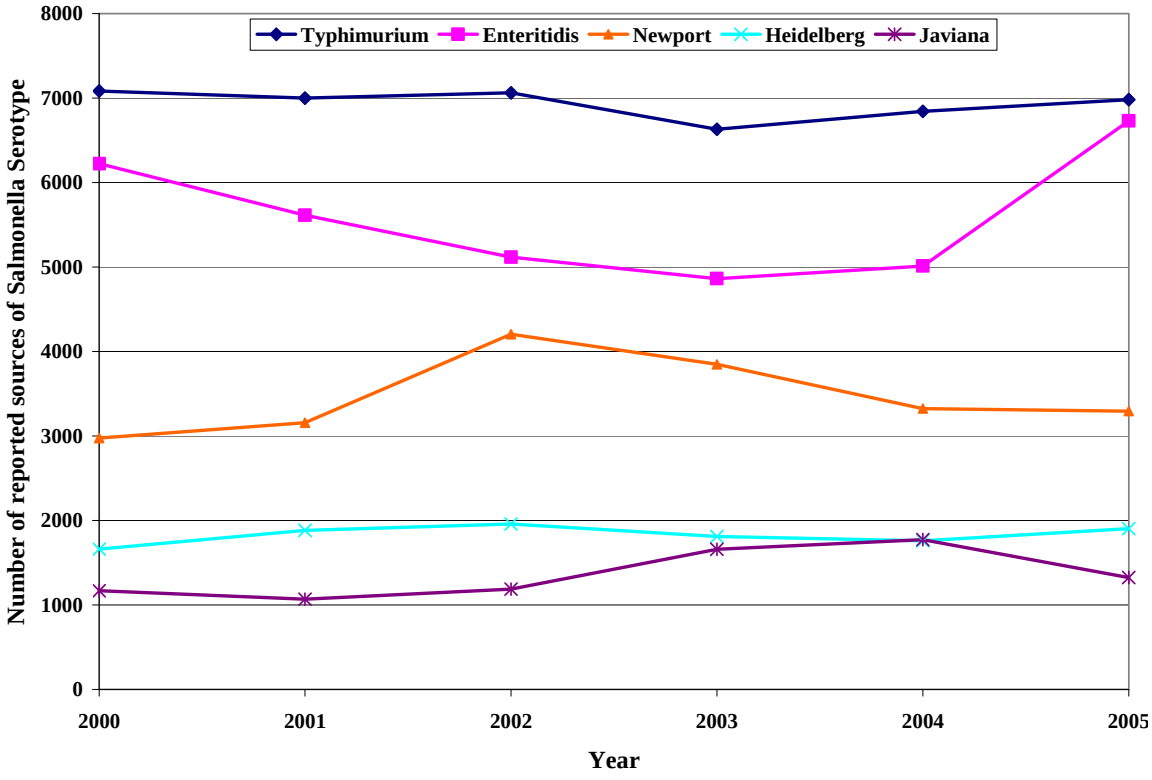

Figure 1-1: Number of reported sources of *Salmonella* serotypes from human sources during the period of 2000 to 2005.

1.1.2 *Salmonella* Related Outbreaks

A number of infamous *Salmonella related* outbreaks of food poisoning around the world have affected a large number of people resulting in discomfort, grief and sometimes even death. The number of cases reported due to *Salmonella* related illnesses is between 6.5 million to 33 million annually, and account for up to 9000 deaths. The Economic Research Service (ERS) estimates the annual economic cost of salmonellosis as $142,552,427. The average cost per case (in the year 2006) was approximately $10,000 including medical costs and productivity loss. Some of the recent *Salmonella typhimurium* related outbreaks are caused by bacterial contamination of tomatoes, eggs, milk, orange juice, fresh vegetables, ground beef and peanut butter. A summary of the recent *Salmonella* outbreaks is given in Table 1-1. A quick look at the table indicates that most of the items on the list are foods of daily consumption, rendering the common man highly vulnerable to any such outbreaks. *Salmonella typhimurium* has been acknowledged to be one of the great threats to human beings, whether it is due to unintentional ingestion of contaminated food or due to a repugnant act by terrorists. In this dissertation, work on the development of a rapid, sensitive and accurate diagnostic biosensor for the detection of *Salmonella typhimurium* is reported.

Table 1-1: *Salmonella* outbreaks in various food products.

Source	**Cases**	**Cause**	**News Article Headline**	
Milk/ Ice-cream	10,000	*S. typhimurium*	Schwain ice cream tainted with *Salmonella*	[8]
Milk	185,000	*S. typhimurium*	*Salmonella Typhimurium* causes scare in Chicago milk	[8, 9]
Milk	80	*S. typhimurium*	Chinese Milk Sickens 80 Children	[8, 9]
Several	70,000	*S. typhimurium*	700,000 killed by bad food and water in Asia each year: UN	[10]
Potato	3,400	*S. typhimurium*	*Salmonella* in potato salad renders several ill	[11]
Oat Cereal	100	*S. typhimurium*	*Salmonella* Outbreak Sickens 100 in 7 States	[2, 12]
Tomatoes	459	*Salmonella*	Tomatoes Blamed in *Salmonella* Outbreak in Pittsburgh, PA	[13]
Beef	6,000	*E. coli*	5.7 Million Pounds Of Ground Beef Recalled Due To *E.Coli*.	[14]
Spinach	5,000	*E. coli*	*E. coli* spinach scare increases to 21 states	[15]
Peanut butter	329	*S. typhimurium*	Tests find *salmonella* in peanut butter.	[16]

1.2. Diagnostic Biosensors: Definition and Components

The ever growing need for rapid detection of pathogenic micro-organisms has resulted in an increased interest in the research and development of biosensor systems. Figure 1-2 illustrates the main components of a biosensor. A biosensor is defined as a device that incorporates a biological recognition element and a transducer for the detection of an analyte/target of interest. The transducer needs to be capable of transferring information about the specific interaction between the analyte and the recognition element into measurable signals with high sensitivity. The bio-recognition element is an integral part of any biosensor. The bio-recognition element is responsible for the selectivity, specificity and thermal stability of a biosensor.

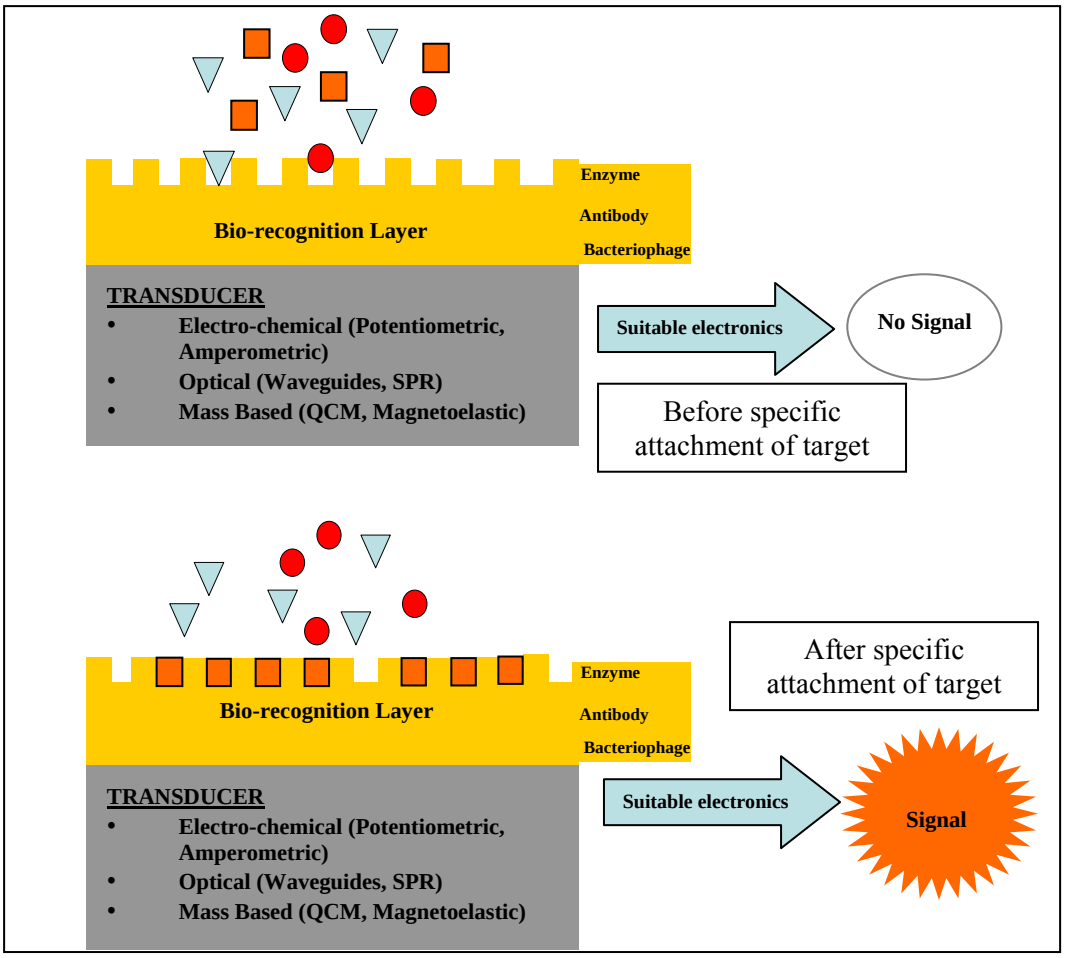

Figure 1-2: Schematic showing the basic components of a diagnostic biosensor.

1.2.1 Bio-recognition Element

The bio-recognition element is vital to the design of a biosensor. There are several types of bio-recognition elements (enzymes (section 2.3.1), antibodies (section 2.3.2), and phage (section 1.2.1.1, section 2.3.3)) that are used for biosensor applications [17]. In this dissertation, bacteriophage was used as the bio-recognition element for the detection of *Salmonella typhimurium*. The application of different types of phages used for diagnostic biosensor applications has been discussed and reviewed in Chapter 2.

1.2.1.1 Filamentous Bacteriophage

Bacteriophage derives its name from a combination of the word "bacteria" and Greek word "phagos" that in English mean "bacteria eater." The first report of the existence of phage was reported by a British scientist Dr. Ernest Hankin in 1896. He observed that the water from the river Ganges (largest river in India) had strong anti-microbial action (against *Vibrio cholerae*). Phage is a type of virus that infects bacteria at very specific sites. There are several types of phage that exist, classified based on their structure and the type of genes they carry.

Filamentous bacteriophage, as its name suggests, is a type of phage that has a thread-like appearance and encloses a circular ss-DNA as its genetic material. Typically filamentous bacteriophage has its genetic components enclosed within a tube with the major coat proteins pVIII covering a large percentage of the entire surface along the tube length. The ends are then capped with minor coat proteins pVI and pIII on one end and pVII and pIX on the other end (Figure 1-3).

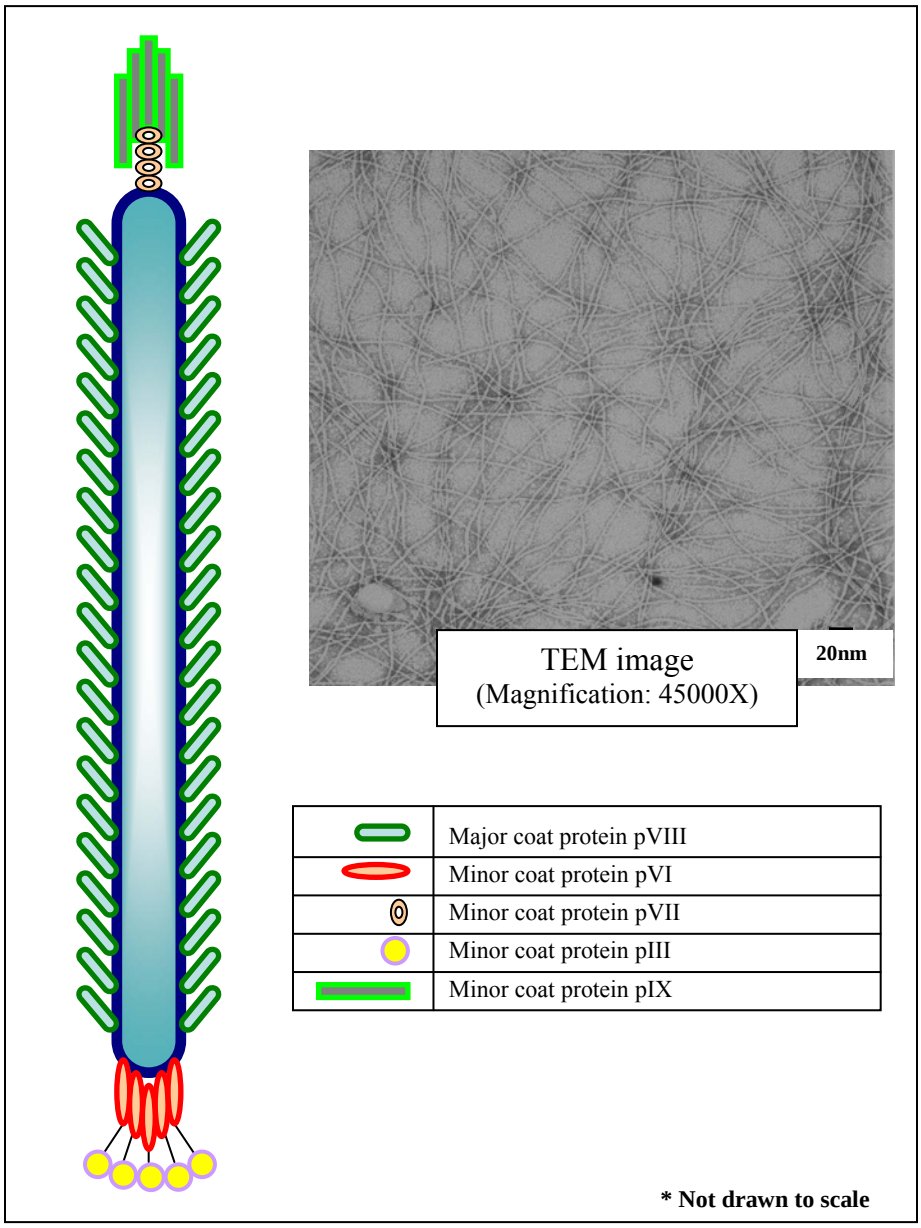

Figure 1-3: Schematic showing basic components of fd filamentous phage. The tube in the center contains the genetic material. Minor coat proteins cap the ends of the tube. The inset shows a TEM picture (Magnification 45000X) of phage filaments at a concentration of 5×10^{11} vir/mL.

Each phage filament is approximately 800-900 nm in length and has a diameter of about 6 nm. A landscape phage is a recombinant phage displaying 4000 copies of random peptides on their surface. Phage display technique is used to modify a small portion of the DNA. This modification leads to a display of desired peptides or "organic landscapes" fused into the major coat proteins [18-23]. Several steps (usually 5-10) of affinity selection (biopanning) procedures are then performed to yield a phage clone displaying peptides that are highly specific to the target analyte. The development of filamentous phage using phage display techniques have been studied extensively with potential applications in the area of biosensors research [18-20]. However, the study of affinity selected filamentous bacteriophage as a bio-recognition probe for biosensor applications is limited [28-35].

1.2.2 Transducer Platform

In this dissertation, the use of a magnetoelastic material as a transducer platform for the rapid, selective and specific detection of *S. typhimurium* is reported. Recently, the use of magnetoelastic materials as transducer platforms for the remote monitoring of food-borne pathogens [34-39] and other applications in chemical detection and environmental monitoring [40-45] have attracted considerable interest. Magnetoelastic transducers have the unique advantage of detection in the absence of physical wire contacts to the sensor, enabling in-situ wireless measurements in sealed containers. Magnetoelastic materials are amorphous ferromagnetic alloys that usually include a combination of iron, nickel, molybdenum and boron. These materials work on the principle of magnetostriction, wherein, the material experiences changes in its

dimensions in presence of a magnetic field. Upon application of a magnetic field, the randomly oriented magnetic domains in the material tend to align in the direction of the applied field. The alignment of the magnetic domains in the magnetoelastic material results in a change in the dimensions. By applying a time varying magnetic field, the magnetoelastic materials can efficiently convert the applied magnetic energy into mechanical oscillations. The characteristic fundamental resonance frequency of these oscillations is dependent on the physical properties (elastic modulus, density and Poisson's ratio) and the dimensions of the material. Both the actuation of the sensor and the detection of the response of the sensor can be measured using changes in the impedance of a non-contact solenoid pick-up coil. Magnetoelastic sensors are actuated by the application of an AC magnetic field that causes the sensors to oscillate mechanically. When the frequency of the applied field is in resonance with the natural frequency of the sensor, the conversion of electrical energy to elastic energy is the largest. For a thin, planar, ribbon shaped sensor of length L, vibrating in its basal plane, the fundamental resonant frequency of longitudinal oscillations is given by [45, 46]

$$f = \sqrt{\frac{E}{\rho(1-\sigma^2)}}\,\frac{1}{2L} \qquad (1\text{-}1)$$

where, E is Young's modulus of elasticity, ρ is the density of the sensor material, σ is the Poisson's ratio, and L is the length of the sensor.

Any non-magnetoelastic mass added to the sensor surface reduces the mechanical oscillations causing the resonance frequencies to shift to a lower value. A scan through the range of applied AC frequencies yields a spectrum. The resonance frequency of the sensor can be read from this spectrum and can be tracked for any changes. The details of

the measurement setup have been described in detail in section 3.3 and section 4.2. The changes in the resonance frequency can then be related to the magnitude of non-magnetoelastic mass attached to the sensor surface. Addition of a small mass of Δm (much smaller than the original mass of the sensor ($\Delta m << M$)) on the sensor surface will result in the change of natural resonance frequency (f_0) by an amount of Δf that can be related to the mass added as:

$$\Delta f = -\frac{f}{2}.\frac{\Delta m}{M} \qquad (1\text{-}2)$$

where f is the initial resonance frequency, M is the initial mass, Δm is the added mass and Δf is the shift in the resonant frequency of the sensor.

1.3. Research Objectives

The primary objective of this work was to characterize the performance of a magnetoelastic diagnostic biosensor for the detection of *S. typhimurium* using affinity-selected filamentous bacteriophage as the bio-recognition element. The experimental work was divided into three different sections.

I. Fabrication and characterization of the sensor platform
II. Characterization of the phage-immobilized biosensor
III. Characterization of phage immobilization on the sensor surface

The research objectives for this dissertation have been shown schematically in Figure 1-4. Details of the experiments done to met the objectives have been described in detail in Chapter 3.

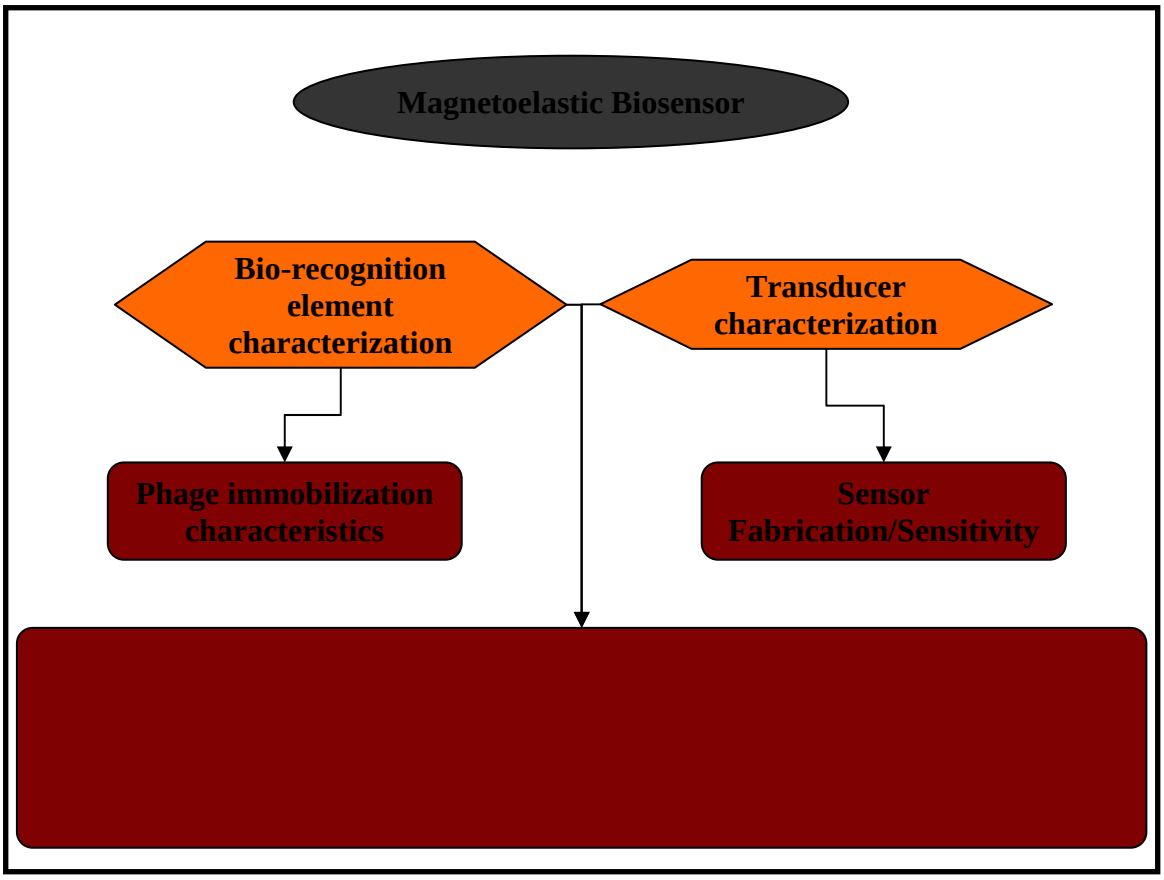

Figure 1-4: Chart depicting experiments to meet the research objectives.

1.3.1 Fabrication and characterization of the sensor platform

The fabrication of the magnetoelastic biosensors of desired dimensions with corrosion resistance and a favorable layer for bio-recognition element immobilization is critical for its performance. Our aim was to:

- Fabricate and measure responses of sensors with different dimensions.
- Establish size dependent mass sensitivity by measuring dose responses of sensors with decreasing the size (L=2 mm, 1 mm and 500 μm) of the sensors.
- Study the equivalent circuit for the measurement of magnetoelastic sensors.

1.3.2 Characterization of phage-immobilized magnetoelastic biosensor

The performance of a biosensor was evaluated by its dose response characteristics, specificity, selectivity, longevity and its capability to detect *Salmonella typhimurium* present in complex matrices. In order to evaluate these parameters the following tests were carried out:

- Study frequency responses of the biosensor upon exposure to different concentrations (5×10^1 through 5×10^8 cfu/mL) of *S. typhimurium*.
- Confirm the phage-*S. typhimurium* binding using measured frequency responses and correlate the responses with the help of electron microscopy images of assayed sensor surfaces.
- Study the thermal stability/longevity of phage-immobilized sensors at 3 different temperatures (25 ºC, 45 ºC and 65 ºC).
- Establish the specificity of the immobilized phage by analyzing cross-reactivity with other species.
- Study the selectivity of the phage-immobilized sensor to *S. typhimurium* in the presence of high concentrations of masking bacteria and in spiked (known concentrations of added bacteria) fat free milk and apple juice samples.

1.3.3 Characterization of phage immobilization on sensor surface

The nature and distribution characteristics of the bio-recognition element are very important towards achieving better sensitivity and stability of sensor responses. Since the use of phage as a bio-recognition element is relatively new, there is little understanding of the characteristics of immobilized phage and the effects it would have on the

performance of diagnostic sensors. In order to study these effects the following experiments were performed:

- Improve sample preparation techniques to enable viewing of phage filaments immobilized on a sensor surface using electron microscopy.
- Study the nature of the distribution of filamentous phage.
- Study the effect of the counterion concentrations on the immobilization characteristics of phage.

REFERENCES

1. Mead, P.S., Slutsker, L., Dietz, V., McCaig, L.F., Bresee, J.S., Shapiro, C., Griffin, P.M., and Tauxe, R.V., *Food-Related Illness and Death in the United States.* Emerging Infectious Diseases, 1999. **5**(5): 607-625.
2. Altekruse, S.F., Cohen, M.L., and Swerdlow, D.L., *Emerging Foodborne Diseases.* Emerging Infectious Diseases, 1997. **3**: 503-510.
3. Slutsker, L., Altekruse, S.F., and Swerdlow, D.L., *FOODBORNE DISEASES: Emerging Pathogens and Trends.* Infectious Disease Clinics of North America, 1998. **12**(1): 199-216.
4. Torok, T.J., Tauxe, R.V., Wise, R.P., Sokolow, R., Mauvais, S., Birkness, K.A., Skeels, M.R., Horan, J.M., and Foster, L.R., *A large community outbreak of salmonellosis caused by intentional contamination of restaurant salad bars.* 1997. **278**: 389-395.
5. Todd, E.C., *Costs of acute bacterial foodborne disease in Canada and the United States.* International Journal of Food Microbiology, 1989. **9**(313-326).
6. Galanis, E., Wong, D.M.A.L.F., Patrick, M.E., Binsztein, N., Cieslik, A., Chalermchaikit, T., Aidara-Kane, A., Ellis, A., Angulo, F.J., and Wegener, H.C., *Web-based Surveillance and Global Salmonella Distribution, 2000–2002.* Emerging Infectious Diseases, 2006. **12**(3): 381-388.
7. CDC. Salmonella Surveillance: Annual Summary, A., Georgia: US Department of Health and Human Services, CDC, 2007.

8. CDC, *Multistate Outbreak of Salmonella Serotype Typhimurium Infections Associated with Drinking Unpasteurized Milk --- Illinois, Indiana, Ohio, and Tennessee, 2002--2003*. 2003. **52**(56): 613-615.

9. CDC, *Salmonella Typhimurium Infection Associated with Raw Milk and Cheese Consumption --- Pennsylvania, 2007*. MMWR, 2007. **56**(44): 1161-1164.

10. *700,000 Killed by bad food, water in Asia each year: UN*, in *ONASA News Agency, Europe Intelligence Wire*. 2004.

11. Angulo, F.J., Getz, J., and Taylor, J.P., *A large outbreak of botulism: the hazardous baked potato*. 1998. **178**: 172-177.

12. CDC, *The Management of Acute Diarrhea in Children: Oral Rehydration, Maintenance, and Nutritional Therapy*. MMWR, 1992. **41**(RR-16): 1.

13. CDC, *Preliminary FoodNet data on the incidence of infection with pathogens transmitted commonly through food---10 sites, United States, 2004*. MMWR, 2005. **54**: 352-356.

14. CDC, *Multistate Outbreak of Salmonella Typhimurium Infections Associated with Eating Ground Beef -United States, 2004*. MMWR, 2006. **55**(7): 180-182.

15. CDC, *Summary of Notifiable Diseases --- United States, 2006*. MMWR, 2008. **55**(53): 1-94.

16. CDC, *Multistate Outbreak of Salmonella Serotype Tennessee Infections Associated with Peanut Butter --- United States, 2006--2007*. MMWR, 2007. **56**(21): 521-524.

17. Feltus, A., Daunert, S. (2002). Genetic engineering of signaling molecules. In: Ligler, F.S., Rowe-Taitt, C.A. (Eds), Optical Biosensors: Present and Future. Elsevier, Amsterdam, pp. 307–329.

18. Petrenko, V.A., *Landscape phage as a molecular recognition interface for detection devices.* Microelectronics Journal, 2008. **39**(2): 202-207.

19. Petrenko, V.A. and Sorokulova, I.B., *Detection of biological threats. A challenge for directed molecular evolution.* Journal of Microbiological Methods, 2004. **58,**(2): 147-168.

20. Sorokulova, I.B., Olsen, E.V., Chen, I.H., Fiebor, B., Barbaree, J.M., Vodyanoy, V.J., Chin, B.A., and Petrenko, V.A., *Landscape phage probes for Salmonella typhimurium.* Journal of Microbiological Methods, 2005. **63**(1): 55-72.

21. Ilyichev, A.A., Minenkova, O.O., Kishchenko, G.P., Tat'kov, S.I., Karpishev, N.N., Eroshkin, A.M., Ofitzerov, V.I., Akimenko, Z.A., Petrenko, V.A., and Sandakhchiev, L.S., *Inserting foreign peptides into the major coat protein of bacteriophage M13.* FEBS Letters, 1992. **301**(3): 322-324.

22. Petrenko, V.A. and Vodyanoy, V.J., *Phage display for detection of biological threat agents.* Journal of Microbiological Methods, 2003. **53**(2): 253-262.

23. Smith, G.P., Petrenko, V.A., and Matthews, L.J., *Cross-linked filamentous phage as an affinity matrix.* Journal of Immunological Methods, 1998. **215**(1-2): 151-161.

24. Benhar, I., Eshkenazi, I., Neufeld, T., Opatowsky, J., Shaky, S., and Rishpon, J., *Recombinant single chain antibodies in bioelectrochemical sensors.* Talanta, 2001. **55**(5): 899.

25. Mittelmann, A.S., Ron, E.Z., and Rishpon, J., *Amperometric Quantification of Total Coliforms and Specific Detection of Escherichia coli.* Analytical Chemistry, 2002. **74**(4): 903-907.

26. Neufeld, T., Schwartz-Mittelmann, A., Biran, D., Ron, E.Z., and Rishpon, J., *Combined Phage Typing and Amperometric Detection of Released Enzymatic Activity for the Specific Identification and Quantification of Bacteria.* Analytical Chemistry, 2003. **75**(3): 580-585.

27. Perez, F., Tryland, I., Mascini, M., and Fiksdal, L., *Rapid detection of Escherichia coli in water by a culture-based amperometric method.* 2001. **427**(2): 149.

28. Wei, D., Oyarzabal, O.A., Huang, T.-S., Balasubramanian, S., Sista, S., and Simonian, A.L., *Development of a surface plasmon resonance biosensor for the identification of Campylobacter jejuni.* Journal of Microbiological Methods, 2007. **69**(1): 78-85.

29. Nanduri, V., Bhunia, A.K., Tu, S.-I., Paoli, G.C., and Brewster, J.D., *SPR biosensor for the detection of L. monocytogenes using phage-displayed antibody.* 2007. **23**(2): 248.

30. Nanduri, V., Balasubramanian, S., Sista, S., Vodyanoy, V.J., and Simonian, A.L., *Highly sensitive phage-based biosensor for the detection of [beta]-galactosidase.* 2007. **589**(2): 166.

31. Jia, Y., Qin, M., Zhang, H., Niu, W., Li, X., Wang, L., Li, X., Bai, Y., Cao, Y., and Feng, X., *Label-free biosensor: A novel phage-modified Light Addressable Potentiometric Sensor system for cancer cell monitoring.* Biosensors and Bioelectronics, 2007. **22**(12): 3261.

32. Olsen, E.V., Sorokulova, I.B., Petrenko, V.A., Chen, I.H., Barbaree, J.M., and Vodyanoy, V.J., *Affinity-selected filamentous bacteriophage as a probe for acoustic wave biodetectors of Salmonella typhimurium.* 2006. **21**(8): 1434.

33. Nanduri, V., Sorokulova, I.B., Samoylov, A.M., Simonian, A.L., Petrenko, V.A., and Vodyanoy, V., *Phage as a molecular recognition element in biosensors immobilized by physical adsorption.* Biosensors and Bioelectronics, 2007. **22**(6): 986-992.

34. Lakshmanan, R.S., Guntupalli, R., Hu, J., Kim, D.-J., Petrenko, V.A., Barbaree, J.M., and Chin, B.A., *Phage immobilized magnetoelastic sensor for the detection of Salmonella typhimurium.* Journal of Microbiological Methods, 2007. **71**(1): 55-59.

35. Lakshmanan, R.S., Guntupalli, R., Hu, J., Petrenko, V.A., Barbaree, J.M., and Chin, B.A., *Detection of Salmonella typhimurium in fat free milk using a phage immobilized magnetoelastic sensor.* Sensors and Actuators B: Chemical, 2007. **126**(2): 544-549.

36. Guntupalli, R., Lakshmanan, R.S., Johnson, M.L., Hu, J., Huang, T.S., Barbaree, J.M., Vodyanoy, V.J., and Chin, B.A., *Magnetoelastic biosensor for the detection of Salmonella typhimurium in food products.* Sensing and Instrumentation for Food Quality and Safety, 2007. **1** (1): 3-10.

37. Guntupalli, R., Hu, J., Lakshmanan, R.S., Huang, T.S., Barbaree, J.M., and Chin, B.A., *A magnetoelastic resonance biosensor immobilized with polyclonal antibody for the detection of Salmonella typhimurium.* Biosensors and Bioelectronics, 2007. **22**: 1474-1479.

38. Ong, K.G., Bitler, J. S., Grimes, C. A., Puckett, L.G., Bachas, L. G., *Remote query resonant-circuit sensors for monitoring of bacteria growth: application to food quality control.* Sensors, 2002. **2**: 219-232.

39. Ong, K.G., Leland, J. M., Zeng, K., Barrett, G., Zourob, M., Grimes, C. A., *A rapid highly-sensitive endotoxin detection system.* Biosensors and Bioelectronics, 2006. **21**: 2270–2274.

40. Grimes, C.A., Kouzoudis, D., *Remote Query Measurement of Pressure, Fluid-Flow Velocity, and Humidity Using Magnetoelastic Thick-Film Sensors.* Sensors and Actuators B, 2000. **84**: 205-212.

41. Jain, M.K., Schmidt, S., Ong, K. G., Mungle, C., Grimes, C. A., *Magnetoacoustic Remote Query Temperature and Humidity Sensors.* Smart Materials and Structures, 2000. **9**: 502-510.

42. Jain, M.K., Schmidt, S., Mungle, C., Loiselle, K., Grimes, C. A., *Measurement of temperature and liquid viscosity using magneto-acoustic/magneto-optical sensors.* IEEE. Trans. on Magnetics, 2001. **37**(4): 2767-2769.

43. Ruan, C., Zeng, K., Varghese, O.K., and Grimes, C.A., *Magnetoelastic Immunosensors: Amplified Mass Immunosorbent Assay for Detection of Escherichia coli O157:H7.* Anal. Chem., 2003. **75**: 6494-6498.

44. Shankar, K., Zeng, K., Ruan, C., and Grimes, C.A., *Quantification of ricin concentrations in aqueous media.* Sensors and Actuators B, 2005. **107**: 640-648.

45. Stoyanov, P.G. and Grimes, C.A., *A Remote Query Magnetostrictive Viscosity Sensor.* Sensors and Actuators A, 2000. **80**: 8-14.

46. Landau, L.D. and Lifshitz, E.M., *Theory of Elasticity*. 1986: Pergamon.

2. LITERATURE REVIEW

In this chapter the current trends and existing methodologies for the detection of food-borne pathogens are described. This chapter begins with two sections discussing micro-biological methods (section 2.1) and diagnostic biosensors (section 2.2). Different bio-recognition probes used for biosensor applications are then described in section 2.3. In section 2.4, a review of various transducers that are used in combination with phage is presented. The transducers that are discussed are based on: electro-chemical (section 2.4.1), optical (section 2.4.2) and mass-change mechanisms (section 2.4.3).

2.1. Conventional micro-biological methods

2.1.1 History

The presence of micro-organisms was reported for the first time in the 17th century by Anton van Leeuwenhoek. In 1676, Anton van Leeuwenhoek used self-crafted lenses to view micro-organisms that he named as animalcules (now known as bacteria). He used beet stains to view the micro-organisms under the microscope. The next significant development in the identification of bacteria was during the years 1881-1885. During these 4 years Robert Koch and his associates Angelina Fannie Hesse, Walter Hesse and Julius Petri isolated bacteria responsible for anthrax, tuberculosis and cholera [1-4]. They

used methylene blue stains to view the micro-organisms with the help of a compound microscope. Robert Koch's group was also responsible for the development of culturing methods for micro-organisms; including discovery of agar gel as a culturing medium and discovery of the Petri dish.

The Gram stain method is one of the oldest techniques of distinguishing bacteria which is widely used even in the present day. This method was originally devised by a Danish doctor Hans Christian Joachim Gram in 1884 and is used to classify bacteria by its ability to retain crystal violet-iodine complex. The bacteria are classified as gram-negative or gram-positive based on the chemical and physical properties of the bacterial cell wall. In gram-positive bacteria, the stain does not penetrate the thick cell wall (peptidoglycan is present) and the cells appear to be violet in color. Gram-negative bacteria have a thinner cell wall (peptidoglycan is absent) and also have an outer layer with lipids that allow the stain to penetrate the cell wall and the cells appear to be pink in color. The problem with this method of distinguishing bacteria is due to the exceptions presented by some species. These bacterial species even in the presence of peptidoglycan in the cell wall are penetrated by the stain and thus result in an inaccurate differentiation of bacteria. The Gram stain method is messy due to the use of staining dyes and is also prone to operator error.

The traditional methods (described above) for the identification of bacteria typically depend on amplification and enrichment of the microbe in favorable media. Enrichment and sampling can take from 4 to 7 days, depending on the growth rate of the micro-organism [1-4]. This results in an increased turn around time for these methods. Table 2-1 shows a timeline of important contributions in microbiology leading to the

development of the now modern techniques of bacterial identification. The widely used modern microbiological methods for identification of bacteria known as Polymerase Chain Reaction (PCR) and Enzyme Linked Immuno Sorbent Assay (ELISA) tests are discussed in section 2.1.2 and section 2.1.3, respectively.

Table 2-1: Timeline showing some of the important contributions in bacteriology

Year	**Researcher**	**Contribution**
1676	Anton van Leeuwenhook	Used lenses to view single celled organisms called "animalcules."
1881	Robert Koch	Isolation of anthrax, tuberculosis and cholera and viewed using beet stains.
1883	Angelina Fannie and Walter Hesse	Development of Agar gels as a medium for culturing micro-organisms.
1883	Julius Petri	Discovery of Petri dish for culturing of micro-organisms.
1884	Hans Christian Gram	Developed a method for distinguishing between two major classes of bacteria
1891	Paul Elrich	Proposed that antibodies are responsible for immunity.
1953	James Watson and Francis Crick	Described the structure of DNA.
1971	Peter Perlmann and Eva Engvall	Development of ELISA.
1983	Kary Mullis	Development of PCR.

2.1.2 Polymerase Chain Reaction (PCR)

Polymerase Chain Reaction (PCR), developed in the mid-1980's, presented several advantages in terms of speed, specificity and sensitivity for the identification of bacteria. In the PCR test, a certain target DNA segment of interest in a bacterial sample is amplified to form millions of copies of the target DNA segment. Since this method is a nucleic acid-based diagnostic method, the identification of bacteria (even when present in small quantities) can be carried out with relative ease [5]. The main ingredients used for this process are an excess of free nucleotides, primers and an enzyme Taq polymerase. The primers are usually around 20-nucleotides long and complimentary to the end of the target DNA segment of interest. The Taq polymerase is an enzyme that is capable of withstanding high temperatures used in the PCR process. A schematic showing the basic steps involved in PCR is depicted in Figure 2-1.

A typical PCR procedure consists of three main steps: denaturing, annealing and extension/polymerization. The denaturing step is carried out by heating to a temperature of 94-98 ºC to break the hydrogen bonds between the two strands of DNA. This step yields single strands of the DNA. In the annealing step the temperature is lowered to 50-65 ºC. At this temperature the primers are attached to the single strands of DNA obtained from the denaturing step. The primer sequence is selected so that nucleotides present on the primer are complimentary to the target DNA. In the final step extension of the primer with help of added free nucleotides is carried out at a temperature of 75-80 ºC. At the end of this step two copies of the target DNA are created. The two copies produced by this first cycle are then returned to the denaturing step for the next cycle. After 25-30

cycles of this procedure, millions of copies of the target DNA have been produced, thus amplifying the initial small quantity of target DNA.

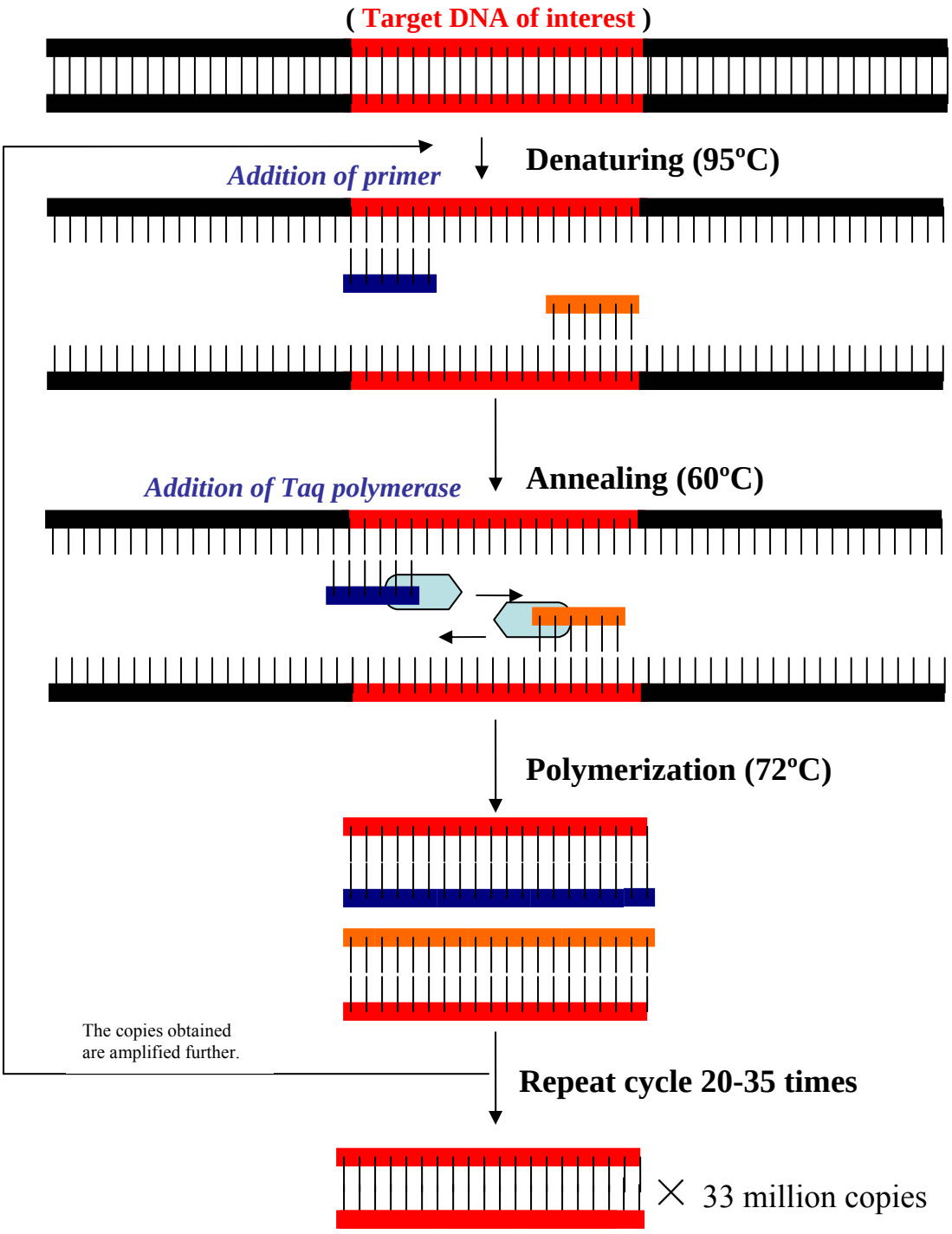

Figure 2-1: Schematic showing basic steps involved in PCR.

There are numerous reports on the detection of bacterial pathogens using PCR in water [6], milk, chicken fecal samples [7], and ground beef [8]. PCR has also been used to detect *Bacillus anthracis* [9-11] in a variety of mediums. Due to the high sensitivity of this method, even a minor contamination of sample DNA can yield erratic results. The selection of a suitable primer is also a challenge due to the need for a prior knowledge of the target DNA sequence. The requirement of extremely clean and controlled environments and the need for trained personnel limits this methodology to laboratory use.

2.1.3 Enzyme-Linked Immunosorbent Assay (ELISA)

The first immunoassay used for identification of bacterial pathogens was the radio immunoassay (RIA). This method involved tagging of an antibody with a radioactive element. The amount of radiation of the radioactive species was then used to determine the concentration of analyte present. In search for a safer alternative to this method (no radio-active elements), enzyme-linked immunoassay (ELISA) was developed. In ELISA the radioactive elements are replaced by enzymes tagged to an antibody. A change in color produced by an enzyme mediated reaction is measured. The amount of target analyte present in a sample can be related to the amount of color change produced. There are three different formats for performing ELISA: “indirect” ELISA, sandwich ELISA and competitive ELISA. A schematic of the three types of ELISA procedures are shown in Figure 2-2.

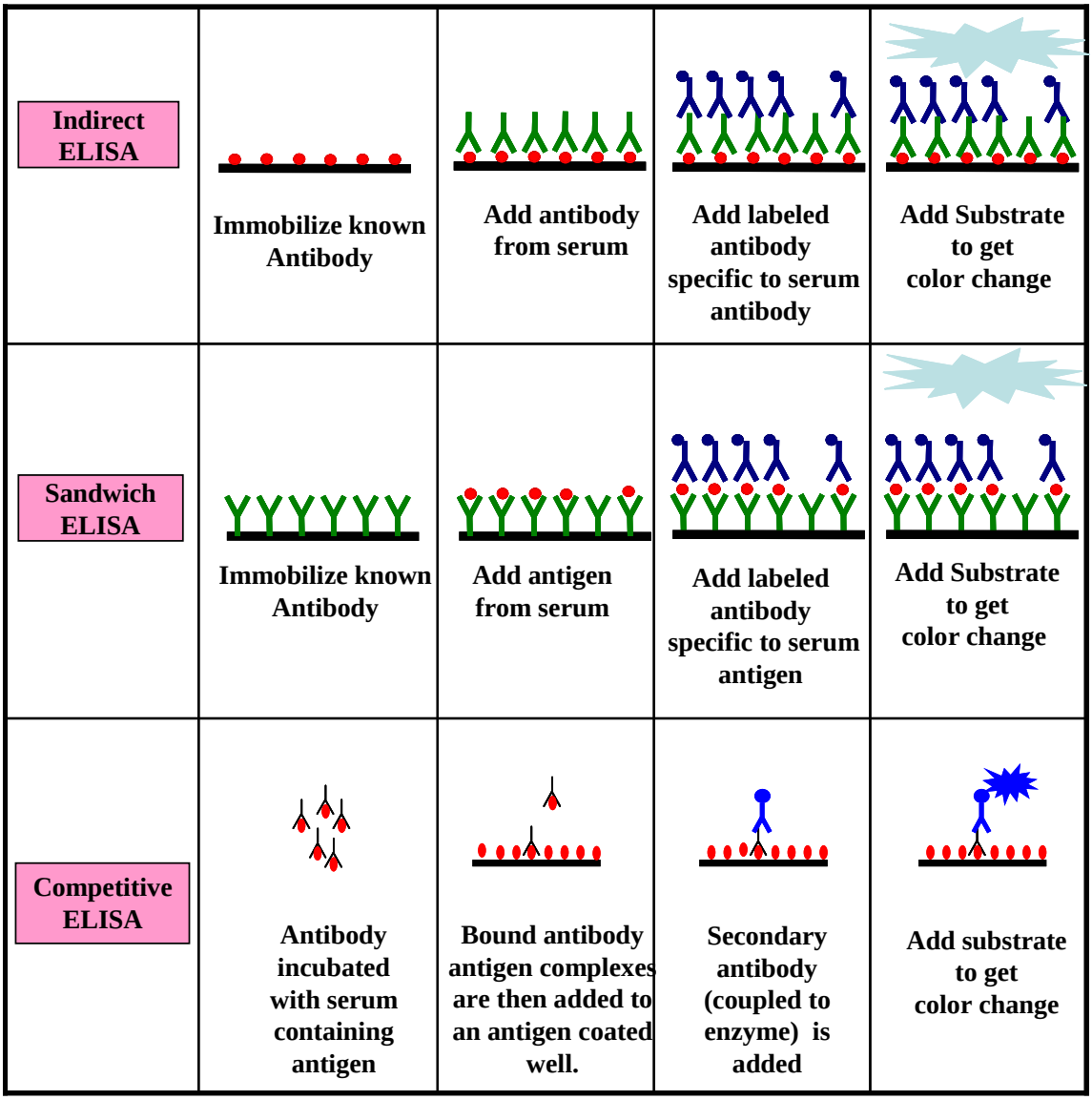

Figure 2-2: Schematic showing basic steps involved in a typical Indirect ELISA, Sandwich ELISA assay and Competitive ELISA.

In an indirect ELISA, the capture antigen is coated on a micro titer plate. The serum containing the antibody is then added and is washed with buffer solutions to remove any unbound antibody. A secondary antibody specific to the serum antibody is then added and allowed to attach. This step is followed by the attachment of an enzyme-conjugated antibody to the secondary antibody. After the excess enzyme-conjugated antibodies are washed away, a substrate is added that will produce a color change that can be detected and quantified using optical methods.

In a sandwich ELISA, the micro titer plate is coated with an antibody with high specificity to the target antigen of interest. The non-specific sites on the micro titer plate are blocked. The serum containing the antigen is then added and allowed to attach to the coated antibody. This is followed by a washing step to remove any unbound or loosely bound antigens. An enzyme-conjugated antibody (specific to the target antigen) is added. Another wash is used to remove any unbound or loosely bound enzyme-conjugated antibodies. Finally a substrate is added that would react with the enzyme to produce a color change depending on the concentration of the antigen present in the serum.

In a competitive ELISA, the steps are somewhat different. Unlabeled antibody is incubated in the presence of antigen. These antibody-antigen complexes are added to an antigen coated micro titer plate. Thus, the higher the amount of antigen in the sample, the smaller the amount of antibody bound to the well. The secondary antibody (coupled to the enzyme) that is specific to the primary antibody is then added. The substrate is then added to produce a color change. In competitive ELISA unlike indirect ELISA or sandwich ELISA, for a sample with higher antigen concentration the signal produced is weaker. Competitive ELISA and sandwich ELISA are usually used to determine the

amount of antigen present in a serum/sample while indirect ELISA is usually used to estimate the amount of antibody present in a serum sample.

2.2. Diagnostic Biosensors

The ever growing need for early, rapid, sensitive and specific identification of micro-organisms present in food, environmental and clinical samples, has attracted considerable interest in research towards the development of novel diagnostic methodologies. The primary focus of research in the field of biosensors is to enable rapid detection of target pathogens outside laboratory confines with minimal need for skilled personnel. Biosensors are now being used in a wide variety of fields such as food safety, detection of liquid contamination, clinical diagnostics, agriculture and in the fight against bio-terrorism [12-17].

A diagnostic biosensor is composed of two major elements: a transducer and a bio-molecular recognition element. A biosensor is defined as a device that incorporates a biological sensing element and a transducer for the detection of an analyte/target of interest. The detection of an analyte by the bio- recognition element is due to a specific interaction that would generate a chemical or physical change. The transducer can directly or indirectly convert this interaction reaction into a measurable effect. Historically, biosensor research evolved from the discovery of the oxygen electrode by Professor Leland C. Clarke Junior. He was the first to develop a biosensor for glucose detection. Since then researchers have developed a plethora of recognition elements (enzymes, antibodies, bacteriophage) and transduction elements (optical, magnetic,

electro-chemical, mass-based) to build novel biosensor systems for a wide range of applications.

2.3. Bio-recognition element

2.3.1 Enzymes

Enzymes have been used as a bio-recognition probe for various biosensors. Enzymes usually aid in catalytic reactions to produce measurable signals. The catalytic power of enzymes, coupled with their high specificity of action, make them the most extraordinary molecules for use in biological systems. Enzyme-based biosensors are used in electrochemical assays, for the detection of glucose, aromatic hydrocarbons, and monitoring of pH changes. However, there is limited use of enzyme-based biosensors for the detection of bacterial pathogens.

2.3.2 Antibody

Antibodies have been the most popular recognition elements for applications in biosensors particularly for detection of bacterial micro-organisms. Antibodies specific to a target bacteria of interest are produced by injecting the target bacteria into an efficient antibody producing animal. The animal's immune system then builds a family of polyclonal antibodies with mildly varying specificities and affinities to the injected bacteria. From this family of antibodies, the antibodies that yield high specificity and affinity to the target bacteria are extracted. This process of immunization and extraction is time consuming and requires specialized facilities. In addition to the complexity of extracting and purifying, antibodies require controlled laboratory environments and are

extremely sensitive to temperature and pH changes. Hence there is need for a more robust bio-recognition element that would be suitable for typical field conditions.

2.3.3 Bacteriophage

Bacteriophages are naturally evolved viruses that attach and infect their host bacteria at highly specific receptors. This principle has been the basis of a method known as phage-typing. The phage-typing method involves the infection and lysis of the bacterial cell. This method has been has been widely used for epidemiological applications and bacterial detection [18, 19]. However, the lytic nature of the phages used in phage-typing limit their applications as bio-recognition probes. A study of the genetics of filamentous phage and recent advances in phage display techniques have resulted in the development of recombinant phage. The recombinant phage can be genetically modified to display peptides, fused into all copies of the major coat protein. The phage clones displaying peptides highly specific to a target analyte of interest [20-28] are then identified and separated using affinity selection procedures.

Filamentous phages are flexible thread-shaped bacterial virus typically 6 nm wide and 800-900 nm long. The genetic material (single stranded circular DNA) is enclosed within the tube containing the outer coat proteins. The outer coat is formed by thousands of equal copies of the major coat protein pVIII and the ends are capped by minor coat proteins (pIII, pVI, pVII and pIX) at each end. Landscape phages are created by modifying the genetic material in such a manner that they display numerous copies of peptides in a repeating fashion on the viral surface. It is called a “Landscape” phage because the viral surface constricts the peptides to a defined conformation [29, 30]. The

surface area density of phage is 300-400 m^2/g, out of which more than 50% of the surface and 90% of the mass is comprised of peptides that form the active binding sites [27]. Studies have shown that, unlike antibodies, phage is stable in harsh environments and can be stored indefinitely at moderate temperatures with minimal loss of activity [20, 31].

Procedures used in the affinity-selection of filamentous phage have been described in detail by Sorokulova et.al. In this method the target antigen is added and spread on a Petri dish. The f8/8 landscape phage library is then added to the target antigen coated Petri dish and is incubated for 1 hour at room temperature. The unbound phage from the Petri dish is washed with a mixture of TBS and tween. An elution buffer is then used to elute the phage bound to the target antigen attached to the Petri dish. The elution process is followed by the neutralization of the eluate. The phage recovered from the eluate is multiplied and used in the subsequent cycles of the selection process. The whole procedure of selection is repeated 5 times to provide the clones highly specific to the target antigen. The phage filaments produced at the end of each cycle is characterized using DNA sequencing techniques to identify the amino acid sequences of the displayed peptides. Common motifs in the amino acid sequences are identified for the clones that have a larger affinity towards the target antigen. A schematic of the affinity selection procedure is shown in Figure 2-3. Table 2-2 shows the International Committee on Taxonomy of Viruses (ICTV) classification of phage [32] based on their morphology and the kind of genetic material they enclose. Filamentous phage (fd) used in this work belongs to the class Inoviridae.

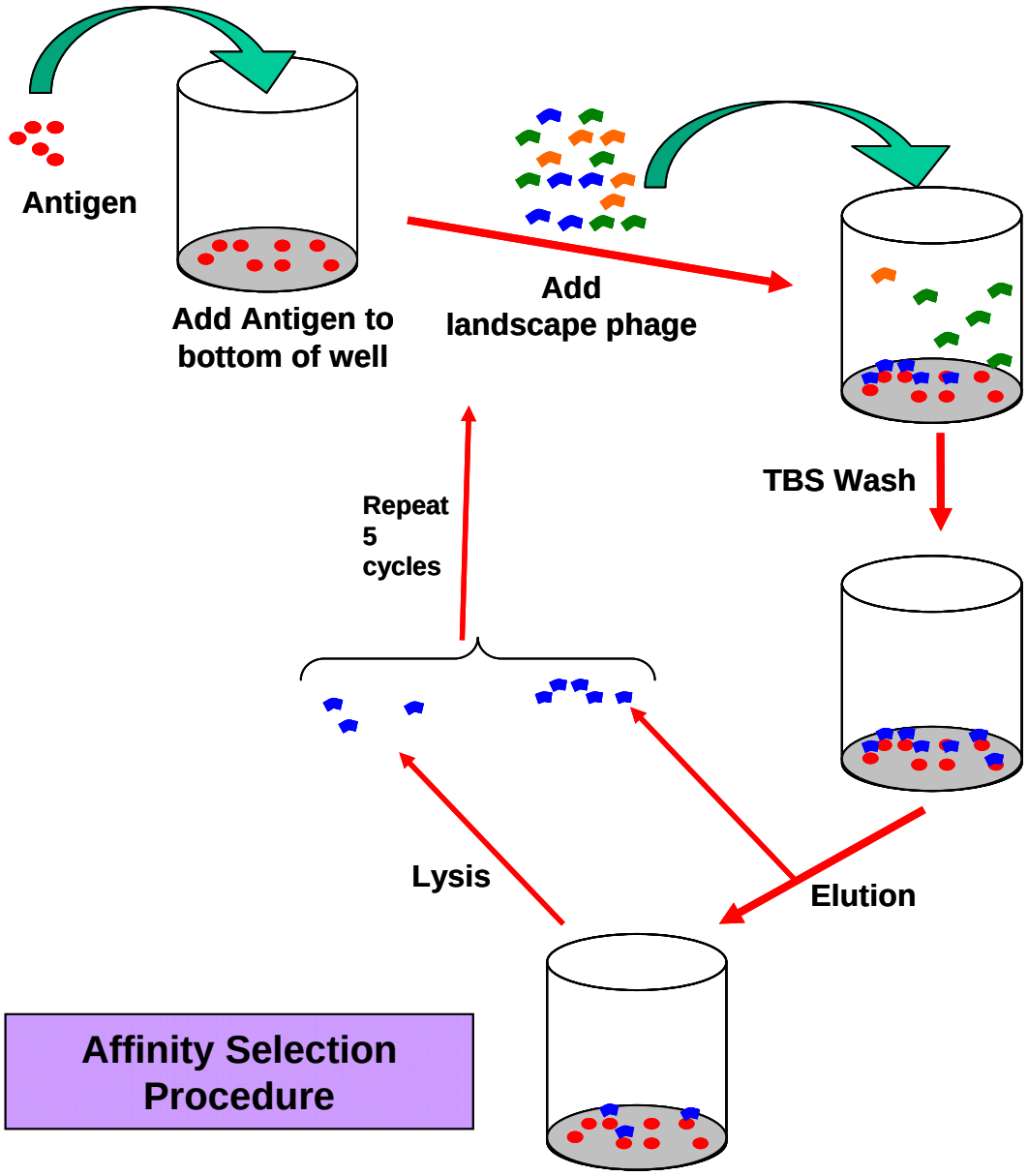

Figure 2-3: Schematic depicting selection procedure for phage.

Table 2-2: ICTV classification of phages based on structural morphology and genetic material enclosed [32].

Family	Morphology	Nucleic acid
Myoviridae	Non-enveloped, contractile tail	Linear dsDNA
Siphoviridae	Non-enveloped, long non-contractile tail	Linear dsDNA
Podoviridae	Non-enveloped, short noncontractile tail	Linear dsDNA
Tectiviridae	Non-enveloped, isometric	Linear dsDNA
Corticoviridae	Non-enveloped, isometric	Circular dsDNA
Lipothrixviridae	Enveloped, rod-shaped	Linear dsDNA
Plasmaviridae	Enveloped, pleomorphic	Circular dsDNA
Rudiviridae	Non-enveloped, rod-shaped	Linear dsDNA
Fuselloviridae	Non-enveloped, lemon-shaped	Circular dsDNA
Inoviridae	Non-enveloped, filamentous	Circular ssDNA
Microviridae	Non-enveloped, isometric	Circular ssDNA
Leviviridae	Non-enveloped, isometric	Linear ssRNA
Cystoviridae	Enveloped, spherical	Segmented dsRNA

2.4. Transduction Methods

In this section, the work done on the application of bacteriophage utilizing either lytic phage or affinity-selected filamentous phage in combination with different transduction methodologies is reviewed. A transducer element is capable of measuring electro-chemical (section 2.4.1), optical (section 2.4.2) and mass-based (section 2.4.3) changes caused by the specific interaction of the bio-recognition element and the target analyte of interest.

2.4.1 Electro-chemical

Electro-chemical transducers are capable of converting the interaction between the target analyte and the bio-recognition probe into measurable electrical signals (usually due to electrons and ions). The magnitude of the changes in the electrical signal can be related to the amount of analyte present. Electro-chemical transducers are categorized as amperometric and potentiometric.

2.4.1.1 Amperometric

As the name suggests, amperometric transducers measure the current produced by the biological interaction of interest. This is done by applying a constant potential across the working and the reference electrode and measuring the changes in the current produced. The applied potential ensures the electron transfer reaction of the electroactive biological species by gaining or losing an electron. The current thus produced can be related to the recognition interaction and thus the amount of target analyte present. Amperometric transducers have found a wide range of applications in gas analysis and chemical/biological detection, primarily due to ease of operation and high sensitivity.

The use of amperometric methods to detect bacteria by the release of intrinsic enzyme markers from the interior of the cells has been widely studied [33-36]. The released enzyme markers are complimented with a suitable substrate to produce electroactive reactions at the electrode. Early amperometric sensors relied on permeabilization (using chemicals) of the antigens for the release of intrinsic enzymes. In their earlier work, Mittleman et. al. [33] established the release of β-galactosidase from *E. coli* by permeabilization. The interaction of β-galactosidase with substrate *p*-aminophenyl α-D-galactopyranoside releases *p*-aminophenol. The *p*-aminophenol oxidizes at the electrode to produce current. The work by Neufeld et. al. and Yemini et. al. [34, 37, 38], used these principles to detect various pathogens (*Bacillus cereus*, *Mycobacterium smegmatis* and *Escherichia coli*).

Recently amperometric sensors in combination with phage typing have been used for the specific detection of various bacteria. In this method, the enzyme markers from the interior of bacterial cells are released by a phage mediated lysis of the analyte. The released intrinsic enzyme then reacts with the substrate. The product of this reaction (usually *p*-aminophenol) oxidizes at the electrode resulting in an electric current proportional to the analyte concentration. The reaction shown in Figure 2-4 is representative of such an amperometric sensor. Here phage mediated lysis of the *E. coli* bacteria was used to release the enzyme β-galactosidase. This enzyme upon its reaction with the substrate (*p*-aminophenyl β-D-galactopyranoside) produces *p*-aminophenol. The oxidation of *p*-aminophenol at the electrode produces a current proportional to the initial concentration of the analyte.

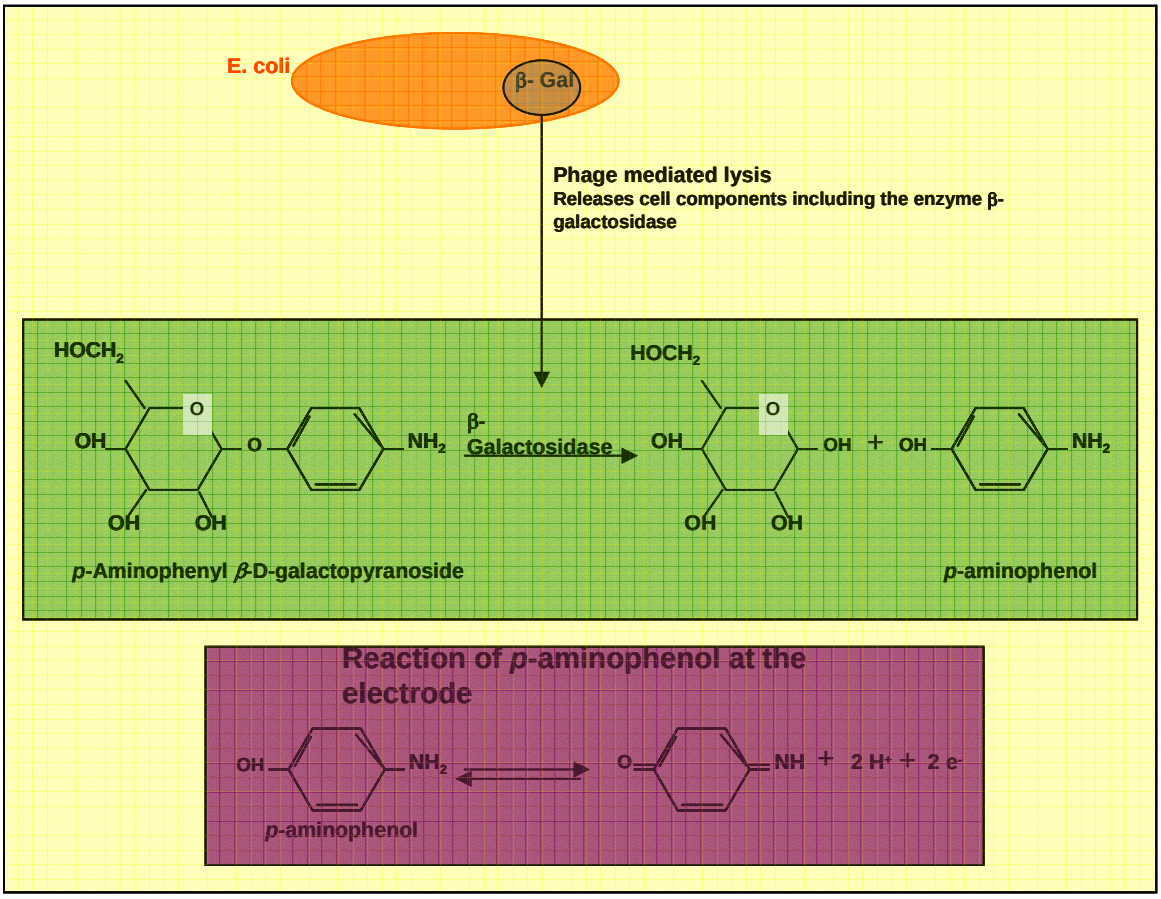

Figure 2-4: Basic reactions involved in amperometric detection of *E. coli* [35]. In this technique the intrinsic enzyme from the bacteria is released by phage-driven lysis of the cells.

In an advanced assay, Neufeld et. al. [37] have published data using a combination of phagemid (a cloning vector of filamentous phage) and a helper M13 phage. In this technique rather than lysing the cell, the substrate and the reporter enzyme reaction occurs in the periplasmic region of the bacterial cell. This reaction results in the subsequent release of *p*-aminophenol and its oxidation at the electrode. The advantage of this method is that the bacterial cells are still undamaged at the end of the test. A similar approach was used for the detection of *Bacillus cereus* and *Mycobacterium smegmatis*,

by a phage mediated release of intrinsic enzymes α-glucosidase and β-glucosidase, respectively. These enzymes catalyzed the hydrolysis of their corresponding substrate to yield *p*-aminophenol. A detection limit of 10 cfu/mL for *E. coli*, *B. cereus* and *M. smegmatis* and a response time of about 10 minutes were demonstrated. The whole process including a pre-incubation step took about 8 hours for detection of the lowest concentrations.

2.4.1.2 Potentiometric

The potentiometric transducers are different from that of the amperometric transducers in the type of electrical signal produced. Potentiometric transducers measure the voltage difference caused by the ions or gases liberated by the probe-analyte interaction. These potential measurements are made using an Ion Selective Electrode (ISE). It is important for the ISE to be highly specific to the ion of interest to avoid false positives and inaccurate results.

With recent advances in semiconductor technology, field effect devices [14, 39] have become widely used in sensor applications. One such application utilizes an electrolyte-insulator-semiconductor configuration (EIS) that is light activated. This device is known as the Light Addressable Potentiometric Sensor (LAPS). These devices [40-44] are different in principle from the conventional electrode-based potentiometric sensors. However, measurement of changes in the surface potential as an output still makes them suitable for discussion in the category of potentiometric sensors. Figure 2-5 depicts a schematic of a basic LAPS.

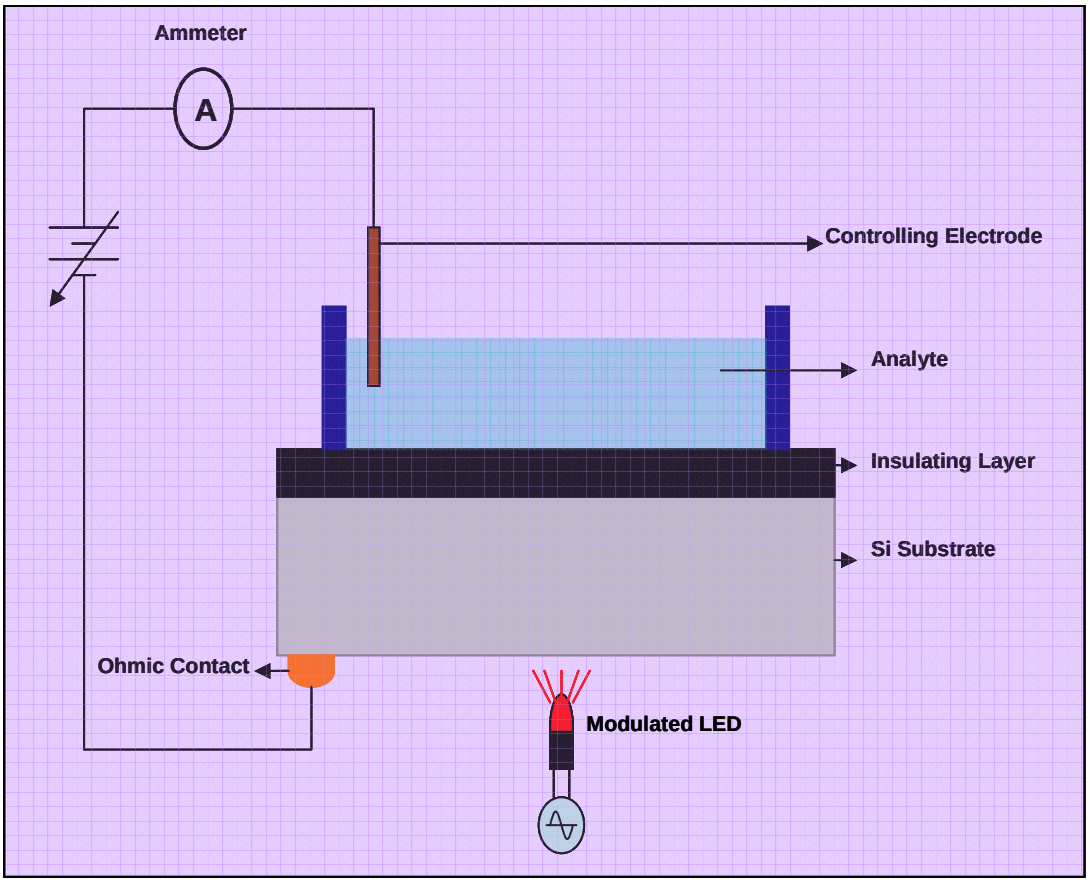

Figure 2-5: Schematic depicting a Light Addressable Potentiometric Sensor (LAPS).

The interaction of the bio-recognition element with the target analyte results in a change in the ion concentrations in the electrolyte. This change in the ion concentrations is responsible for changes in the surface potential of the EIS interface. The width of the depletion layer is dependant on the surface potential. The depletion layer appears at the insulator-semiconductor interface when a DC bias is applied. The width of the depletion layer changes with changes in the surface potential. Illuminating the bottom of the semiconductor substrate with a modulated light (LED) produces electron hole pairs and thus an ac photocurrent is generated depending on the width of the depletion layer. The magnitude of the photocurrent generated is thus used to determine the surface potential.

The primary advantage presented by this type sensor is ease of miniaturization. Light addressability also enables investigation of localized changes at different regions on a sensor surface. Due to this unique advantage LAPS can be used to map profiles of localized chemical changes at different regions on a sensor surface.

In a recent study [45] affinity-selected filamentous phage was used to detect human phosphatase of regenerating liver-3 (hPRL-3) and the mammary adenocarcinoma cell (MDAMB231) using a light addressable potentiometric sensor. The protein hPRL-3 is a cancer marker and MDAMB231 is a cancer cell. The interaction of the immobilized phage and the cancer cells/cancer marker caused a change in the surface potential. Changes in the surface potential were then related to the concentration of the target cells in the analyte. A detection limit of 1×10^3 cells/mL was reported by the authors. However the authors did not investigate or explain the mechanisms causing the surface potential changes. The disadvantages of these sensors are the dependence of the sensor response on pH and ionic strength of the analyte test solutions. Additionally, difficulties in miniaturization and proper selection of the reference electrodes limit the performance of LAPS devices.

2.4.2 Optical

Optical methods for the detection of micro-organisms can be divided into two categories depending on the type of interaction that produces an output signal. Methods that utilize flouresence, bio-luminescence resulting from the antigen-probe interactions assisted by labels are categorized as indirect methods. On the other hand, in direct optical methods the analyte-probe interactions result in a direct change in the properties

of the light. The total internal reflection of light incident at the interface of mediums with different refractive indices is the principle utilized in the direct optical methods. Tapered optical fibers, planar waveguides and surface plasmon resonance based sensors are examples of direct optical methods.

2.4.2.1 Indirect optical methods

In this section the work done towards detection of bacteria using label assisted phage-based optical methods is reported. The use of labels for detection using flourescence or bio-luminescence have been studied extensively and reviewed [46, 47]. Recombinant phage has been used extensively for the indirect optical methods. Goodridge et. al. [48, 49] used flourescently labeled phage in combination with antibody-immobilized immunomagnetic beads for the detection of *E. coli* O157:H7 in inoculated ground beef and milk. They quantified the amount of antigen using flow cytometry and epiflourescence microscopy. They reported a detection limit and detection time of 50 cfu/mL and 7 hours (including a pre-enrichment step of 6 hours), respectively. In this method phage was tagged with labels and the interaction of phage with the target analyte produced optical signals. The optical signals produced could then be related to the amount of analyte present in the sample.

Some other notable indirect optical techniques that have been reported utilize luciferase induced bioluminiscence [47, 50, 51]. Banaiee et. al. [50] used luciferase reporter bacteriophage for the detection of *Mycobacterium tuberculosis*. In this work they established the ability to detect and evaluate the anitbiotic susceptibility of *Mycobacterium tuberculosis* in clinical samples using luciferase reporter phage. Blasco

et. al. [51] reported detetion of *Escherichia coli* and *Salmonella newport* using a different approach. In this method the phage mediated lysis was used to release adenylate kinase (AK) and adenosine-triphosphate (ATP) from the interior of the cells. When adenosine-diphosphate (ADP) is used as a substrate, AK acts as a catalyst to produce more ATP. The ATP then reacts with firefly luciferase to produce luminescence. Blasco et. al. reported a detection limit of 10^3 cfu/mL for both *E. coli* and *S. newport* and assay times of 1 and 2 hours, respectively. There have been numerous reports of several variations of the indirect optical methods (described above) wherein a fluorophor is involved to produce an output optical signal.

Recent advances in nanotechnology have resulted in a new class of flourescence based assays [52-54]. Quantum dots are highly flourescent semiconductor nanocrystals capable of producing stronger flourescence signals. They are more resistant to photobleaching in comparison to conventional flourescent dyes [54-56]. Edgar et.al. [57] utilized this technology to detect *E.coli.* They used filamentous phage with surface peptides that could be biotinylated upon interaction with biotin present in the host cell. The biotinylated phage was then exposed to the streptavidin-conjugated quantum dots. The phage thus bound to the quantum dots was characterized for the amount of the target analyte using flow cytometry and fluorescence microscopy. Edgar et. al. established a minimum detection limit of 20 cells/mL in an assay time of 1 hour. The need for suitable equipment and microscopes to quantify the amount of analyte would limit the use of these methods for field application.

2.4.2.2 Direct methods

In direct optical methods, the biological recognition event is measured directly based on changes in the properties of the light used. Most of the direct optical methods depend on total internal reflection (TIR) of light. When light is incident at the interface of an optically rare and dense medium at an angle greater than a certain critical angle (Equations 2-1, 2-2) TIR occurs. Since all the energy is not reflected there is a decaying evanescent field that is produced at the interface. The penetration depth (Equation 2-3) of the evanescent field is approximately 100 nm. Hence this method is highly sensitive to the interactions or changes occuring in the vicinity of the interface. These are the principles utilized in optical fiber, planar waveguide and surface plasmon resonance based direct optical methods.

$$n_d \sin\theta_d = n_r \sin\theta_r \quad (2\text{-}1)$$

$$\theta_c = \sin^{-1}\left(\frac{n_r}{n_d}\right) \quad (2\text{-}2)$$

$$d_p = \frac{\lambda}{2\pi(n_d^2 \sin^2\theta_d - n_r^2)^{1/2}} \quad (2\text{-}3)$$

where n_d *and* n_r are the refractive indices of the denser and the rarer medium, θ_d and θ_r are the incident and the refracted angle, λ is the wavelength of the incident light beam and d_p is the depth of penetration of the evanescent wave. The depth of penetration of the evanescent wave is the distance at which the intensity of the wave is lesser by a factor of '***e***' to that at the interface.

There have been several reports on biosensors based on total internal reflection and/or evanescent waves. However most of these techniques utilize antibodies as the bio-

recognition element. Recently Balasubramanian et. al., Nanduri et. al and Wei et. al. [58-61] have used a surface plasmon resonance-based sensor with phage as the bio-recognition element towards detection of various micro-organisms. In their work they used SPREETA^{TM}, an integrated device produced by Texas instruments. This sensor is a miniature (approximately 7 g) surface plasmon resonance device. This device is configured with an AlGaAs light emitting diode (LED, 840 nm), a polarizer, temperature sensor, two photodiode arrays, and a reflecting mirror. Light from the LED illuminates the gold-coated thin glass with a wide range of angles after passing through a polarizer which allows only the transverse magnetic component. After reflection from the gold-coated glass slide, the light is directed towards the two independent Siphotodiode arrays with the help of a mirror. The entire assembly is encased in an optically clear material while the interference from the external light is blocked with an opaque coating. Figure 2-6 shows a schematic of the setup used for their experiments.

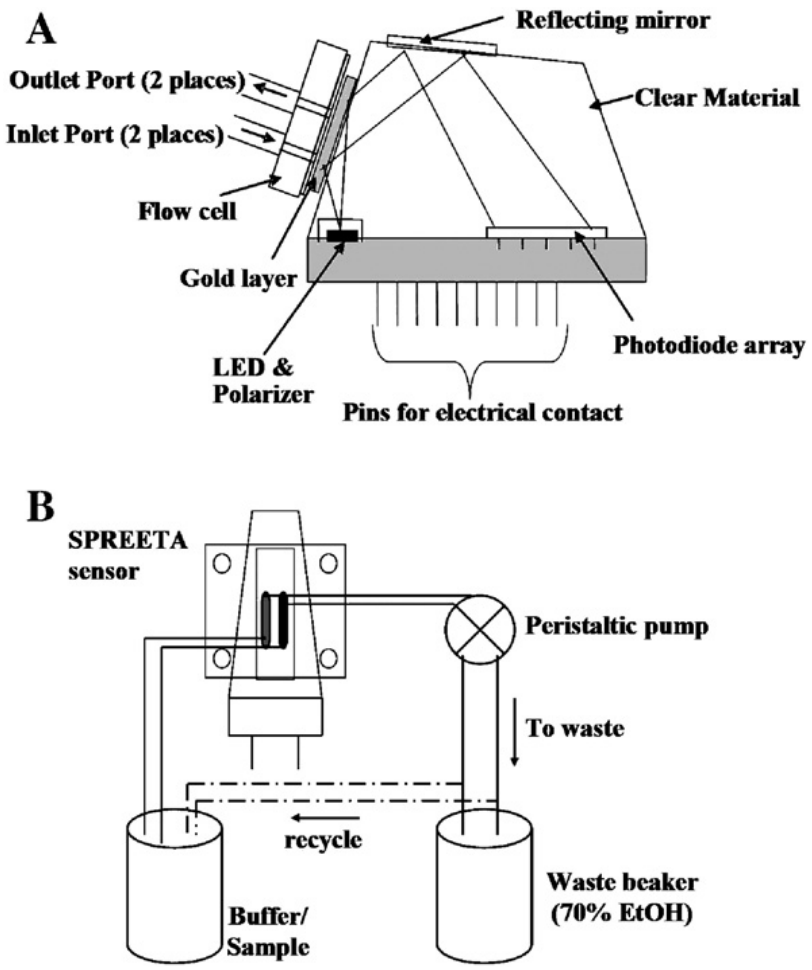

Figure 2-6: "Schematic of SPREETA$^{(TM)}$ system used" Adapted from [60].

Balasubramanian et. al. [60] used lytic phage, immobilized on the gold surface by physical adsorption to detect different concentrations of *Staphylococcus aureus.* They reported a detection limit of 10^4 cfu/mL in absence of any amplification or enrichment steps. Using the same transducer (SPREETA^{TM}) Nanduri et. al. and Wei et. al. have reported detection of β-galactosidase [58] and *L. monocytogenes* [59] using a phage-based interface. However in their work Nanduri et. al. used affinity-selected filamentous phage. A detection limit on the order of 10^4 cfu/mL of *L. monocytogenes* was reported.

The high cost of the apparatus and bulkiness of equipment limit the application of optical biosensors for on-site measurements.

2.4.3 Mass based

2.4.3.1 Piezoelectric Transducer Platforms

QCM sensors work on the principle of piezoelectricity. Piezoelectricity is the ability of certain materials to generate an electric potential in response to an applied mechanical stress. The piezoelectric effect was discovered by the Pierre Curie and Jacques Curie in 1880. The materials that exhibit piezoelectric effect also exhibit the converse piezoelectric effect. In the converse piezoelectric effect an applied electric potential causes a change in the dimensions of the material. Piezoelectric transducers utilize the principle of converse piezoelectricity to actuate the sensors. Surface Acoustic Wave (SAW) devices, Flexural Plate Wave (FPW) devices, Thickness Shear Mode (TSM) devices, Quartz crystal Microbalance (QCM) devices and Love Wave Devices are examples of such sensors. All these sensors are actuated by the application of an electric potential. The direction of deformation/oscillation is different for each of the above transducer platforms. Piezoelectric transducers have been used for numerous applications such as blood characterization, organic vapor sensing, monitoring of biofilm growth, liquid property measurements [62-68], detection of gas and vapor concentrations [69, 70], relative humidity [71-74], ion concentrations [75-77] and bacterial pathogen detection.

Olsen et. al. [79] have reported on a QCM biosensor immobilized with landscape phage probes for the detection of *Salmonella typhimurium* in aqueous samples. The

immobilization of phage was carried out using physical adsorption, exposure of the sensor surface to the phage. This method of immobilizing phage on sensor surfaces is very simple compared to the often complex immobilization procedures used with traditional antibodies. Olsen et. al. reported a detection limit of 100 cells/mL. The authors reported detection times of 5-10 minutes. The physical wire contacts to piezoelectric sensors make them unsuitable for use in sealed containers.

2.4.3.2 Magnetoelastic

The principle of magnetostriction was discovered by James Joule in 1840. However, the use of magnetostrictive materials as transducers for sensor applications has gained significant attention over the last two decades. Magnetostriction is a property observed in ferromagnetic materials. A magnetostrictive material experiences a change in shape when exposed to a magnetic field. The opposite effect is known as the Villari effect or inverse magnetostriction. In this inverse effect, the application of a mechanical stress on a magnetostrictive material results in a change in the magnetization of the material. In a typical sensor application both these effects are utilized. Most of the reported magnetostrictive sensors are free-standing strips of the magnetoelastic material. However, recently there have been some explorations into the use of magnetoelastic cantilever sensors. Magnetoelastic sensors are actuated by the application of an AC magnetic field. The applied varying magnetic field causes the sensors to oscillate mechanically. There have been several reports describing the application of magnetoelastic materials as sensors for measuring density [80], viscosity [81], pH [82], temperature [83, 84], humidity [83, 84], fluid flow velocity and CO_2 [85]. Recently these

sensors have been used for the detection of food-borne pathogens [21, 86-92] and toxins [93-95]. The wireless nature of magnetostrictive sensors allows these sensors to be used *in-vivo* in closed containers. Magnetoelastic sensors are disposable because of their extremely low cost. In this research, we have characterized the performance of a magnetoelastic biosensor for the detection of *S. typhimurium*. The following table (Table 2-3) summarizes the literature reports on the use of phage as a bio-recognition element for different sensor applications.

Table 2-3: Summary of literature reports on the use of phage as a bio-recognition element in various assays

Transduction	*Assay type and Mechanism*	*Target*	*Ref.*
Amperometric	Phage induced cell lysis causing release of components (such as β-galactosidase, α-glucosidase and β-glucosidase.)	*E. coli* (K-12, MG 1655) *B. anthracis* *M. Smegmatis*	[33-36]
LAPS	Phage display technology to engineer display peptides specific to the target analyte.	hPRL-3 MDAMB231	[45]
Bio-luminescence	Luciferase reporter phage	*M. tuberculosis* *L. monocytogenes*	[47, 96]
Fluorescence	Fluorosecently labeled phage in combination with	*E. coli* O157:H7	[48, 49]

	immunomagnetic beads		
Quantum Dots	Biotinylated phage and streptavidin conjugated quantum dot.	*E. coli* BL-21	[57]
SPR	Affinity-selected phage-immobilized using physical adsorption	*S. aureus* β-galactosidase *L. monocytogenes*	[58, 59]
QCM	Phage display technology to engineer display peptides specific to the target analyte. Affinity-selected phage-immobilized using physical adsorption	*S. typhimurium*	[79]
Magnetoelastic material	Phage display technology to engineer display peptides specific to the target analyte. Affinity-selected phage-immobilized using physical adsorption	*B. anthracis* *S. typhimurium*	[21, 87, 88]

REFERENCES

1. Dusch, H. and Altwegg, M., *Evaluation of Five New Plating Media for Isolation of Salmonella Species.* Journal of Clinical Microbiology, 1995. **33**(4): 802-804.
2. Ruiz, J., Nunez, M.L., Diaz, J., Lorente, I., Perez, J., and Gomez, J., *Comparison of five plating media for isolation of Salmonella species from human stools.* Journal of Clinical Microbiology, 1996. **34**(3): 686-688.
3. Perry, J.D., Ford, M., Taylor, J., Jones, A.L., Freeman, R., and Gould, F.K., *ABC Medium, a New Chromogenic Agar for Selective Isolation of Salmonella spp.* Journal of Clinical Microbiology, 1999. **37**(3): 766-768.
4. Perry, J.D., Riley, G., Gould, F.K., Perez, J.M., Boissier, E., Ouedraogo, R.T., and Freydière, A.M., *Alafosfalin as a Selective Agent for Isolation of Salmonella from Clinical Samples.* Journal of Clinical Microbiology, 2002. **40**(11): 3913-3916.
5. Mullis, K.B., Faloona, F.A., and Ray, W., *Specific synthesis of DNA in vitro via a polymerase-catalyzed chain reaction.* Methods in Enzymology, 1987. **155**: 335-350.
6. Higgins, J.A., Nasarabadi, S., Karns, J.S., Shelton, D.R., Cooper, M., Gbakima, A., and Koopman, R.P., *A handheld real time thermal cycler for bacterial pathogen detection.* Biosensors and Bioelectronics, 2003. **18**(9): 1115-1123.
7. Lund, M., Nordentoft, S., Pedersen, K., and Madsen, M., *Detection of Campylobacter spp. in chicken fecal samples by real-time PCR.* Journal of Clinical Microbiology, 2004. **42**: 5125-5132.

8. Fu, Z., Rogelj, S., and Kieft, T.L., *Detection of Escherichia coli 0157:H7 by immuno-magnetic separation and real-time PCR.* International Journal of Food Microbiology, 2005. **99**: 47-57.

9. Castanha, E.R., Swiger, R.R., Senior, B., Fox, A., Waller, L.N., and Fox, K.F., *Strain discrimination among B. anthracis and related organisms by characterization of bclA polymorphisms using PCR coupled with agarose gel or microchannel fluidics electrophoresis.* Journal of Microbiological Methods, 2006. **64**(1): 27-45.

10. Jensen, G.B., Fisker, N., Sparso, T., and Andrup, L., *The possibility of discriminating within the Bacillus cereus group using gyrB sequencing and PCR-RFLP.* International Journal of Food Microbiology, 2005. **104**(1): 113-120.

11. Reiman, R.W., Atchley, D.H., and Voorhees, K.J., *Indirect detection of Bacillus anthracis using real-time PCR to detect amplified gamma phage DNA.* Journal of Microbiological Methods, 2007. **68**(3): 651-653.

12. Abdel-Hamid, I., Atanasov, P., Ghindilis, A.L., and Wilkins, E., *Development of a flow-through immunoassay system.* Sensors and Actuators B, 1998. **49**: 202-210.

13. Abdel-Hamid, I., Ivnitski, D., Atanasov, P., and Wilkins, E., *Highly sensitive flow-injection immunoassay system for rapid detection of bacteria.* Analytica Chimica Acta, 1999. **399**: 99-108.

14. Cass, A.E.G., *Biosensors: A Practical Approach*. 1990: Oxford University Press. 271.

15. Ivnitski, D., Abdel-Hamid, I., Atanasov, P., and Wilkins, E., *Biosensors for detection of pathogenic bacteria.* Biosensors & Bioelectronics, 1999. **14**: 599-624.

16. Jones, C., Patel, A., Griffin, S., Martin, J., Young, P., O'Donnell, K., Silverman, C., Porter, T., and Chaiken, I., *Current trends in molecular recognition and bioseparation.* Journal of Chromatography A, 1995. **707**(1): 3-9.

17. Mead, P.S., Slutsker, L., Dietz, V., McCaig, L.F., Bresee, J.S., Shapiro, C., Griffin, P.M., and Tauxe, R.V., *Food-Related Illness and Death in the United States.* Emerging Infectious Diseases, 1999. **5**(5): 607-625.

18. Capita, R., Alonso-Calleja, C., Mereghetti, L., Moreno, B., del Camino García-Fernández, M., *Evaluation of the international phage typing set and some experimental phages for typing of Listeria monocytogenes from poultry in Spain.* Journal of Applied Microbiology, 2002. **92** (1): 90-96.

19. Doi, K., Zhang, Y., Nishizaki, Y., Umeda, A., Ohmomo, S., and Ogata, S., *A Comparative study and phage typing of silage-making Lactobacillus bacteriophages.* Journal of Bioscience and Bioengineering, 2003. **95**(5): 518-525.

20. Brigati, J.R. and Petrenko, V.A., *Thermostability of landscape phage probes.* Analytical and Bioanalytical Chemistry, 2005. **382**(6): 1346-1350.

21. Wan, J., Johnson, M.L., Guntupalli, R., Petrenko, V.A., and Chin, B.A., *Detection of Bacillus anthracis spores in liquid using phage-based magnetoelastic micro-resonators.* Sensors and actuators B, 2007. **127**: 559-566.

22. Petrenko, V.A. and Smith, G.P., *Phages from landscape libraries as substitute antibodies.* Protein Engineering, 2000. **13**: 589-592.

23. Petrenko, V.A., Smith, G.P., Gong, X., and Quinn, T., *A library of organic landscapes on filamentous phage.* Protein Engineering, 1996. **9**(9): 797.

24. Petrenko, V.A. and Sorokulova, I.B., *Detection of biological threats. A challenge for directed molecular evolution.* Journal of Microbiological Methods, 2004. **58**(2): 147.

25. Petrenko, V.A. and Vodyanoy, V.J., *Phage display for detection of biological threat agents.* Journal of Microbiological Methods, 2003. **53**(2): 253.

26. Smith, G.P. and Petrenko, V.A., *Phage display.* Chemical Reviews, 1997. **97**(2): 391-410.

27. Smith, G.P., Petrenko, V.A., and Matthews, L.J., *Cross-linked filamentous phage as an affinity matrix.* Journal of Immunological Methods, 1998. **215**(1-2): 151-161.

28. Sorokulova, I.B., Olsen, E.V., Chen, I.H., Fiebor, B., Barbaree, J.M., Vodyanoy, V.J., Chin, B.A., and Petrenko, V.A., *Landscape phage probes for Salmonella typhimurium.* Journal of Microbiological Methods, 2005. **63**(1): 55.

29. Petrenko, V.A., *Landscape phage as a molecular recognition interface for detection devices.* Microelectronics Journal, 2008. **39**(2): 202-207.

30. Petrenko, V.A. and Sorokulova, I.B., *Detection of biological threats. A challenge for directed molecular evolution.* Journal of Microbiological Methods, 2004. **58,**(2): 147-168.

31. Petrenko, V.A. and Vodyanoy, V.J., *Phage display for detection of biological threat agents.* Journal of Microbiological Methods, 2003. **53**(2): 253-262.

32. Fauquet, C.M., Mayo, M.A., Maniloff, J., Desselberger, U., and Ball, L.A., *Virus Taxonomy, 8th Reports of the International Committee on Taxonomy of Viruses*. 2005: Elsevier Publication. 1162.

33. Mittelmann, A.S., Ron, E.Z., and Rishpon, J., *Amperometric Quantification of Total Coliforms and Specific Detection of Escherichia coli.* Analytical Chemistry, 2002. **74**(4): 903-907.

34. Neufeld, T., Schwartz-Mittelmann, A., Biran, D., Ron, E.Z., and Rishpon, J., *Combined Phage Typing and Amperometric Detection of Released Enzymatic Activity for the Specific Identification and Quantification of Bacteria.* Analytical Chemistry, 2003. **75**(3): 580-585.

35. Perez, F., Tryland, I., Mascini, M., and Fiksdal, L., *Rapid detection of Escherichia coli in water by a culture-based amperometric method.* 2001. **427**(2): 149.

36. Benhar, I., Eshkenazi, I., Neufeld, T., Opatowsky, J., Shaky, S., and Rishpon, J., *Recombinant single chain antibodies in bioelectrochemical sensors.* Talanta, 2001. **55**(5): 899.

37. Neufeld, T., Schwartz-Mittelmann, A., Buchner, V., and Rishpon, J., *Electrochemical Phagemid Assay for the Specific Detection of Bacteria Using Escherichia coli TG-1 and the M13KO7 Phagemid in a Model System.* Analytical Chemistry, 2005. **77**: 652-657.

38. Yemini, M., Levi, Y., Yagil, E., and Rishpon, J., *Specific electrochemical phage sensing for Bacillus cereus and Mycobacterium smegmatis.* Bioelectrochemistry 2005, Selection of papers from the 18th International Symposium, Coimbra, Portugal, 19 - 24 June 2005, 2007. **70**(1): 180.

39. Turner, A.P.F. and Wilson, G.S., *Biosensors: Fundamentals and Applications*. 1990: Oxford University Press, Incorporated. 786.

40. Owicki, J.C., Bousse, L.J., Hafeman, D.G., Kirk, G.L., Olson, J.D., Wada, H.G., and Parce, J.W., *The light-addressable potentiometric sensor: principles and biological applications.* Annual Review of Biophysics and Biomolecular Structure, 1994. **23**: 87-113.

41. Hafeman, D.G., Parce, J.W., and McConnell, H.M., *Light-Addressable Potentiometric Sensor for Biochemical Systems.* 1988. **240**(4856): 1182.

42. Parak, W.J., Hofmann, U.G., Gaub, H.E., and Owicki, J.C., *Lateral resolution of light-addressable potentiometric sensors: an experimental and theoretical investigation.* 1997. **63**(1): 47.

43. Yoshinobu, T., Schoning, M.J., Otto, R., Furuichi, K., Mourzina, Y., Ermolenko, Y., and Iwasaki, H., *Portable light-addressable potentiometric sensor (LAPS) for multisensor applications.* Selected Papers from Eurosensors XVI, 2003. **95**(1-3): 352.

44. Yoshinobu, T., Iwasaki, H., Ui, Y., Furuichi, K., Ermolenko, Y., Mourzina, Y., Wagner, T., Nather, N., and Schoning, M.J., *The light-addressable potentiometric sensor for multi-ion sensing and imaging.* Biosensors, 2005. **37**(1): 94.

45. Jia, Y., Qin, M., Zhang, H., Niu, W., Li, X., Wang, L., Li, X., Bai, Y., Cao, Y., and Feng, X., *Label-free biosensor: A novel phage-modified Light Addressable Potentiometric Sensor system for cancer cell monitoring.* Biosensors and Bioelectronics, 2007. **22**(12): 3261.

46. Petty, N.K., Evans, T.J., Fineran, P.C., and Salmond, G.P.C., *Biotechnological exploitation of bacteriophage research.* 2007. **25**(1): 7.

47. Billard, P. and DuBow, M.S., *Bioluminescence-Based Assays for Detection and Characterization of Bacteria and Chemicals in Clinical Laboratories.* Clinical Biochemistry, 1998. **31**(1): 1.

48. Goodridge, L., Chen, J., and Griffiths, M., *The use of a fluorescent bacteriophage assay for detection of Escherichia coli O157:H7 in inoculated ground beef and raw milk.* International Journal of Food Microbiology, 1999. **47**(1-2): 43.

49. Goodridge, L., Chen, J., and Griffiths, M., *Development and Characterization of a Fluorescent-Bacteriophage Assay for Detection of Escherichia coli O157:H7.* Applied and Environmental Microbiology, 1999. **65**(4): 1397.

50. Banaiee, N., Bobadilla-del-Valle, M., Bardarov, S., Jr., Riska, P.F., Small, P.M., Ponce-de-Leon, A., Jacobs, W.R., Jr., Hatfull, G.F., and Sifuentes-Osornio, J., *Luciferase Reporter Mycobacteriophages for Detection, Identification, and Antibiotic Susceptibility Testing of Mycobacterium tuberculosis in Mexico.* Journal of Clinical Microbiology, 2001. **39**(11): 3883-3888.

51. Blasco, R., Murphy, M.J., Sanders, M.F., and Squirrell, D.J., *Specific assays for bacteria using phage mediated release of adenylate kinase.* Journal of Applied Microbiology, 1998. **84**(4): 661.

52. Dubertret, B., Skourides, P., Norris, D.J., Noireaux, V., Brivanlou, A.H., and Libchaber, A., *In Vivo Imaging of Quantum Dots Encapsulated in Phospholipid Micelles.* Science, 2002. **298**(5599): 1759-1762.

53. Sukhanova, A., Devy, J., Venteo, L., Kaplan, H., Artemyev, M., Oleinikov, V., Klinov, D., Pluot, M., Cohen, J.H.M., and Nabiev, I., *Biocompatible fluorescent*

nanocrystals for immunolabeling of membrane proteins and cells. 2004. **324**(1): 60-67.

54. Chan, W.C. and Nie, S.M., *Quantum dot bioconjugates for ultrasensitive nonisotopic detection.* Science, 1998. **281**: 2016-2018.

55. Bruchez Jr, M., Moronne, M., Gin, P., Weiss, S., and Alivisatos, A.P., *Semiconductor nanocrystals as flourescent biological labels.* Science, 1998. **281**: 2013-2015.

56. Michalet, X., Pinaud, F., Lacoste, T.D., Dahan, M., Bruchez, M.P., Alivisatos, A.P., and Weiss, S., *Properties of Fluorescent Semiconductor Nanocrystals and their Application to Biological Labeling.* Single Molecules, 2001. **2**(4): 261-276.

57. Edgar, R., McKinstry, M., Hwang, J., Oppenheim, A.B., Fekete, R.A., Giulian, G., Merril, C., Nagashima, K., and Adhya, S., *High-sensitivity bacterial detection using biotin-tagged phage and quantum-dot nanocomplexes.* Proceedings of the National Academy of Sciences, 2006. **103**(13): 4841-4845.

58. Nanduri, V., Balasubramanian, S., Sista, S., Vodyanoy, V.J., and Simonian, A.L., *Highly sensitive phage-based biosensor for the detection of [beta]-galactosidase.* 2007. **589**(2): 166.

59. Nanduri, V., Bhunia, A.K., Tu, S.-I., Paoli, G.C., and Brewster, J.D., *SPR biosensor for the detection of L. monocytogenes using phage-displayed antibody.* 2007. **23**(2): 248.

60. Balasubramanian, S., Sorokulova, I.B., Vodyanoy, V.J., and Simonian, A.L., *Lytic phage as a specific and selective probe for detection of Staphylococcus aureus—A*

surface plasmon resonance spectroscopic study. Biosensors and Bioelectronics, 2007. **22**(6): 948-955.

61. Wei, D., Oyarzabal, O.A., Huang, T.-S., Balasubramanian, S., Sista, S., and Simonian, A.L., *Development of a surface plasmon resonance biosensor for the identification of Campylobacter jejuni.* Journal of Microbiological Methods, 2007. **69**(1): 78-85.

62. Bandey, H.L., Cernosek, R.W., Lee, I., William E., and Ondrovic, L.E., *Blood rheological characterization using the thickness-shear mode resonator.* Biosensors and Bioelectronics, 2004. **19**(12): 1657-1665.

63. Helle, H., Vuoriranta, P., Valimaki, H., Lekkala, J., and Aaltonen, V., *Monitoring of biofilm growth with thickness-shear mode quartz resonators in different flow and nutrition conditions.* Sensors and Actuators B: Chemical, 2000. **71**(1-2): 47-54.

64. Holloway, A.F., Nabok, A., Thompson, M., Ray, A.K., and Wilkop, T., *Impedance analysis of the thickness shear mode resonator for organic vapour sensing.* Sensors and Actuators B: Chemical, 2004. **99**(2-3): 355-360.

65. Martin, S.J., Frye, G.C., and Wessendorf, K.O., *Sensing liquid properties with thickness-shear mode resonators.* Sensors and Actuators A: Physical, 1994. **44**(3): 209-218.

66. Zhang, C., Schranz, S., and Hauptmann, P., *Surface microstructures of TSM resonators and liquid properties measurement.* Sensors and Actuators B: Chemical, 2000. **65**(1-3): 296-298.

67. Adanyi, N., Varadi, Maria., Kim, Namsoo., Szendro, Istvan., *Development of new immunosensors for determination of contaminants in food.* Current Applied Physics Engineering Aspects of Nanomaterials and Technologies, 2006. **6**(2): 279-286.

68. Su, X.-L. and Li, Y., *A self-assembled monolayer-based piezoelectric immunosensor for rapid detection of Escherichia coli O157:H7.* Biosensors and Bioelectronics, 2004. **19**(6): 563-574.

69. Caliendo, V.I.A., Fedososv, C., Koelyanskii, V. I., Verardi, I. M. and Verona, E. *Characterization of Pd and Pd:Ni films for SAW hydrogen sensors*. in *190th Meeting Acoustic Wave Based Sensor Symp*. 1996. SanAntonio, TX.

70. Caliendo, C.D.A., A.; Varadi, P.; Verona, E. *Surface acoustic wave H2 sensor on silicon substrate*. in *Ultrasonics Symposium, Proceedings. IEEE 1988*. 1988. Chicago, IL: New York: IEEE.

71. Ippolito, S.J., Ponzoni, A., Kalantar-Zadeh, K., Wlodarski, W., Comini, E., Faglia, G., and Sberveglieri, G., *Layered WO3/ZnO/36[deg] LiTaO3 SAW gas sensor sensitive towards ethanol vapour and humidity.* Sensors and Actuators B: Chemical, 2006. **In Press, Corrected Proof**.

72. Penza, M., Anisimkin, V. I., *Surface acoustic wave humidity sensor using polyvinyl-alcohol film.* Sensors and Actuators A: Physical, 1999. **76**(1-3): 162-166.

73. Shen, C.-Y., Huang, Chun-Pu., Huang, Wang-Tsung., *Gas-detecting properties of surface acoustic wave ammonia sensors.* Sensors and Actuators B: Chemical, 2004. **101**(1-2): 1-7.

74. Korsah, K., Ma, C.L., and Dress, B., *Harmonic frequency analysis of SAW resonator chemical sensors: application to the detection of carbon dioxide and humidity.* Sensors and Actuators B: Chemical, 1998. **50**(2): 110-116.

75. Chang, H.-W. and Shih, J.-S., *Surface acoustic wave immunosensors based on immobilized C60-proteins.* Sensors and Actuators B: Chemical, 2006. **In Press, Corrected Proof**.

76. Kostial, P., *Surface acoustic wave control of the ion concentration in water.* Applied Acoustics, 1994. **41**(2): 187-193.

77. Cai, Q., Wang, R., Wu, L., Nie, L., and Yao, S., *Surface Acoustic Wave (SAW)-Impedance Sensor for Kinetic Assay of Trypsin.* Microchemical Journal, 1997. **55**(3): 367-374.

78. Sorokulova, I.B., Olsen, E.V., Chen, I.H., Fiebor, B., Barbaree, J.M., Vodyanoy, V.J., Chin, B.A., and Petrenko, V.A., *Landscape phage probes for Salmonella typhimurium.* Journal of Microbiological Methods, 2005. **63**(1): 55-72.

79. Olsen, E.V., Sorokulova, I.B., Petrenko, V.A., Chen, I.H., Barbaree, J.M., and Vodyanoy, V.J., *Affinity-selected filamentous bacteriophage as a probe for acoustic wave biodetectors of Salmonella typhimurium.* 2006. **21**(8): 1434.

80. Kouzoudis, D., Grimes, C. A., *The Frequency Response of Magnetoelastic Sensors to Stress and Atmospheric Pressure.* Smart Materials and Structures, 2000. **8**: 885-889.

81. Stoyanov, P.G. and Grimes, C.A., *A Remote Query Magnetostrictive Viscosity Sensor.* Sensors and Actuators A, 2000. **80**: 8-14.

82. Cai, Q.Y., Grimes, C. A., *A salt independent pH sensor.* Sensors and Actuators B, 2001. **79**: 144-149.

83. Grimes, C.A. and Kouzoudis, D., *Remote Query Measurement of Pressure, Fluid-Flow Velocity, and Humidity Using Magnetoelastic Thick-Film Sensors.* Sensors and Actuators B, 2000. **84**: 205-212.

84. Jain, M.K., Schmidt, S., Ong, K.G., Mungle, C., and Grimes, C.A., *Magnetoacoustic Remote Query Temperature and Humidity Sensors.* Smart Materials and Structures, 2000. **9**: 502-510.

85. Cai, Q.Y., Cammers-Goodwin, A., and Grimes, C.A., *A Wireless, Remote Query Magnetoelastic CO2 Sensor.* Journal of Environmental Monitoring, 2000. **2**: 556-560.

86. Guntupalli, R., Lakshmanan, R., Wan, J., Kim, D.J., Huang, T., Vodyanoy, V., and Chin, B., *Analytical performance and characterization of antibody immobilized magnetoelastic biosensors.* Sensing and Instrumentation for Food Quality and Safety, 2007. **DOI: 10.1007/s11694-007-9025-x**: Accepted/ Online First.

87. Lakshmanan, R.S., Guntupalli, R., Hu, J., Kim, D.-J., Petrenko, V.A., Barbaree, J.M., and Chin, B.A., *Phage immobilized magnetoelastic sensor for the detection of Salmonella typhimurium.* Journal of Microbiological Methods, 2007. **71**(1): 55-59.

88. Lakshmanan, R.S., Guntupalli, R., Hu, J., Petrenko, V.A., Barbaree, J.M., and Chin, B.A., *Detection of Salmonella typhimurium in fat free milk using a phage*

immobilized magnetoelastic sensor. Sensors and Actuators B: Chemical, 2007. **126**(2): 544-549.

89. Ong, K.G., Wang, J., Singh, R.S., Bachas, L.G., Grimes, C.A., *Monitoring of bacteria growth using a wireless, remote query resonant-circuit sensor: application to environmental sensing.* Biosensors and Bioelectronics, 2001. **16**: 305-312.

90. Ong, K.G., Bitler, J.S., Grimes, C.A., Puckett, L.G., and Bachas, L.G., *Remote query resonant-circuit sensors for monitoring of bacteria growth: application to food quality control.* Sensors, 2002. **2**: 219-232.

91. Ruan, C., Zeng, K., Varghese, O.K., and Grimes, C.A., *Magnetoelastic Immunosensors: Amplified Mass Immunosorbent Assay for Detection of Escherichia coli O157:H7.* Anal. Chem., 2003. **75**: 6494-6498.

92. Wan, J., Shu, H., Huang, S., Fiebor, B., Chen, I.-H., Petrenko, V.A., and Chin, B.A., *Phage-based Magnetoelastic wireless biosensors for detecting Bacillus anthracis spores.* IEEE Sensor Journal, 2007. **7**(3): 470-477.

93. Ong, K.G., Leland, J.M., Zeng, K., Barrett, G., Zourob, M., and Grimes, C.A., *A rapid highly-sensitive endotoxin detection system.* Biosensors and Bioelectronics, 2006. **21**: 2270–2274.

94. Shankar, K., Zeng, K., Ruan, C., and Grimes, C.A., *Quantification of ricin concentrations in aqueous media.* Sensors and Actuators B, 2005. **107**: 640-648.

95. Wu, S., Zhu, Y., Cai, Q., Zeng, K., Grimes, C.A., *A wireless magnetoelastic α-amylase sensor.* Sensors and Actuators B, 2006. **121**(2): 476-481.

96. Loessner, M.J., Rees, C.E., Stewart, G.S., and Scherer, S., *Construction of luciferase reporter bacteriophage A511:luxAB for rapid and sensitive detection of viable Listeria cells.* Applied Environmental Microbiology, 1996. **62**(4): 1133-1140.

3. MATERIALS AND METHODS

3.1. Sensor Fabrication

The magnetoelastic material chosen for this work was METGLAS™ 2826MB (Honeywell Inc., Conway, SC). METGLAS is an iron rich amorphous alloy fabricated using a water-cooled, tape-casting technique. The composition of this alloy is $Fe_{40}Ni_{38}Mo_4B_{18}$. The as-received material is in the form of a long roll of ribbon about 6 mm in width and 28 μm in thickness. This material has a large magnetostriction (12 ppm) and a high magnetoelastic coupling coefficient (90%). These properties result in an efficient conversion of magnetic to elastic energies making it ideal for sensor applications Table 3-1 presents the physical and magnetic properties of METGLAS™ 2826MB.

Table 3-1: Physical and magnetic properties of METGLAS™ 2826MB.

Tensile Strength (GPa)	1-2
Elastic Modulus (GPa)	100-110
Tensile Strength (GPa)	1-2
Density (gm/cc)	7.9
Thermal Expansion (ppm/°C)	11.7
Crystallization Temperature (°C)	410
Curie Temperature (°C)	353
Continuous Service Temp. (°C)	125
Saturation Induction (Tesla)	0.88
Maximum D.C. Permeability (μ): Annealed	800,00

Maximum D.C. Permeability (μ): As Cast	>50,000
Saturation Magnetostriction (ppm)	120

A 50 mm long strip was cut out of the roll of ribbon and polished using fine grit polishing paper (1000 micron and 2000 micron). The polishing was used to reduce the thickness to 15 μm and to provide a smooth surface on both sides. The reduced thickness of the sensor (smaller mass) increases the mass sensitivity of the device. The polished strips were then diced to the desired sizes for experimentation using a computer controlled automatic micro-dicing saw. Any debris or grease remaining from the dicing process was removed by cleaning the diced sensors ultrasonically in acetone for 20 minutes. The cleaned sensor platforms were then subjected to a thermal anneal in a vacuum oven at 200 ^{o}C for 2 hours and oven cooled under vacuum ($\approx 10^{-3}$ torr). Upon cooling, the sensors were transferred to a Denton™ (Moorestown, NJ) high-vacuum, RF sputtering system. Chromium and Gold (in that order) were sputtered onto both sides of the sensor platforms. Chromium was sputtered (DC) to a thickness of approximately 50 nm and gold was sputtered (RF) to a thickness of about 100 nm. The layer of chromium was sputtered to improve the adhesion of the gold film to the substrate. In addition, chromium was also expected to electro-chemically protect the iron rich substrate from corrosion when exposed to saline environments for extended periods of time. The thin film of chromium was then covered with a thin layer of gold. The gold layer provides a suitable surface for phage immobilization. The fabricated sensor platforms were stored in a dessicator until their use. The sensor platforms were washed with hexane and air dried prior to immobilization of the bio-recognition element. The basic steps in the fabrication of the magnetoelastic biosensor are shown in Figure 3-1.

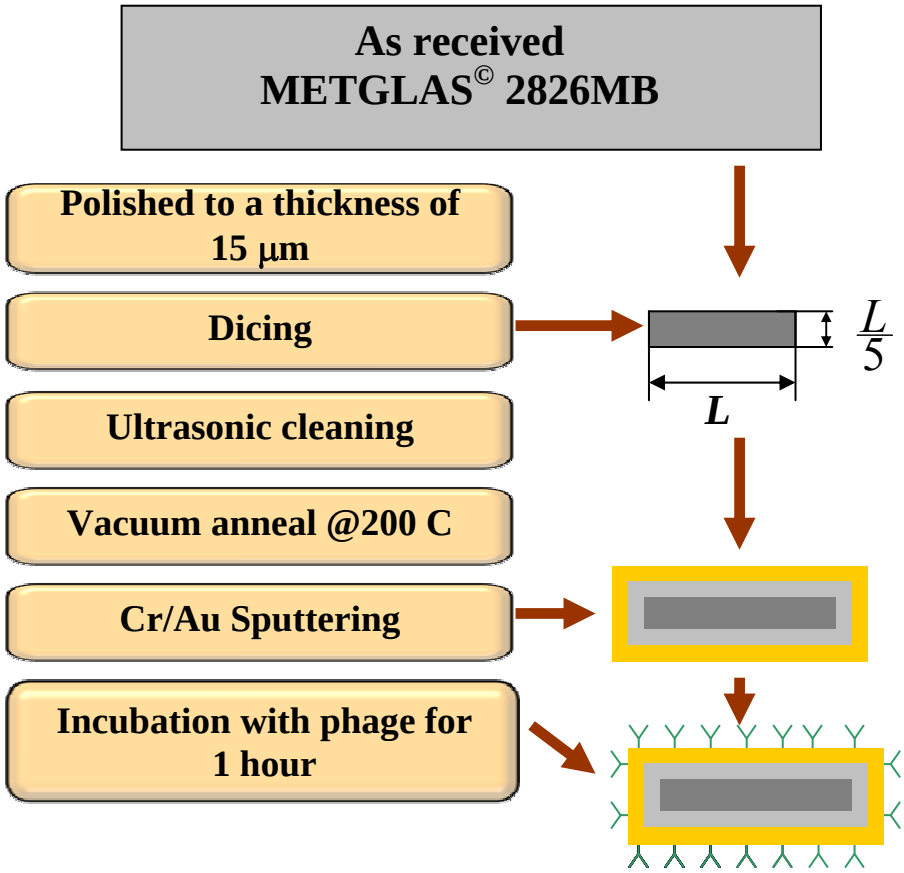

Figure 3-1: Steps in the fabrication of magnetoelastic biosensor.

3.2. Phage immobilization on the sensor surface

The filamentous phage E2, used in this work, was provided by Dr. James M. Barbaree's lab in the Department of Biological Sciences at Auburn University. The magnetoelastic sensor platforms were placed in vials containing 100 μL of phage E2 (5×10^{11} virions/mL). The immobilization of phage on the sensor surface was done by placing these vials on a rotor (running at 8 rpm) for 1 hour. The use of a rotor for the immobilization step resulted in a uniform distribution of phage on the sensor surface. These sensors were then washed three times with Tris-Buffered Saline (TBS) solution

and two times with sterile distilled water in order to remove any unbound or loosely bound phage. The resonance frequency of the sensors was measured at this point to obtain a baseline signal.

3.3. Resonance frequency measurement

A solenoid coil wound around a glass tube was used to measure responses of the sensor platform. The sensor platform was placed in the center of the solenoid coil. A time-varying current applied to the solenoid generates a time-varying magnetic field. This time-varying magnetic field causes the sensors to oscillate [1-4]. Along with the AC magnetic field, an external DC magnetic field was used to bias the magnetoelastic sensor. At the mechanical resonance frequency of the sensor, there is a maximum transfer of mechanical energy to magnetic energy. The resonance frequency of the sensor's oscillations was determined using a HP8751A network analyzer. The measurements using the network analyzer have been described in detail in section 4.2. The solenoid coil is connected to the network analyzer and is calibrated before the sensor is placed in the coil. This calibration step cancels any ambient electrical noise. 801 points were recorded over the frequency range of interest with a 11.31 sec sweep time. The data measured by the network analyzer was transferred to a personal computer with the help of the HP-VEE program.

3.4. Bacterial suspensions

The *S. typhimurium* (ATCC13311), *S. enteritidis*, *E. coli and L. monocytogenes* used in this work were provided by Dr. James M. Barbaree's lab in the Department of Biological Sciences at Auburn University, Auburn, AL. One colony of bacteria from a

master plate was inoculated into NZY (Casein Hydrolysate (10 g), Yeast extract (5 g), NaCl (5 g), $MgCl_2$ (2 g)) broth and incubated at 37 °C for 12 hours. Following incubation, the culture was gently mixed for homogeneity and transferred into sterile tubes. The sterile tubes containing the bacterial cells were then centrifuged. The supernatant solution obtained from the centrifugation was decanted. After the first round of centrifugation and decantation, the bacterial cells were resolubilized in distilled water. The *S. typhimurium* cultures obtained from Dr. Barbaree's lab were obtained in the form of a suspension at a concentration of 5×10^8 cfu/mL. The concentration of the cultures was confirmed using a spectrophotometer. The suspensions were serially diluted in water or desired food matrices to prepare bacterial suspensions ranging from 5×10^1 to 5×10^8 cfu/mL. Prior to each dilution, the solution was mixed using a vortex mixer to ensure homogeneity of concentration in the solution. All test solutions were prepared on the same day as the biosensor testing. The test solutions were stored at 4°C (during transfer and storage) and equilibrated to room temperature in a water bath prior to the experiments.

3.5. Scanning Electron Microscopy (SEM)

The surface of the biosensors was viewed at different stages of experimentation using scanning electron microscopy. SEM provided a visual verification of *Salmonella* cells bound to the sensor surface. Assayed sensors were washed one time with sterilized distilled water. The sensors were then placed on cylindrical aluminum stubs with the help of an adhesive double sided carbon conductive tape (Ted Pella Inc.). These sensors were then allowed to dry in air for 15 minutes. The aluminum stubs with the sensor

platforms were placed in a Petri dish containing a small volume (60 μL) of Osmium tetraoxide (OsO_4) for 10 minutes. Osmium tetraoxide is commonly used as a stain for biological samples for electron microscopy. The diffusion of Os (heavy metal) into the cell membrane provides a better contrast to the images in an electron microscope. For some of the initial set of experiments, a gold layer of 50nm was sputtered (PELCO sputter coater, SC-7) onto the sensor surface. A JEOL-7000F Field Emission Scanning Electron Microscope was used for imaging. The images were taken at an accelerating voltage of 10 or 15 kV, a working distance of 10 mm, an aperture of 3, and a probe current of 54 μA. SEM images of the sensor surface at desired magnifications were recorded in electronic format (jpeg files) using JEOL-Imaging software. The number of bacterial cells attached to the sensor was estimated by counting the number of bacterial cells bound to several different regions on the sensor surface. These results were then extrapolated to obtain the total number of cells bound to the sensor surface. The sample preparation technique limited the imaging to only one side of the sensor. The number of cells bound to either side of the sensor platform was assumed to be the same. Hence, the total number of cells attached to the sensor surface was calculated as two times that obtained for one side of the sensor.

3.6. Estimation of bound bacteria based on sensor responses

The sensor's response to a small added mass (Δm), much smaller than the initial mass (M) of the sensor, will result in a change in frequency (Δf) given as (rewritten from equation 1-2):

$$\Delta m = -\frac{2M\Delta f}{f} \qquad (3-1)$$

For a sensor with initial dimensions of 2×0.4×0.015 mm, the frequency (f) can be calculated using equation 1-1 by substituting parameters from Table 3-1. The initial mass was calculated using the density (ρ) and initial volume of the sensor (L×w×t). Upon substitution of these values, the equation 3-1 can be rewritten as

$$\Delta m = -5863\Delta f \qquad (3-2)$$

where Δf is in Hz and Δm is in picograms. For all calculations that were used to estimate the number of bacteria attached to the sensors, the mass of each bacterium was assumed to be 2 pg. Hence the number of bacteria attached ($n_{calculated}$) was determined using the following equation

$$n_{calculated} = \frac{\Delta m}{2} \qquad (3-3)$$

3.7. Estimation of bound bacteria based on SEM analysis

SEM micrographs were taken at 10 different regions on the sensor surface. The number of bacterial cells attached on the sensor surface was counted manually for each of the pictures taken. The average number of bound cells per unit area was calculated. The resulting number was multiplied by the entire surface area of the sensor to obtain the total number of bound cells. Each picture was divided into nine equal sections as shown in Figure 3-2. The number of bacteria in each of these sections (A_n, B_n, and C_n (n=1, 2, 3)) was counted. The total number was calculated as shown in equation 3-4.

$$n_{ST} = \sum_{n=1}^{3}(A_n + B_n + C_n) \qquad (3-4)$$

The viewing area (A_P) for each of the SEM image was used calculate the surface area coverage density for the bacterial cells. The average area coverage density obtained from the 10 pictures was then extrapolated to obtain the total number of cells bound to the sensor surface.

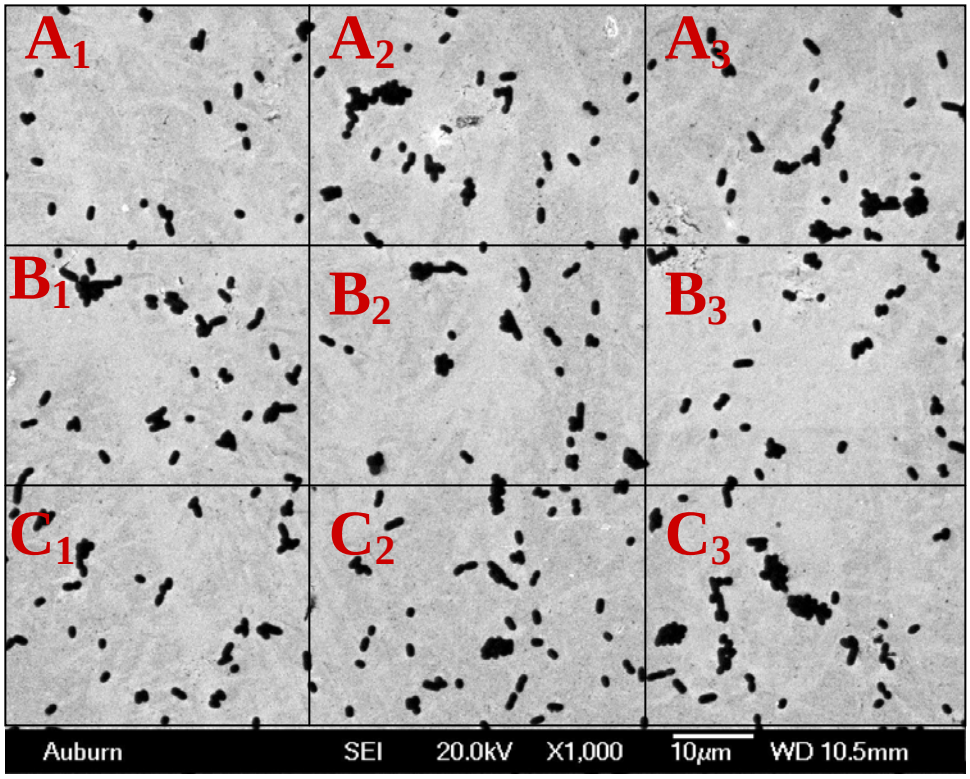

Figure 3-2: SEM image of a magnetoelastic sensor surface after immunoreaction with 5 $\times 10^6$ cfu/mL concentration of *S. typhimurium*. An overlay grid is shown to illustrate the bacterial counting technique on the sensor surface.

3.8. Testing procedures

3.8.1 Static tests

In static tests, the sensor resonance frequency was measured before and after exposure to solutions containing the pathogens of interest. The prepared biosensor was

allowed to dry after final immobilization with phage had been completed. At this point, the resonance frequency of the biosensor was measured. The sensor was then incubated in a vial containing a desired concentration of pathogens (suspended in water). After 45 minutes of incubation, the sensor was again dried. The resonance frequency of the sensor was then compared with that measured prior to incubation. The difference in the resonance frequency of the biosensor before (f_{before}) and after (f_{after}) incubation was calulated ($\Delta f_{measured}=f_{before} - f_{after}$). The assayed biosensors were then analyzed using SEM and compared with the obtained frequency shifts. Static tests were used in the study of specificity and longevity of the biosensors.

3.8.2 Specificity

The specificity of the biosensor was studied by exposing the biosensor to pathogens other than *S. typhimurium*. The affinity of the biosensor to other pathogens was compared with the biosensor's affinity to *S. typhimurium*. Three gram-negative pathogens (*S. typhimurium*, *S. Enteritidis* and *E. coli*) and one gram-positive pathogen (*L. monocytogenes*) were used in this test. The biosensors were exposed to each of the pathogens individually. After exposure the $\Delta f_{measured}$ was obtained using the static test procedure (section 3.8.1). The number of pathogens attached to the biosensor was calculated using the methods described in section 3.7. The $\Delta f_{measured}$ for the assayed biosensors was then compared with Δf_{SEM}.

3.8.3 Longevity

The thermal stability of the biosensor was studied at three different temperatures (25 ºC, 45 ºC and 65 ºC). A large number of biosensors were prepared and distributed

into three groups. The three groups of sensors were incubated in humidified ovens at 25 ºC, 45 ºC and 65 ºC, respectively. At specified intervals of time (in days) 5 biosensors, from each of the three groups, were taken out of the ovens and equilibrated to room temperature. These 15 biosensors were then exposed to a high concentration (5×10^8 cfu/mL) of *S. typhimurium* for 45 minutes. The biosensors were then dried and prepared for SEM. SEM micrographs were taken of all the tested biosensors. The average area coverage densities for the three temperatures of incubation were calculated and plotted as a function of time.

3.8.4 Dose response

Dose response of the biosensor was studied by monitoring the resonance frequency of the biosensor, upon exposure to different concentrations of *S. typhimurium* in a single flow-through mode. The different concentrations (5×10^1 cfu/mL through 5×10^8 cfu/mL) were prepared by successive dilutions of the as-received *S. typhimurium* (5×10^8 cfu/mL). Each successive dilution reduced the concentration of *S. typhimurium* by a factor of 10. The biosensor was placed in the center of a solenoid coil wound around a glass tube (Figure 3-3).

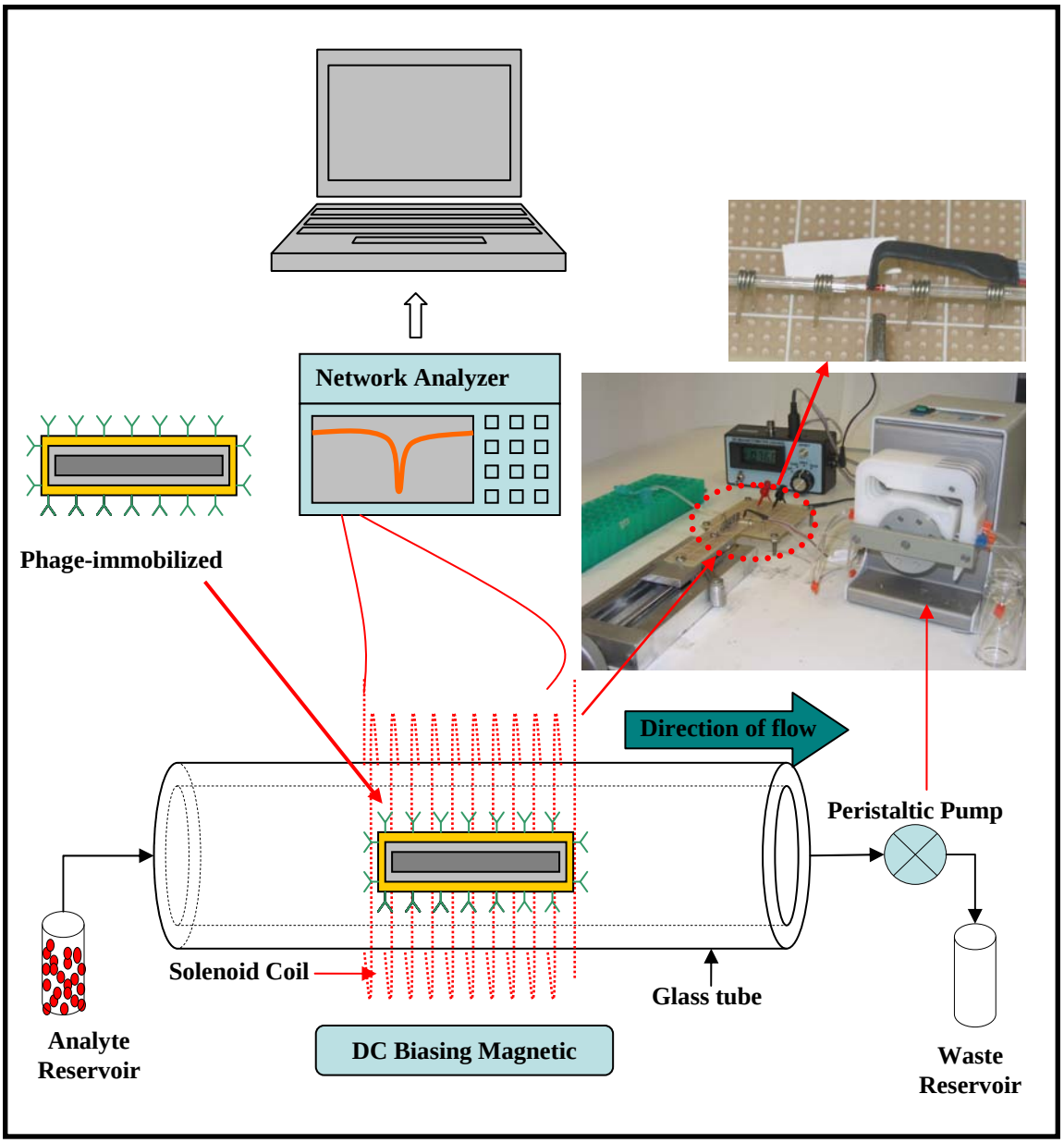

Figure 3-3: Schematic of experimental setup for dose response studies.

A peristaltic pump was used to flow the analyte through the glass tube. A low flow rate (50 µL/min) was maintained to ensure a laminar flow (Reynold's Number=2.37) over the sensor. The biosensor was exposed to flowing water for 20 minutes after obtaining a steady-state resonance frequency. The resonance frequency of the biosensor

at t=20 minutes was used as the baseline resonance frequency. At time t=20 minutes, the biosensor was exposed to a single pass, flowing suspension containing *S. typhimurium* (5×10^1 cfu/mL). One ml of suspension was passed across the biosensor at a flow rate of 50 μL/min every 20 minutes. The change in the resonance frequency due this concentration was calculated as the difference between the baseline resonance frequency and the resonance frequency of the biosensor at t=40 minutes. The resonance frequency of the biosensor was monitored using the network analyzer. The biosensor was then successively exposed to the different concentrations of *S. typhimurium* (5×10^2 cfu/mL through 5×10^8 cfu/mL) in an increasing order. The resonance frequency at t=60, 80, 100, 120, 160 and 180 minutes were used to calculate the resonance frequency changes due to the different concentrations.

The resonance frequency was measured at two minute interval throughout the entire experiment. A computer recorded the resonance frequencies and a plot of frequency as a function of exposure time (exposure concentration) was produced. The assayed biosensors were then analyzed using SEM (section 3.5).

3.8.5 Selectivity and detection in food matrices

Milk and apple juice samples were spiked with known concentrations of *Salmonella typhimurium* (5×10^1 cfu/mL through 5×10^8 cfu/mL). The spiked samples were prepared using fat free milk (Parmalat® brand) and clear apple juice (Kroger® brand) purchased from a local grocery store. The frequency response of the biosensor platforms was then studied as described in section 3.8.4.

Selectivity tests were performed to determine whether *Salmonella typhimurium* could be detected in a mixed microbial population. The selectivity tests were conducted using two different masking mixtures: 1) a mixture of *S. typhimurium* with one masking bacteria (*E. coli*) and 2) a mixture of *S. typhimurium* with two masking bacteria (*E. coli* and *L. monocytogenes*). The dilutions of *S. typhimurium* (5×10^1 cfu/mL through 5×10^8 cfu/mL) were prepared in such a way that all the suspensions contained a high concentration (5×10^7 cfu/mL) of the masking bacteria. A high concentration of the masking bacteria was used to investigate the maximum masking effect that a non-specific bacteria may have on the performance of the biosensor. The biosensors were then exposed to the two different masking mixtures (containing 5×10^1 cfu/mL through 5×10^8 cfu/mL of *S. typhimurium*) using the procedures explained in the section 3.8.4.

3.9. Hill plot construction

A Hill plot, constructed from the dose response curves, was used to study the kinetics of the *Salmonella*-phage binding. This plot was also used to determine the apparent dissociation constant and binding valency. The *S. typhimurium* binding to the phage immobilized on the sensor's surface can be expressed as a reversible reaction:

$$nST + phage \Leftrightarrow ST_n.phage \qquad (3-5)$$

where $1/n$ represents binding valency of the *ST* (*S. typhimurium*) attaching to the phage immobilized on the sensor surface. The association (k_a) and the dissociation constant (k_d) for the above reversible reaction is:

$$k_a = \frac{[ST]^n[phage]}{[ST_n.phage]} = \frac{1}{k_d} \qquad (3-6)$$

The reaction of association is primarily due to the movement of bacteria in solution and its interaction with the immobilized phage. The dissociation is governed by the strength with which bacteria binds to the immobilized phage on the sensor surface. The calculations to determine the values of dissociation constant (k_d) and binding valency ($1/n$) were done by constructing a hill plot. The value of k_d can be determined as the reciprocal of the ordinate intercept. The binding valency is determined as the reciprocal of the slope of the hill plots. The binding valency is the number of phage binding sites that interact with *Salmonella typhimurium*.

$$k_d(\text{apparent}) = k_d^{1/n} \qquad (3\text{-}7)$$

The Hill plots were traditionally used to study kinetics of reactions, where the reactant and the product concentrations were expressed using molar concentrations. However, in this method the concentration of *S. typhimurium* has the units of cfu/mL. The use of k_d (apparent) takes into account the scaling factor due to the use of different units for the concentrations of the analyte. The k_d (apparent) is defined as the concentration at which half of the available binding sites are occupied. Hence, a stronger *Salmonella*-phage binding is indicated by lower values for k_d (apparent). The Hill plot was constructed by plotting log X versus the $\log[\boldsymbol{ST}]$, where X is given as

$$X = \frac{Y}{(1-Y)} \qquad (3\text{-}8)$$

$$\& \quad Y = \frac{\Delta m}{\Delta m_{\max}} = \frac{\Delta f}{\Delta f_{\max}} \qquad (3\text{-}9)$$

Here Δf denotes the frequency shift obtained as a response to the binding of each concentration of *S. typhimurium* to the biosensor. Δf_{max} denotes the maximum frequency that can be detected before the biosensor has reached saturation. Δf_{max} was calculated

from the sigmoidal curve fitting of the dose response curve obtained for the biosensor. The values of the apparent dissociation constant and binding valency were used to compare the biosensor's performance in different matrices.

REFERENCES

1. Vincent, J.H., *Further experiments on magnetostrictive oscillators at radio-frequencies.* Proceedings of the Physical Society, 1931. **43**(2): 157-165.
2. Muzzey, D.S., *Some Measurements of the Longitudinal Elastic Frequencies of Cylinders Using a Magnetostriction Oscillator.* Physical Review, 1930. **36**(5): 935-947.
3. Pierce, G.W., *Magnetostriction Oscillators.* Proceedings of the IRE, 1929. **17**(1): 42-88.
4. Vincent, J.H., *Experiments on magnetostrictive oscillators at radio frequencies.* Proceedings of the Physical Society, 1928. **41**(1): 476-486.
5. *"Agilent 4395A Network/Spectrum/Impedance Analyzer Operation Manual," Agilent Technologies.*
6. Landau, L.D. and Lifshitz, E.M., *Theory of Elasticity*. 3 ed. Vol. 7. 1986: Butterworth-Heinemann. 187.

4. Theory and Measurement Circuit

4.1. Theory

A theoretical derivation of the basic equations to determine the resonance frequency of magnetoelastic sensor platform is presented in this section. The sensor platforms used in this work are thin rectangular plates. A thin rectangular plate of length L, width w and a thickness t ($<< L, w$) is shown in Figure 4-1.

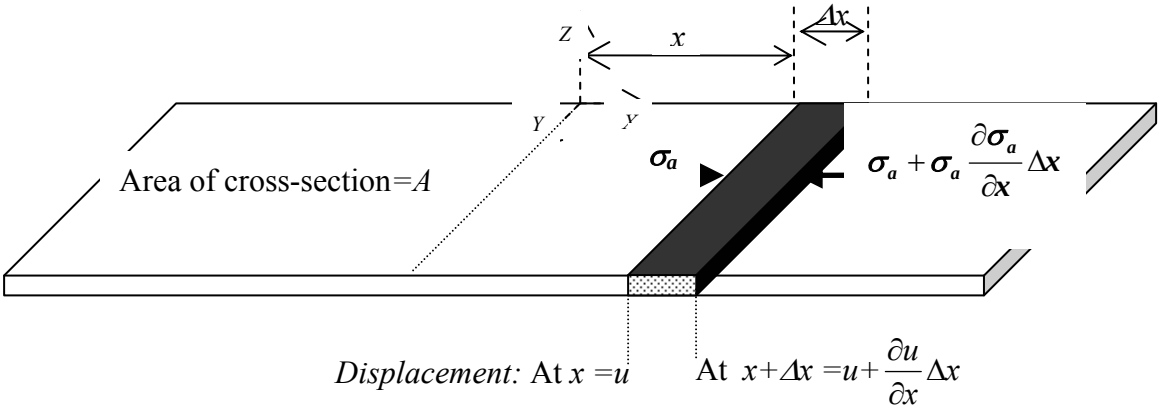

Figure 4-1: Thin rectangular plate discussed in the derivation with a length L, width w and thickness t ($<< L, w$).

For the thin plate shown, we consider an element of length, Δx,extending from X=x to X=x+Δx. The center of the thin plate is defined at X=0. Let σ_T be the total stress and u be the displacement of the element Δx at X=x. For mathematical simplicity, the effects of eddy currents and the viscoelastic damping have been neglected. The thickness of the

plate was assumed to be negligible in comparison to the width and the length of the plate (t<<L,w). A force balance equation for the element Δx is given by:

$$A\left(\sigma_T - \left\{\sigma_T + \frac{\partial \sigma_T}{\partial x}\Delta x\right\}\right) = M\frac{\partial^2 u}{\partial x^2}$$

$$\Rightarrow -A\Delta x\frac{\partial \sigma_T}{\partial x} = \rho A\Delta x\frac{\partial^2 u}{\partial x^2}$$

$$\Rightarrow -\frac{\partial \sigma_T}{\partial x} = \rho\frac{\partial^2 u}{\partial x^2} \text{.....(4-1)}$$

where A is the area of cross-section of the thin plate and ρ is the density of the material. The total stress (σ_T) is comprised of two components: the elastic stress (σ_E) and the magnetostrictive stress (σ_M).

$$\sigma_T = \sigma_E + \sigma_M \ldots\ldots(4-2)$$

Now by substituting for σ_T from equation 4-2, equation 4-1 can be rewritten as:

$$-\left(\frac{\partial \sigma_E}{\partial x} + \frac{\partial \sigma_M}{\partial x}\right) = \rho\frac{\partial^2 y}{\partial x^2}\ldots\ldots(4-3)$$

4.1.1.1 Elastic component of stress (σ_E)

From the Hooke's law equations for the stress and the strain we know that [6]:

$$\sigma_{xx} = \frac{E}{(1+\nu)(1-2\nu)}\left[(1-\nu)u_{xx} + \nu(u_{yy}+u_{zz})\right]\ldots(4-4a) \;\&\; u_{xx} = \frac{1}{E}\left[\sigma_{xx} - \nu(\sigma_{yy}+\sigma_{zz})\right]\ldots(4-4d)$$

$$\sigma_{yy} = \frac{E}{(1+\nu)(1-2\nu)}\left[(1-\nu)u_{yy} + \nu(u_{xx}+u_{zz})\right]\ldots(4-4b) \;\&\; u_{yy} = \frac{1}{E}\left[\sigma_{yy} - \nu(\sigma_{xx}+\sigma_{zz})\right]\ldots(4-4e)$$

$$\sigma_{zz} = \frac{E}{(1+\nu)(1-2\nu)}\left[(1-\nu)u_{zz} + \nu(u_{yy}+u_{xx})\right]\ldots(4-4c) \;\&\; u_{zz} = \frac{1}{E}\left[\sigma_{zz} - \nu(\sigma_{yy}+\sigma_{xx})\right]\ldots(4-4f)$$

In the above equations σ represents stress, u represents displacement and the subscripts represent the respective directions. For a thin plate, $\sigma_{iz} = 0 \Rightarrow \sigma_{xz} = \sigma_{yz} = \sigma_{zz} = 0$. Substituting for σ_{zz}=0 in equation (4-4c) we get

$$u_{zz} = \frac{-\nu}{(1-\nu)}\left(u_{xx} + u_{yy}\right).....(4-5)$$

Substituting the value of u_{zz} from equation 4-5 and rearranging equation (4-4a) we get

$$\sigma_{xx} = \frac{-E}{(1-\nu^2)}\left(u_{xx} + u_{yy}\right).....(4-6)$$

For longitudinal oscillations, the deflections or displacements were assumed to be negligible in the direction of the width ($\boldsymbol{u_{yy}}$=0)**.** Hence,

$$\sigma_{xx} = \frac{-E}{(1-\nu^2)}u_{xx}.....(4-7)$$

$$\sigma_{E} = \frac{-E}{(1-\nu^2)}\frac{\partial y}{\partial x}.....(4-8)$$

4.1.1.2 Magnetic component of stress (σ_M)

The magnetic component of stress arises due to the magnetoelastic nature of the material. The magnetic component of stress in the material is proportional to the magnetic field (B) in the coil.

$$\sigma_M = aB.....(4-9)$$

In equation 4-9, a is the coefficient of magnetostriction. The magnetic field in the solenoid coil has two components. One component (B_i) is due to the applied current in the coil. The other component (B_m) is caused due to inverse magnetostriction. According

to Villari effect, this magnetic field component will be directly proportional to the strain in the material. Thus,

$$B_m = a' \frac{\partial u}{\partial x} \ldots\ldots (4-10)$$

In equation 4-10, a' is the inverse magnetostriction coefficient. The applied magnetic field is a time-varying magnetic field. However, the gradient of the magnetic field was assumed to be constant in the longitudinal direction. Thus, $\frac{\partial \boldsymbol{B_i}}{\partial \boldsymbol{x}} = 0$. Substituting the above values in equation 4-9 we get,

$$\sigma_M = aa' B_M \Rightarrow \sigma_M = aa' \frac{\partial u}{\partial x} \ldots\ldots (4-11)$$

Substituting for $\boldsymbol{\sigma_M}$ and $\boldsymbol{\sigma_E}$ from equation 4-11 and equation 4-8 into equation 4-3 we get,

$$\frac{E}{(1-\nu^2)} \frac{\partial^2 y}{\partial x^2} - aa' \frac{\partial^2 y}{\partial x^2} = \rho \frac{\partial^2 y}{\partial t^2}$$

$$\left(\frac{E}{(1-\nu^2)} - aa' \right) \frac{\partial^2 y}{\partial x^2} = \rho \frac{\partial^2 y}{\partial t^2} \ldots\ldots (4-12)$$

Solving for equation (4-12) we get,

$$f = \frac{1}{2L} \sqrt{\frac{\left(E \big/ (1-\nu^2) - aa' \right)}{\rho}} \ldots\ldots\ldots (4\text{-}13)$$

Reports by Pierce [3] and Muzzy Jr. [2] have experimentally shown that the value of the constant $\boldsymbol{aa'}$ is significantly smaller than the elastic modulus of the material. Hence, the resonance frequency of magnetoelastic sensors can be considered to be the same as that of the mechanical resonance frequency of a similar plate in the absence of magnetic fields.

$$f = \frac{1}{2L} \sqrt{\frac{E}{\rho(1-\nu^2)}} \ldots\ldots\ldots (4-14)$$

Addition of a small mass ($\Delta m << M$) on the sensor surface causes a change in the resonance frequency (Δf). Δf is proportional to the initial frequency f, initial mass M and the mass added (Δm) and is given as,

$$\Delta f = -\frac{f\Delta m}{2M} \text{.....(4-15a)}$$

$$\Rightarrow \frac{\Delta f}{\Delta m} = -\frac{f}{2M} \text{.....(4-15b)}$$

$$\Rightarrow \frac{\Delta f}{\Delta m} = -\frac{1}{L^2 wt}\sqrt{\frac{E}{\rho(1-\nu^2)}} \text{.....(4-15c)}$$

The quantity $\Delta f/\Delta m$ is defined as the mass sensitivity of the sensor platform. The equation 4-14 and equation 4-15 were used for all theoretical calculations presented in this dissertation.

4.2. Measurement Setup

The measurement setup used for magnetoelastic sensors consisted of a solenoid coil wound around a glass tube and a network analyzer. The magnetoelastic sensor was placed in the center of the coil. The frequency spectrum of the sensors was measured using a HP network analyzer 8751A with S-parameter test in the reflected mode. A network analyzer provides a known stimulus to a device-under-test (DUT) and measures its response. The device is characterized by a ratio of the incident signal to the reflected signal. In the reflected mode the network analyzer measures $\mathbf{S}_{11}$ (scattering parameter in reflected mode) [1] which is defined as:

$$S_{11} = \frac{Power_{\text{Reflected}}}{Power_{Incident}} \quad (4\text{-}16)$$

The magnitude of the S_{11} has a minimum value at the mechanical resonance. This is because there is a maximum conversion of the incident power into mechanical oscillations at the mechanical resonance frequency. The frequency at which a minimum occurred in the S_{11} frequency spectrum was taken as the resonance frequency of the sensor. Measurements were taken using an empty solenoid coil to obtain a measurement of the ambient background electrical noise. This background noise was then calibrated out once a sensor is placed in the coil. A coaxial cable (with a capacitance of approximately 30 pF/ft) was used to connect the solenoid coil to the network analyzer. It is important to note that the coaxial cable will affect the frequency measurements. The background effects of the coaxial cable were calibrated out using a standard S_{11} single port calibration (open, closed and a 50 Ω load calibration). 801 points were recorded over the frequency range of interest with an 11.31 seconds sweep time.

4.3. Equivalent circuit for the measurement setup

This section describes the construction of an equivalent circuit that would theoretically predict the interaction and responses of the measurement system and magnetoelastic sensor. The measurement of magnetoelastic sensors was done by obtaining S_{11} signals from a solenoid coil. In the following section, the inductance (L_l), DC resistance (R_l) and self capacitance (C_s) of the solenoid coil were evaluated.

4.3.1 Determination of Inductance, Capacitance and Resistance of the solenoid coil

A typical solenoid coil would have an equivalent circuit arrangement as shown in Figure 4-2. The circuit consists of three components: 1) a resistance (R_l), 2) an

inductance (L_l) and 3) a self capacitance (C_s). The DC resistance (R_l) of the copper wire was determined using a digital multi-meter (Agilent 34401A). The solenoid coils were home built and there was little control on the spacing of the wires and the number of turns. When using theoretical equations to calculate L_l and C_s, variations in the wire spacing and the number of turns are a major source of error. Hence, in this work, the measured electrical resonance frequency responses were used to calculate values for the inductance and self capacitance of the coil.

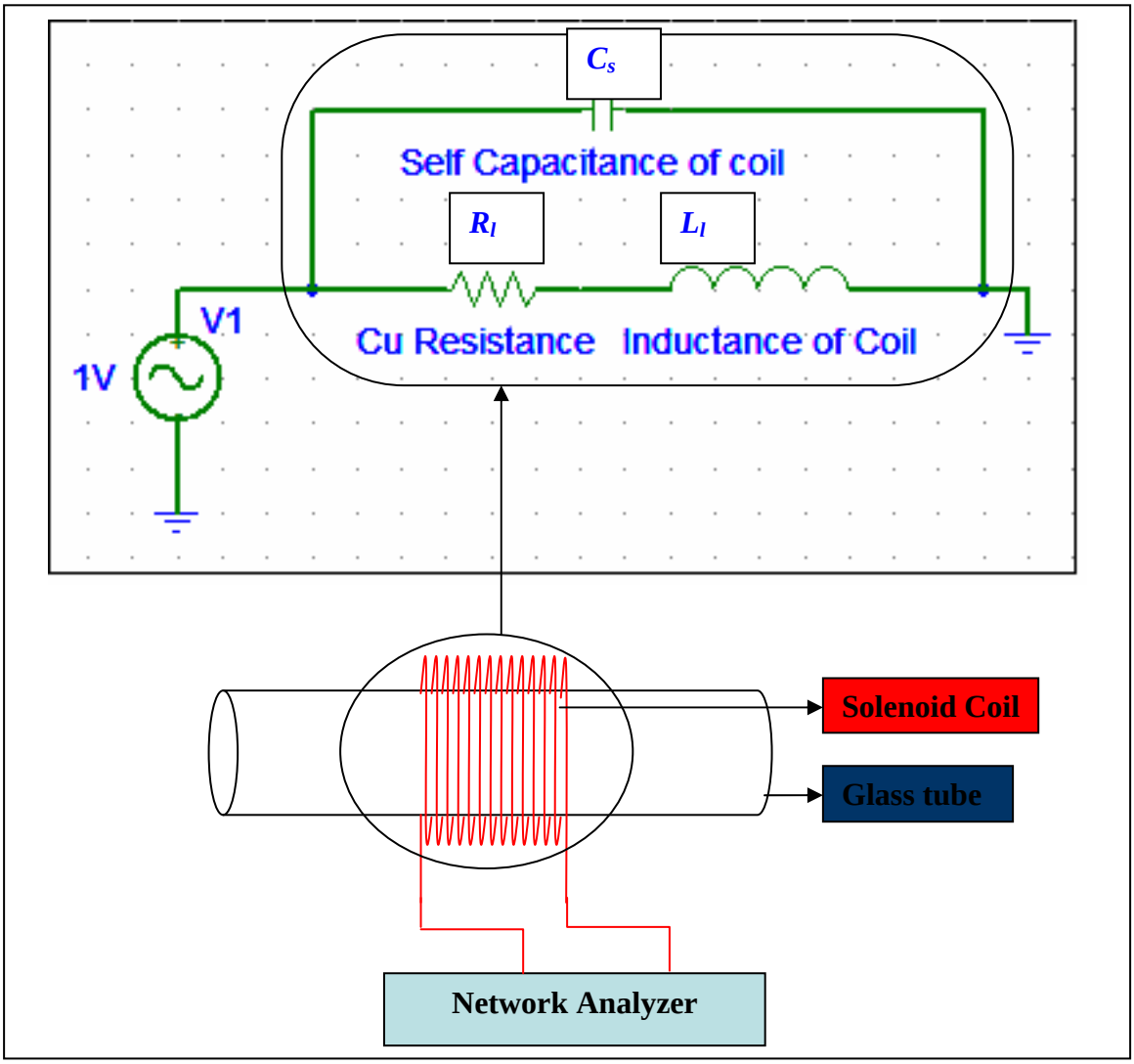

Figure 4-2: Equivalent circuit for the solenoid coil.

The electrical resonance frequency for the above circuit (Figure 4-2) is given as:

$$\omega_0^2 = \frac{1}{LC} - \frac{R_c^{\,2}}{L^2} \qquad (4-17)$$

Here $\boldsymbol{\omega_0}$ (= $2\pi f_0$) is the self resonance frequency of the coil.

The unknown values in equation 4-17 are the inductance ($\boldsymbol{L_l}$) and the self capacitance ($\boldsymbol{C_s}$) of the coil. Figure 4-3 shows a typical frequency response of a home built solenoid coil wound around a glass tube. The $\boldsymbol{S}_{11}$ responses were converted into impedance spectrums using the following equations.

Since S_{11} is a complex number

$$S_{11} = A + iB \qquad (4\text{-}18)$$

Where A is the Real part and B is the Imaginary part.

$$Z = 50 \times \frac{(1 + S_{11})}{(1 - S_{11})} \qquad (4\text{-}19)$$

$$\mathrm{Re}(Z) = 50 \times \frac{\left(1 - A^2 - B^2\right)}{\left((1 - A)^2 + B^2\right)} \qquad (4\text{-}20)$$

$$\mathrm{Im}(Z) = 50 \times \frac{2 \times B}{\left((1 - A)^2 + B^2\right)} \qquad (4\text{-}21)$$

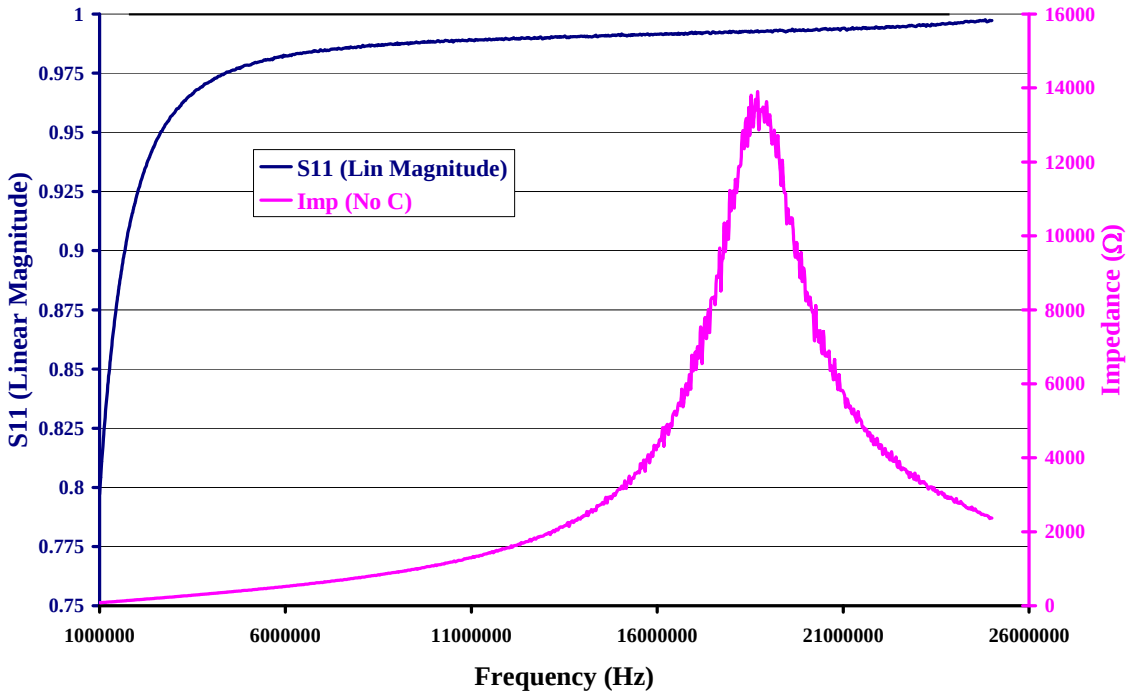

Figure 4-3: Typical frequency response of a solenoid coil wound around a glass tube (O.D.=200 μm), measured using an Agilent 4395A network analyzer with an S-parameter test set (87511A).

It can be seen that the solenoid coil has a resonance frequency of 18.7 MHz. This resonance is caused by the inductance and self capacitance of the coil. Figure 4-3 shows that the impedance spectrum has a peak at the resonance frequency. Such a peak is characteristic of a circuit with an inductor and capacitor in parallel. By adding known capacitances (***C1*** and ***C2***) in parallel to the solenoid the resonance frequency changes to a lower value.

$$\omega_1^2 = \frac{1}{L_l(C_s + C1)} - \frac{R_l^2}{L_l^2} \qquad (4\text{-}22)$$

$$\omega_2^2 = \frac{1}{L_l(C_s + C2)} - \frac{R_l^2}{L_l^2} \qquad (4\text{-}23)$$

Where ω_1 (=$2\pi f_1$) and ω_2 (=$2\pi f_2$) are resonance frequencies corresponding to ***C1*** and ***C2***, respectively. The frequency spectrums obtained by adding the known capacitors in parallel to the coil are shown in Figure 4-4.

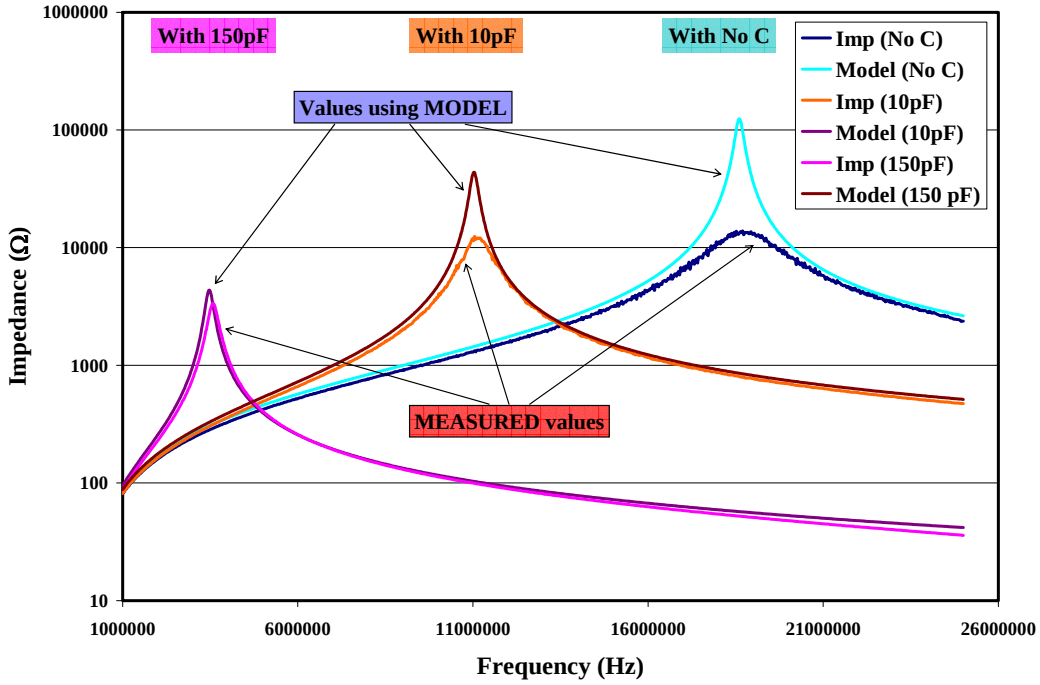

Figure 4-4: Impedance-Frequency spectrums used for calculating the inductance and self capacitance of solenoid coil. Curves also compare the responses obtained using the PSPICE model.

It can be clearly seen that an increase in the capacitance changes the frequency to a lower value. These values of resonance frequencies were then used to evaluate the inductance and self capacitance of the coil. Subtracting Equation 4-22 and Equation 4-23 from Equation 4-17, respectively, we get

$$\Rightarrow \omega_0^2 - \omega_1^2 = \frac{1}{LC} - \frac{1}{L(C+C1)} = \frac{1}{L}\left(\frac{C1}{C(C+C1)}\right) \qquad (4-24)$$

$$\Rightarrow \omega_0^2 - \omega_2^2 = \frac{1}{L_l C_s} - \frac{1}{L_l(C_s+C2)} = \frac{1}{L_l}\left(\frac{C2}{C_s(C_s+C2)}\right) \qquad (4-25)$$

Dividing Equation 4-24 by Equation 4-25 gives a linear relation for the evaluation of $\boldsymbol{C_s}$.

$$\Rightarrow \frac{\omega_0^2 - \omega_1^2}{\omega_0^2 - \omega_2^2} = \frac{C1(C_s+C2)}{C2(C_s+C1)}$$

$$\Rightarrow \frac{C2(\omega_0^2 - \omega_1^2)}{C1(\omega_0^2 - \omega_2^2)} = \frac{C_s+C2}{C_s+C1} = P$$

$$\Rightarrow C_s = \frac{C2-(C1\times P)}{1-P} \qquad (4-26)$$

By substituting for $\boldsymbol{C_s}$ in Equation 4-17 we can evaluate the value of $\boldsymbol{L_l}$. For the measurements shown in Figure 4-4, two different capacitances ***C1***=150 pF and ***C2***=10 pF were chosen.

The measured values for resonance frequency for each of the conditions were f_0=18.85 MHz, f_1=3.61 MHz and f_2=11.21 MHz. The DC resistance of the coil was measured as $\boldsymbol{R_l}$=19.8 Ω. By substituting the measured values for resonance frequency, resistance and ***C1*** and ***C2*** in the equations 4-26 and 4-17, it was determined that:

DC Resistance of Coil: $\boldsymbol{R_l}$=19.8 ± 0.2 Ω

Self Capacitance of Coil: $\boldsymbol{C_s}$=5.4 ± 0.23 pF

Inductance of Coil: $\boldsymbol{L_l}$=10.5 ± 0.35 μH

Using this method the self capacitance and the inductance of different coils can be determined with ease. The software program (PSPICE) was then used to compare the measured and the modeled frequency responses of the equivalent circuit.

The electrical resonance frequencies obtained from the model and the measurements matched fairly well. However, the magnitude of impedance values (at resonance) obtained from the measured responses was significantly lower than those obtained from the model. This difference can be attributed to the fact that the signals measured using network analyzers have high noise when measuring large impedances ($|Z|>>50\ \Omega$). To check the validity of the circuit representing the solenoid, a capacitor was added in series with the solenoid coil. Simulations were run for two different values of the added series capacitance. In Figure 4-5 there are two resonance peaks: one for a series resonance (seen as a minima); and one for a parallel resonance (seen as a maxima). The series resonance is due to the added capacitance ($\boldsymbol{C_a}$) in series with the inductance ($\boldsymbol{L_l}$) of the solenoid coil. The parallel resonance is due to the self capacitance of the solenoid coil ($\boldsymbol{C_s}$) in parallel with the inductance of the solenoid coil ($\boldsymbol{L_l}$). It is also important to observe that the measured and modeled values in terms of the magnitude of the peak and the resonance frequency followed similar trends. The observed trends due to the addition of capacitors in parallel or in series with the coil (Figure 4-5) support the validity of the model.

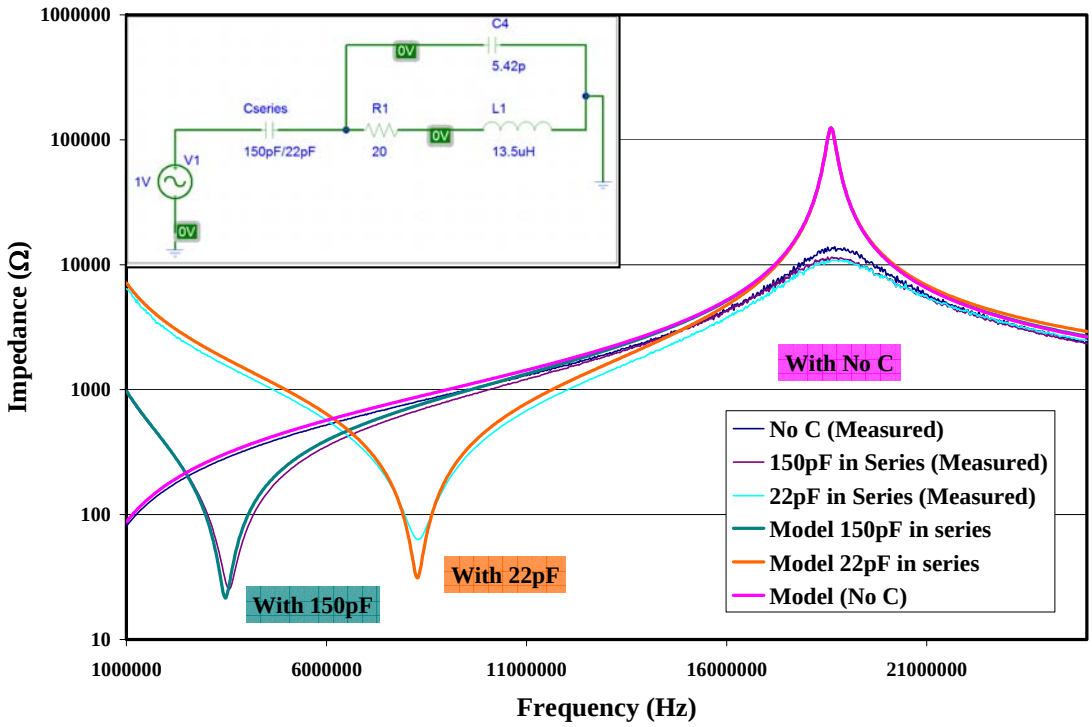

Figure 4-5: Comparison of impedance data from PSPICE model and measured values. Similar trends in changes (frequency and magnitudes) showing the accuracy of the model.

4.3.2 Equivalent circuit with sensor present in the coil

In this section, a similar model to describe the electrical circuit of the free-standing thin rectangular sensor platforms is presented. Free-standing magnetoelastic sensor platforms are allowed to freely oscillate in the presence of a biasing field. The biasing field moves the sensor response into the linear region of strain and magnetic field. S. Butterworth [6] used equations for changes in magnetic flux in the solenoid coil and arrived at an equation of the form:

$$I = V\left(\frac{1}{Z_c} + \frac{1}{Z_m}\right) \qquad (4\text{-}27)$$

Thus, the sensor in the solenoid coil consists of two impedances ($\boldsymbol{Z_c}$ and $\boldsymbol{Z_m}$) in parallel. In addition to these two impedances, Butterworth also defined another impedance $\mathbf{Z_l}$. The three different impedances described by Butterworth were called:

1. Leakage Impedance (Z_l): The impedance of the coil when the sensor platform is not present in the coil.
2. Core Impedance (Z_c): The contribution of the permeability of the magnetoelastic sensor platform to the impedance of the coil.
3. Motional Impedance (Z_m): The contribution of the oscillating magnetoelastic sensor platform in the circuit.

The equivalent circuit described by Butterworth with the inclusion of the self capacitance of the coil is shown in Figure 4-6. This self capacitance was not considered by Butterworth in his work. It is important to note that the effects of eddy currents on the sensor platform's responses were neglected. This assumption is reasonable because of the small cross-sectional area of the sensor that is parallel to the applied magnetic fields. The contributions due to the eddy currents could be incorporated into the circuit by modifying the expressions for $\boldsymbol{Z_c}$. Hence, the overall equivalent circuit representing the oscillations of the magnetoelastic sensor is shown in Figure 4-6. To establish the validity of the model, simulations were performed for the above circuit using PSPICE.

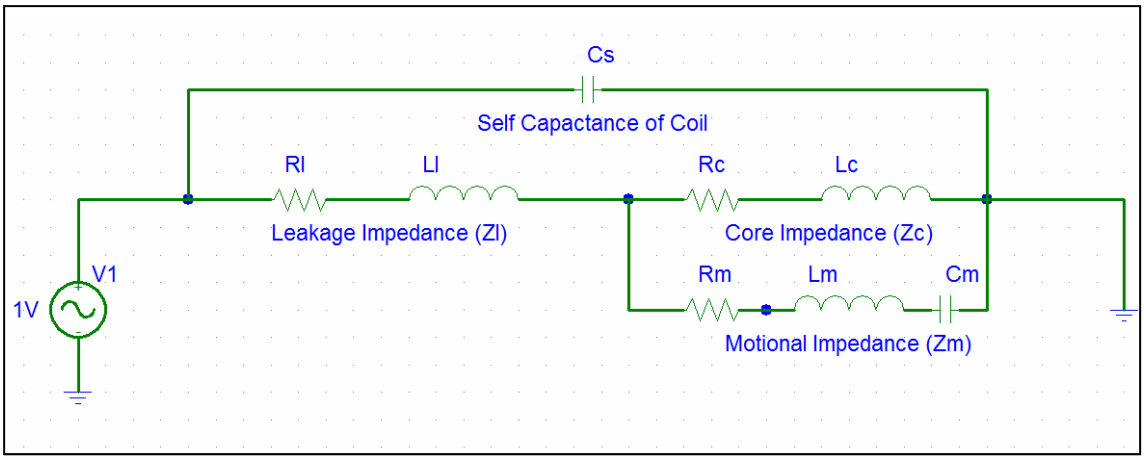

Figure 4-6: Equivalent circuit for the sensor oscillations. The AC voltage source with an amplitude of 1 V was arbitrarily chosen to obtain a frequency spectrum.

When the sensor is placed in the solenoid coil, in the absence of a biasing magnetic field, the inductance of the coil is increased. This increase is due to the presence of a ferromagnetic material in the coil. The increased inductance results in a decrease in the self resonant frequency of the solenoid coil. The placement of the sensor in the coil will not alter the self capacitance ($\boldsymbol{C_s}$) or the DC resistance ($\boldsymbol{R_l}$) of the coil. The core inductance ($\boldsymbol{L_c}$) can then be calculated using equation 4-17.

The values for the motional inductance ($\boldsymbol{L_m}$) and motional capacitance ($\boldsymbol{C_m}$) were calculated from the measured frequency spectrum for the sensor platform. A sensor platform with dimensions of 500×100×8 μm was used to calculate the values for $\boldsymbol{L_m}$ and $\boldsymbol{C_m}$. The measured frequency spectrum shown in Figure 4-7 has a maxima and minima for impedance. The two frequency values corresponding to the maxima and minima of the frequency spectrum were used to calculate the values for $\boldsymbol{L_m}$ and $\boldsymbol{C_m}$. The values for the leakage resistance ($\boldsymbol{R_l}$), leakage inductance ($\boldsymbol{L_l}$) and self capacitance ($\boldsymbol{C_s}$) used in the models were determined by methods described in section 4.3.1.

The calculations of the core resistance (R_c) and motional resistance (R_m) are very complex. For mathematical simplicity, values were chosen by trial and error to match the measured signal damping. It is important to mention that the values of Z_c and Z_m used in this model were constant. However, according to the equations described by Butterworth, these values are frequency dependent. In the vicinity of the resonance frequency, this assumption is reasonable because the frequency dependence of Z_c and Z_m is small.

Table 4-1 summarizes the results of the model for a coil with a self resonance frequency of 18.7 MHz. This table lists all the calculated values for components of the equivalent circuit. The calculated values (Table 4-1) for the components of the equivalent circuit were then input in the PSPICE program. The frequency response obtained from the PSPICE model was compared with the measured frequency response for a 500μm (Figure 4-7) long sensor. The frequency response obtained from the PSPICE model matched the experimental measurements. This result validates the equivalent circuit model (Figure 4-6) for the measurement of magnetoelastic sensor responses.

Table 4-1: Calculated values for components of the equivalent circuit.

Component	**Value**	**Calculation method**
R_l	*19.5 Ω*	DC multimeter.
L_l	*10.5 μH*	By adding parallel capacitor and calculating using method described in Section 4.1.1.
C_s	*5.4 pF*	By adding parallel capacitor and calculating using method described in Section 4.1.1.
R_c	*1 Ω*	Chosen by trial and error to match signal damping.

L_c	*0.5 μH*	Calculated by placing the sensor in the coil in the absence of DC magnetic bias and from resonance frequency measurements describes in Section 4.1.1.
R_m	*10 Ω*	Chosen by trial and error to match signal damping.
L_m	*100 μH*	Calculated using measured resonance and anti-resonance frequency of sensor.
C_m	*14.25 pF*	Calculated using measured resonance and anti-resonance frequency of sensor.

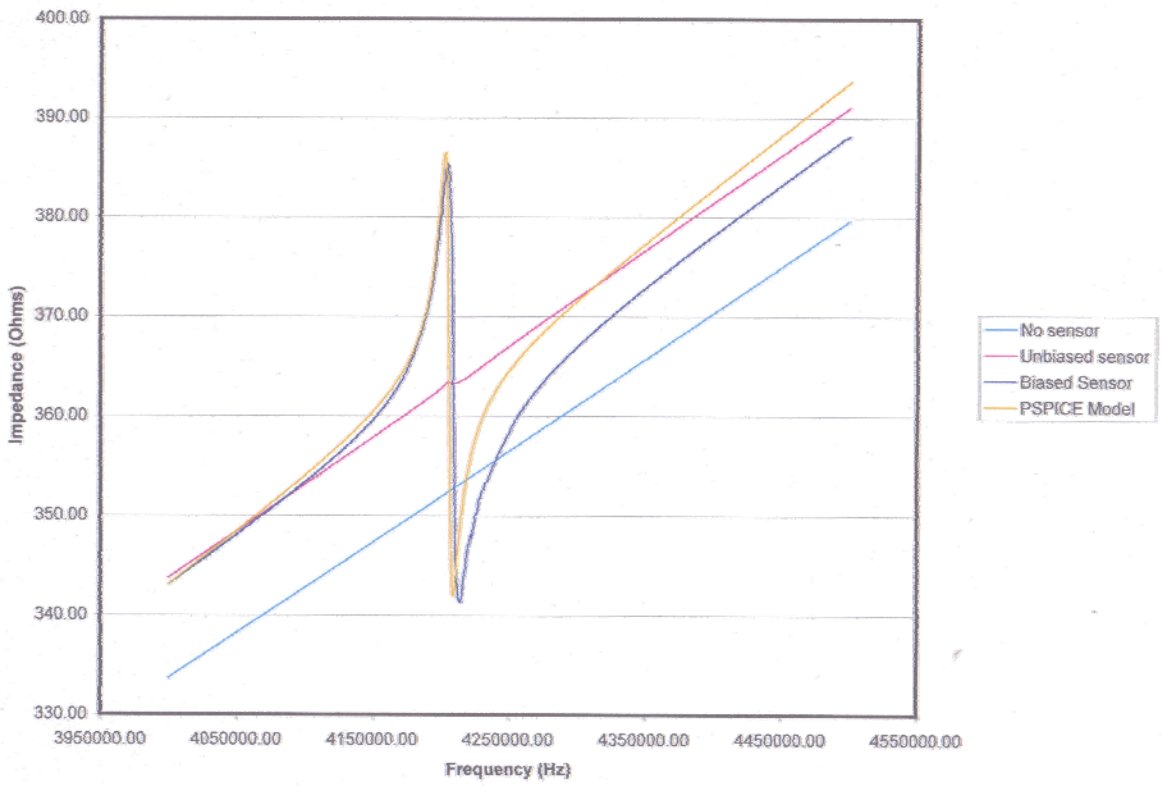

Figure 4-7: Comparison of actual signal and that obtained from PSPICE model.

4.3.3 Enhancement of sensor responses

In this section, a modification to the measurement setup is described that enhances the signal amplitude of the resonance frequency response (enhanced oscillation displacements) of magnetoelastic sensors. A solenoid coil measures changes in magnetic flux caused by changes in the magnetization of the oscillating magnetoelastic sensor platform. A sensor with smaller dimensions will produce smaller changes in the magnetic flux. This will affect the frequency response of the sensors. The smaller sized sensors had lower amplitudes of the resonance peaks.

During the development of the equivalent circuit (section 4.3.2), it was observed that the addition of a capacitor in series with the solenoid coil resulted in enhanced signal amplitudes. A variable capacitor was added in series to the solenoid coil. By tuning the variable capacitor, the series resonance frequency of the circuit changes. When this series resonance frequency of the circuit is equal to the sensor's mechanical resonance, an increase in the amplitude of the resonance peak was observed. The addition of the tuned capacitor in the circuit resulted in an increase in the signal amplitudes. The signal amplitudes increased by 6 times for a 200 μm length sensor and by 20 times for a 500 μm length sensor. Figure 4-8 shows a comparison of the $\boldsymbol{S}_{11}$ frequency responses of a tuned and an untuned circuit for a 200 μm length sensor.

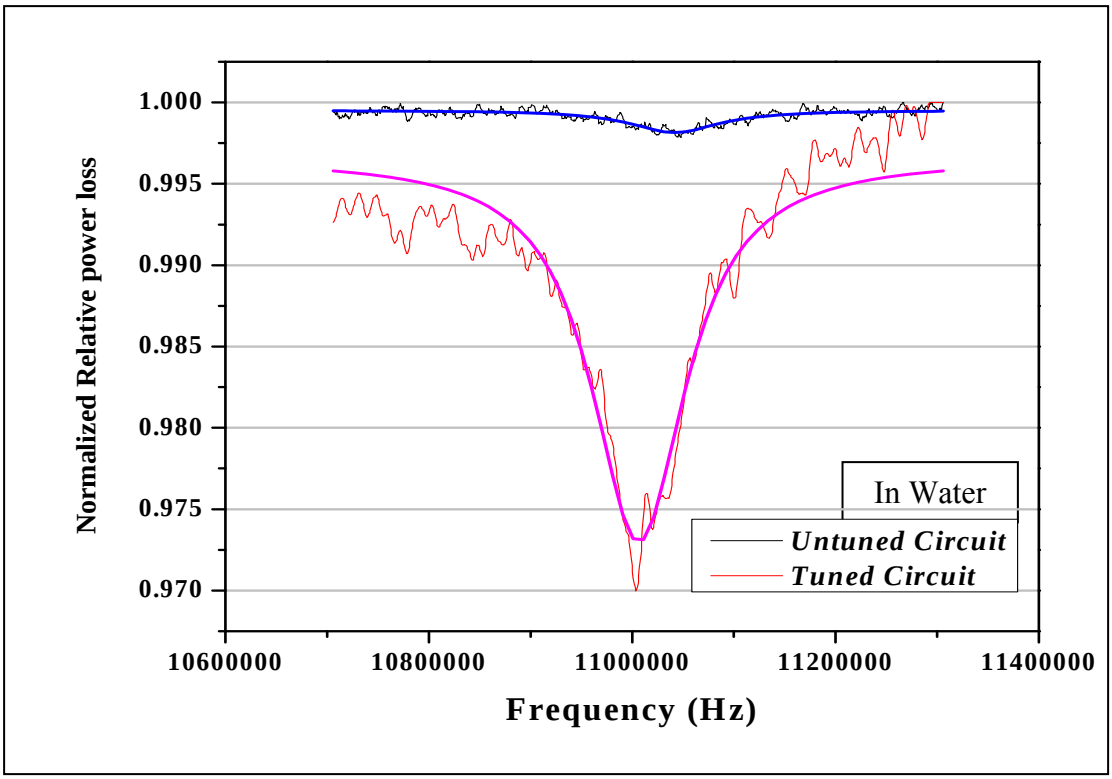

Figure 4-8: Comparison of frequency responses of a 200 μm sensor in water with a tuned and an untuned circuit.

4.4. Discussion

In the late 1920's and early 1930's several authors published their work describing the theoretical aspects of magnetostrictive oscillators G. W. Pierce [2] was the first to provide a detailed theoretical understanding of magnetostrictive oscillators. Further work by J. H. Vincent [3], D. S. Muzzey Jr. [4], F. D. Smith [5], S. Butterworth [6] and J. M. Ide [7] studied different geometries of the magnetostrictive oscillator, using the theory described by G. W. Pierce.

G.W. Pierce used a variable capacitor in series with the solenoid coil to determine the resonance frequency of the sensor platform. By tuning the capacitance to a critical

value, he observed a sharp change in the "plate current." He used the values of the coil inductance and the critical value of the capacitance to evaluate the resonance frequency of the sensor platform. An enhanced sensor response due to the addition of a capacitor in series with the solenoid coil was discussed in section 4.3.3. Theoretically an inductor and capacitor in series will have a low impedance value at resonance. The low value of impedance would result in a higher current in the coil. The higher current in the coil produces larger oscillations on the sensor. The increased oscillations (elastic strains) of the sensors is hypothesized to be the reason for the observed enhanced responses (section 4.3.3).

In summary, an equivalent circuit model has been developed to describe the behavior of the measurement system and magnetostrictive platform. Methods to calculate the circuit parameters have been demonstrated. The use of a tuned circuit was shown to enhance the sensor's resonance peak amplitude. Additional work needs to be performed to verify that the increased resonance peak amplitudes are the result of larger elastic oscillations of the sensor. Measurement of these larger elastic oscillations maybe confirmed using a laser vibrometer.

REFERENCES

1. *"Agilent 4395A Network/Spectrum/Impedance Analyzer Operation Manual," Agilent Technologies.*
2. Pierce, G.W., *Magnetostriction Oscillators.* Proceedings of the IRE, 1929. **17**(1): 42-88.
3. Vincent, J.H., *Further experiments on magnetostrictive oscillators at radio-frequencies.* Proceedings of the Physical Society, 1931. **43**(2): 157-165.
4. Muzzey, D.S., *Some Measurements of the Longitudinal Elastic Frequencies of Cylinders Using a Magnetostriction Oscillator.* Physical Review, 1930. **36**(5): 935-947.
5. Smith, F.D., *The magnetostriction constant for alternating magnetic fields.* Proceedings of the Physical Society, 1930. **42**: 181-191.
6. Butterworth, S. and Smith, F.D., *The equivalent circuit of the magnetostriction oscillator.* Proceedings of the Physical Society, 1931. **43**: 166-185.
7. Ide, J.M., *Magnetostrictive alloys with low temperature coefficients of frequency.* 1934. **22**(2): 177-190.
8. Dapino, M.J., Smith, R.C., Calkins, F.T., and Flatau, A.B., *A Coupled Magnetomechanical Model for Magnetostrictive Transducers and its Application to Villari-Effect Sensors.* Journal of Intelligent Material Systems and Structures, 2002. **13**(11): 737-747.

5. RESULTS AND DISCUSSION

5.1. Outline

This chapter begins with the results of experiments designed to validate the theoretical behavior of the magnetostrictive platforms. Experiments were conducted to measure the effects of size, mass, and mass loading on the resonance frequency of the sensor platforms (Section 5.2.1). In section 5.2.2 the relationship between the biosensor's resonance frequency and exposure to a specific concentration of *Salmonella typhimurium* bacteria in a static system is established. Section 5.2.3 describes the results of experiments to determine the saturation response times of the biosensor when exposed to two different concentrations of *Salmonella typhimurium* using a flowing system (section 5.2.3).

In section 5.3, the biosensor's specificity (section 5.3.1), longevity (section 5.3.5) and dose response in different media (water (section 5.3.2), spiked milk, spiked apple juice (section 5.3.3) and in bacterial mixtures (section 5.3.4)) are discussed.

In section 5.4, the dose response of biosensors of 4 different lengths (L=5 mm, 2 mm, 1 mm and 500 μm) in response to increasing concentrations of *S. typhimurium* is presented and discussed.

In section 5.5, electron microscopy results are described that detail the structure and distribution of immobilized phage on the sensor surface. Different immobilization conditions were also investigated in these experiments.

5.2. Preliminary studies

5.2.1 Frequency response and mass sensitivity

The resonance frequencies of sensor platforms with different lengths were recorded. Sensor platforms, ranging in lengths from 500 μm to 30 mm, were hand-cut from the as-received METGLAS^{TM} 2826MB. The measured values of the resonance frequency were compared with the theoretical values (equation 4-14). Figure 5-1 shows a comparison between the theoretical values and the experimentally measured values. The measured values of the resonance frequency for the sensor platforms matched fairly well with the theoretically predicted values.

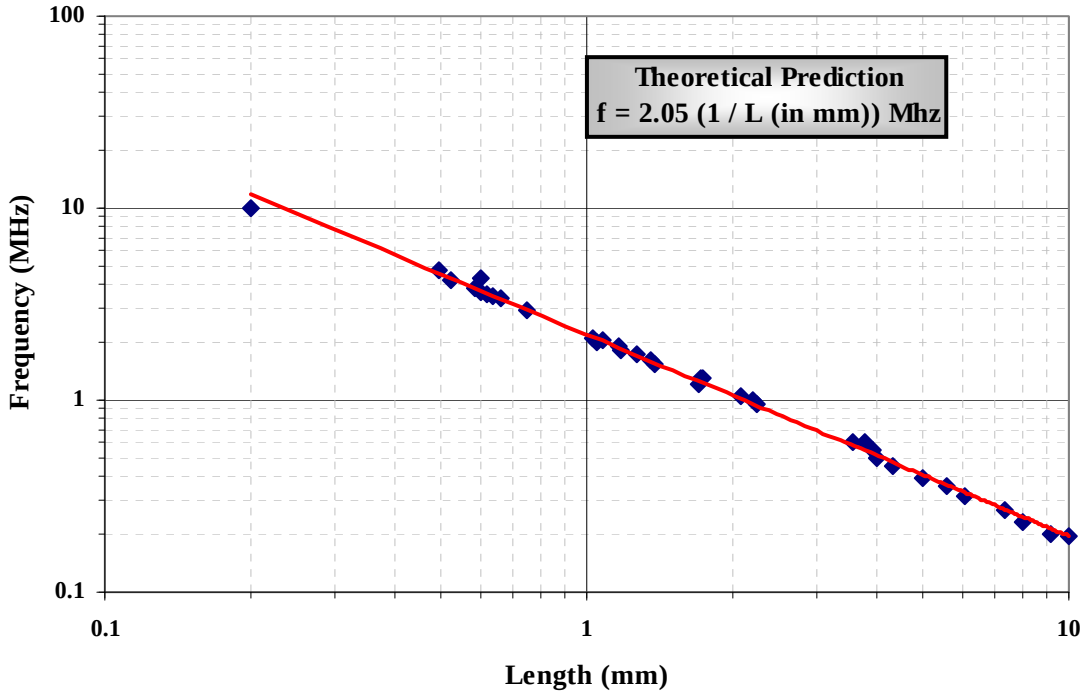

Figure 5-1: Frequency dependence on length (200 μm-10 mm) of magnetoelastic sensors.

Another experiment was done to study the change in the resonance frequency caused by the addition of mass on the sensor surface. Mass was added to the sensor surface by sputtering gold onto the sensor platform. The resonance frequency of the sensor platform was measured before and after the gold deposition. Figure 5-2 shows how the resonance frequency changes for a typical magnetoelastic sensor after the sputtering of gold onto the sensor platform. The resonance frequency of the sensor platform was found to decrease in response to the added mass.

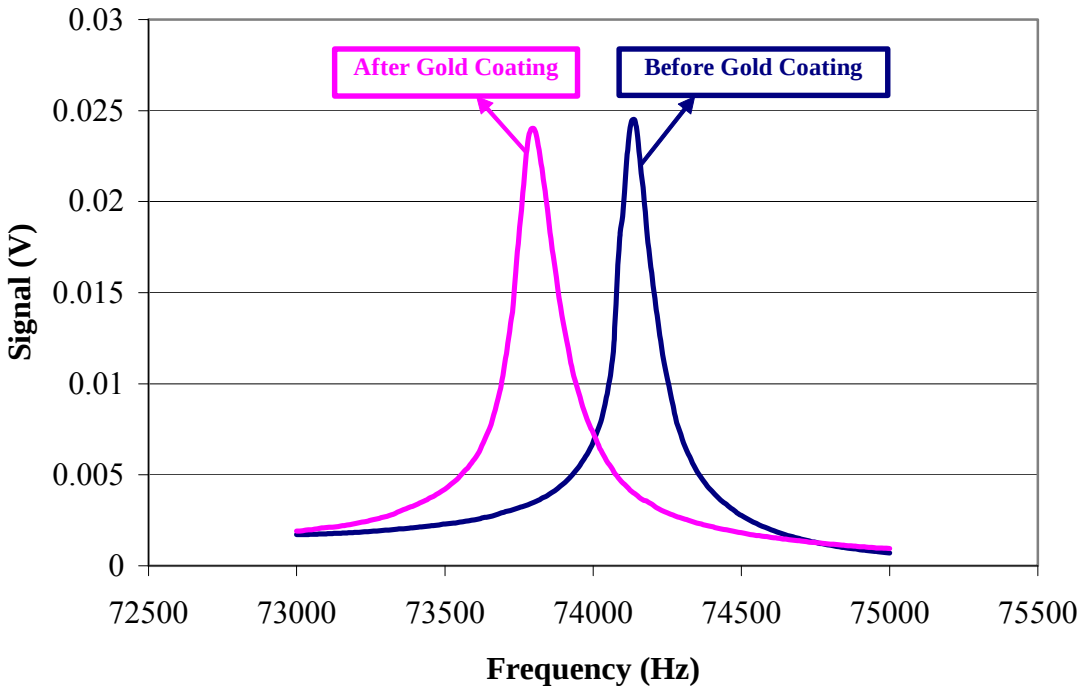

Figure 5-2: Typical frequency response of a magnetoelastic sensor before and after addition of thin film of gold.

Theoretical equation 4-15c predicts that the mass sensitivity of magnetoelastic sensor platforms is higher for sensors with smaller initial mass (smaller dimensions). To experimentally establish this relationship, resonance frequency measurements were made

on sensor platforms of different lengths ranging from 200 μm to 30 mm. Sputtered thin films of gold were used to simulate mass loading on the sensor surface. Gold films were chosen because they can be uniformly deposited and are chemically inert and oxidation resistant. Five successive layers of gold (3 nm each in thickness) were sputtered on the sensor platforms. Resonance frequencies were measured before and after the deposition of each layer. The mass added (Δm_{gold}) was calculated as a product of the density and the volume of gold deposited on the surface. Figure 5-3 shows the frequency shifts (Δf) obtained for successive layers of gold added to three different sensors (L=1.3 mm, 1.0 mm and 0.5 mm). The mass sensitivity ($\Delta f/\Delta m$) was calculated as the slope of Δf vs Δm_{gold} curve.

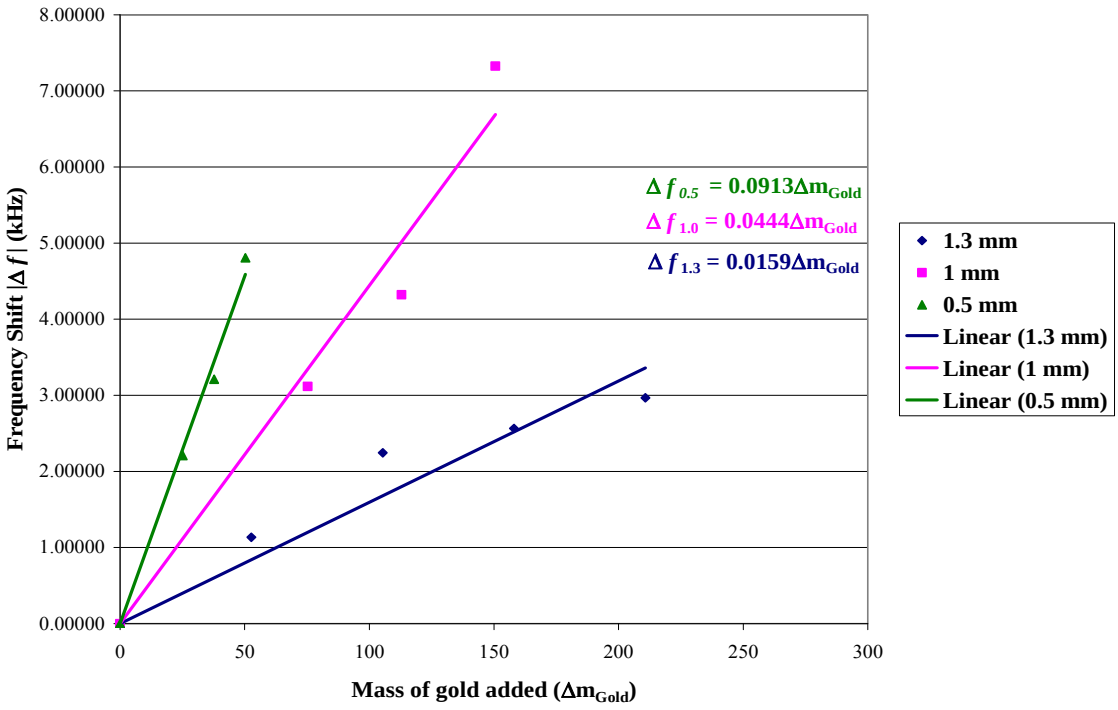

Figure 5-3: Frequency shifts calculated as function of mass of gold added to the sensor surface. The three different lengths shown are L=1.3, 1.0 and 0.5 mm.

The results of the mass sensitivity measurements are shown in Figure 5-4 with $\Delta f/\Delta m$ (Hz/pg) as the ordinate and length (mm) as the abscissa. The theoretical equation shown in Figure 5-4 was calculated by substituting for f and M in equation 4-15c. The thickness (28 μm) and the length to width ratio (5:1) of all the sensor platforms used in this experiment, were held constant. The plot clearly shows that sensor platforms with smaller physical dimensions have a higher mass sensitivity. It is important to note that for the sensitivity study described in this section, the frequency response measurements were performed in air.

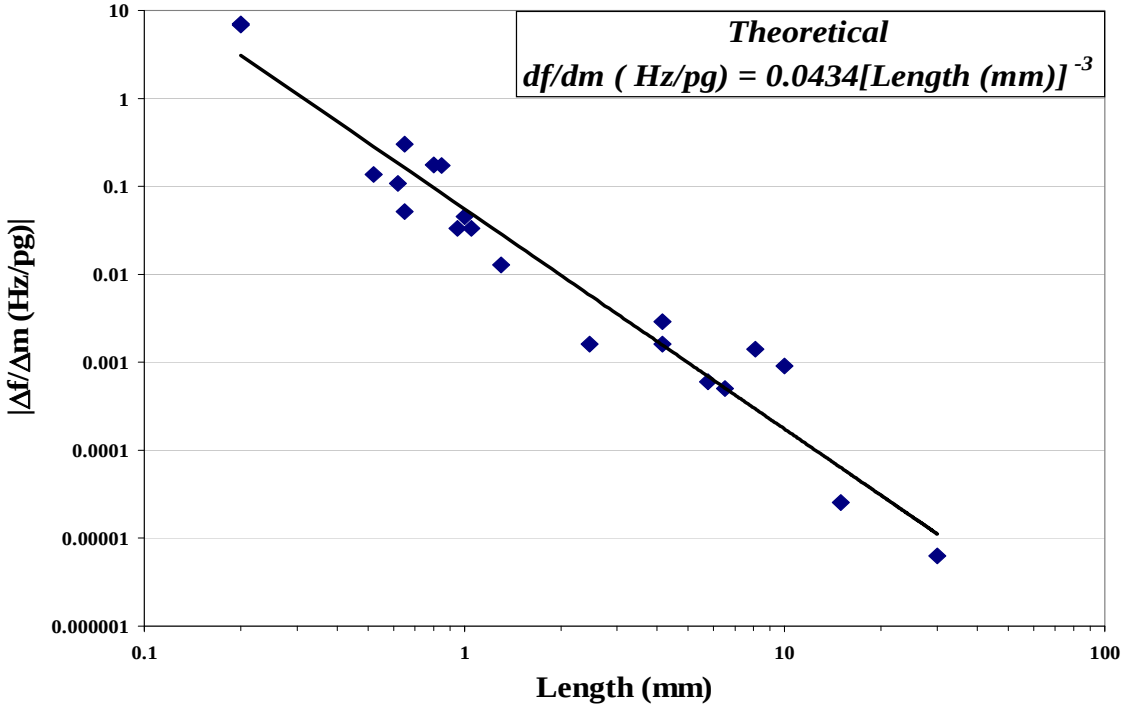

Figure 5-4: Dependence of length on the mass sensitivity $(\Delta f/\Delta m)$ of magnetoelastic sensors with air as surrounding media.

5.2.2 Sensor response to *S. typhimurium* in static conditions

In this section, the change in resonance frequency of the biosensor upon exposure to *S. typhimurium* was studied. This experiment was performed using static test procedures described in section 3.8.1. The biosensor was exposed to *S. typhimurium* (5×10^8 cfu/mL) for 30 minutes. The resonance frequency of the biosensor was measured before and after the exposure. The total number of bacteria attached to the sensor surface was counted from the SEM micrographs of different regions on the biosensor surface. The measured frequency responses and the SEM micrographs for a 2mm length biosensor are shown in Figure 5-5 and Figure 5-6, respectively. The attachment of bacterial mass to the biosensor resulted in a measured frequency shift of 1290 Hz. The total number of *S. typhimurium* attached (counted from SEM micrographs) to the biosensor was 1.232×10^5 cells. This bacterial mass attachment corresponds to a theoretical frequency shift of 1346 Hz. The resonance frequency shifts obtained for 5 different biosensors using this procedure are summarized in Table 5-1.

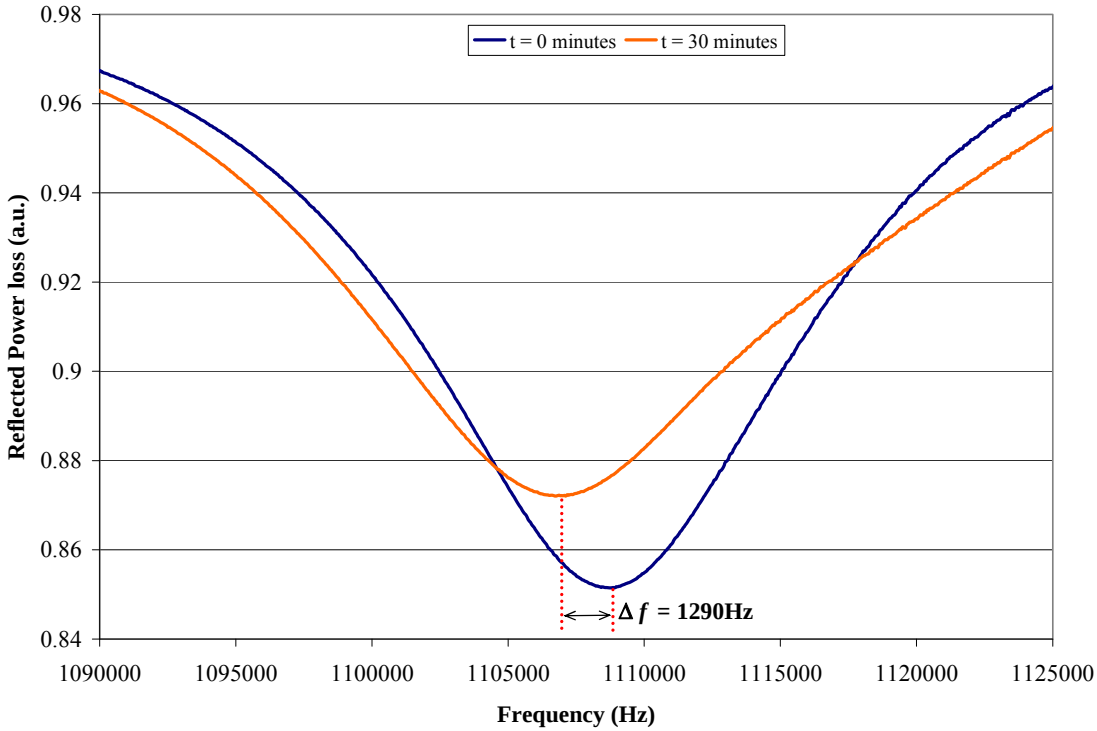

Figure 5-5: Typical response of a 1×0.2×0.015 mm sensor to 5×10^{8} cfu/mL of *S. typhimurium* at different time intervals (t=0, 10, 20, 30, 40 and 50 minutes). A total frequency shift (Δf) of 1290 Hz was observed.

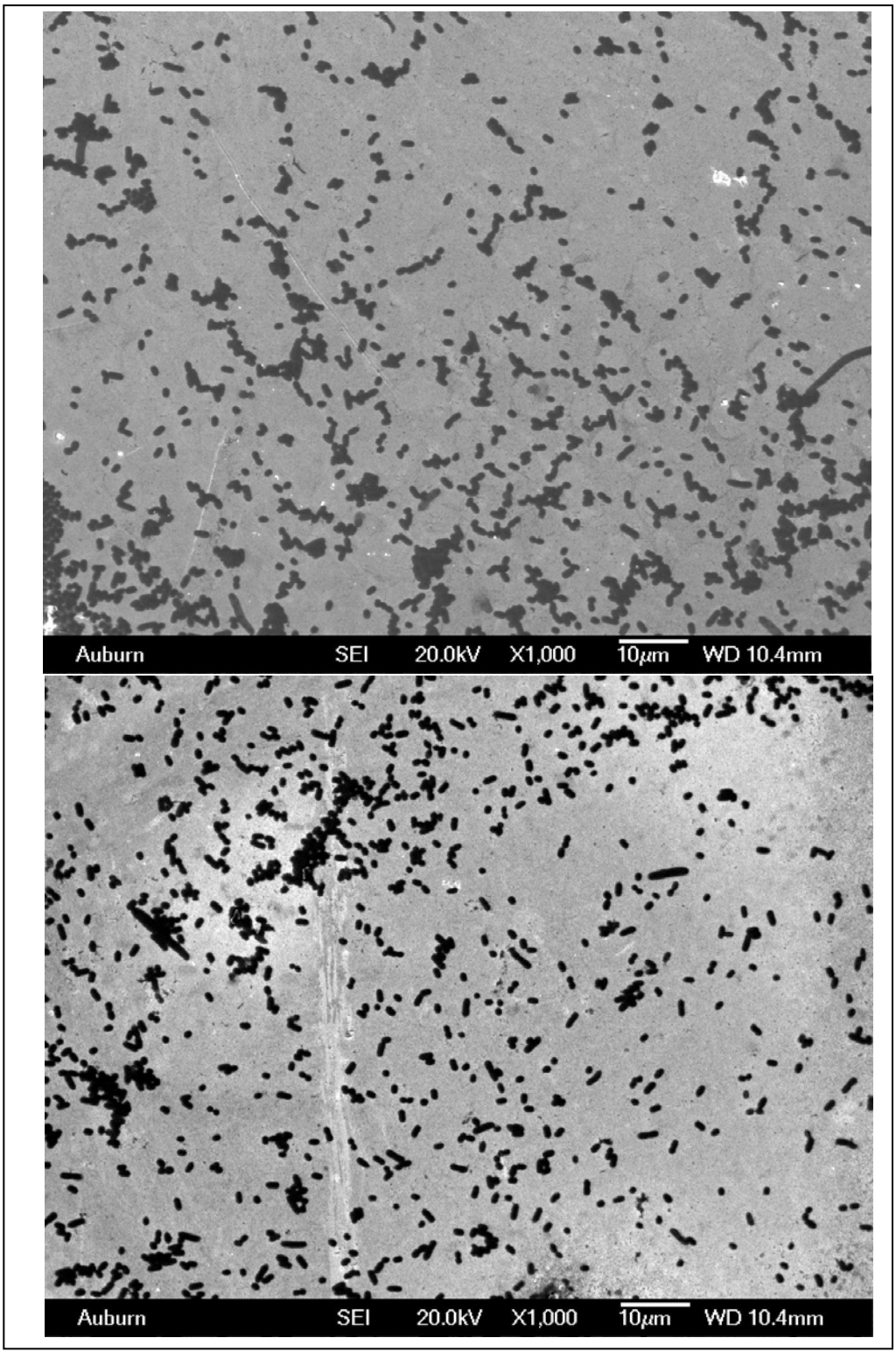

Figure 5-6: SEM pictures (Magnification: 1000X) of two different regions on the sensor (2×0.4×0.015 mm) with a frequency shift of 1290 Hz.

Table 5-1: Comparison of number of bacterial cells attached estimated from frequency shifts obtained and the extrapolated number calculated from SEM images.

	Measured Frequency Shift (Hz)	**Number of cells estimated from frequency shifts**	**Total number of cells from SEM**	**Estimated *Salmonella typhimurium* mass (pg)**
Sensor 1	1291	118107	123200	1.987
Sensor 2	1163	106397	152000	1.451
Sensor 3	1048	95876	142000	1.399
Sensor 4	973	89014	118600	1.556
Sensor 5	947	86636	115200	1.559

From the results shown in Table 5-1 it was confirmed that the measured frequency shifts were due to the attachment of *S. typhimurium* to the biosensor. The mass of *S. typhimurium* was estimated from the observed experimental frequency shifts. Equation 4-15a was used to calculate the mass of one *S. typhimurium* cell. The dimensions of the sensors used in this calculation were 2×0.4×0.015 mm. The average mass of *Salmonella typhimurium* obtained from the calculation was 1.59±0.23 pg.

5.2.3 Saturated response time

This experiment was performed to study the time required to achieve a saturated frequency response of the biosensor upon exposure to *S. typhimurium*. The biosensors were placed in the center of a solenoid coil. Water was then allowed to flow over the sensor at a flow-rate of 50 μL/min. Fifteen minutes after obtaining a steady-state resonance frequency in flowing water, the biosensor was exposed to 1mL of *S.*

typhimurium suspension (5×10^8 cfu/mL). Figure 5-7 shows the changes in the resonance frequency of the biosensor as a function of time.

The introduction of the *S. typhimurium* (5×10^5 cfu/mL) to the biosensor resulted in a gradual decrease in the resonance frequency during the first 20 minutes of exposure. After 20 minutes, the resonance frequency of the biosensor reached saturation. Similarly, when the biosensor was exposed to *S. typhimurium* of 5×10^8 cfu/mL concentration, the saturated resonance frequency response was achieved in 30 minutes. Hence, for all the static tests performed, the sensors were exposed to *S. typhimurium* for more than 30 minutes to ensure saturation.

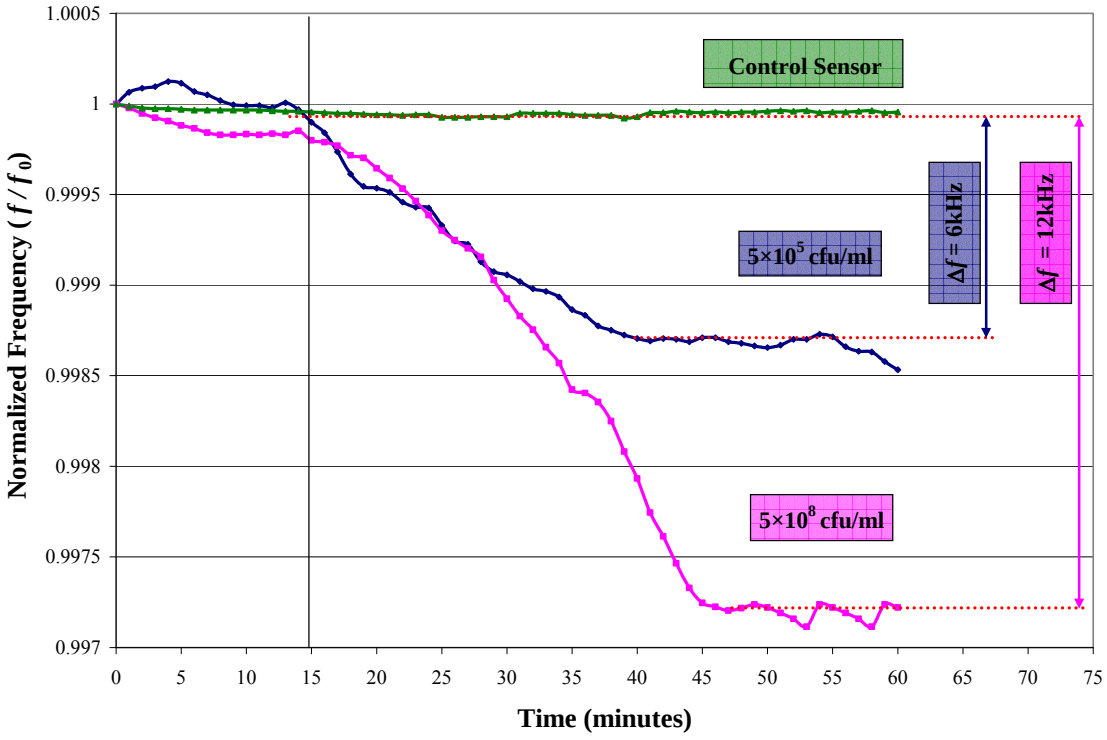

Figure 5-7: Responses of three different sensors (L=500 μm) to *S. typhimurium*. An average saturation response could be seen at the end of 30 minutes.

5.3. Biosensor Characterization

5.3.1 Sensor specificity

In evaluating the performance of a biosensor, it is essential to establish specificity (cross-reactivity with other pathogenic species) of the immobilized bio-recognition element. The response of the biosensor upon exposure to *S. typhimurium*, *E. coli, S. Enteritidis* and *L. monocytogenes* was studied. A significantly lower affinity of the immobilized phage to pathogens other than *S. typhimurium* will establish the biosensor's specificity. The biosensors were exposed to each pathogen using the static test procedure. In the section 5.2.3, it was established that the biosensor resonance frequency achieved saturation in 30 minutes. In this experiment the biosensor was exposed to the pathogenic solution for 45 minutes. Figure 5-8 shows the measured values of normalized area coverage density, $\Delta f_{measured}$ and Δf_{SEM} obtained for the biosensors. These values were compared for biosensors exposed to the different pathogens. The normalized area coverage density shown in Figure 5-8 was calculated as the ratio of the area coverage density of a certain pathogen (N_P) to the area coverage density of *S. typhimurium* (N_{ST}). The $\Delta f_{measured}$ and Δf_{SEM} were calculated using procedures described in section 3.7.

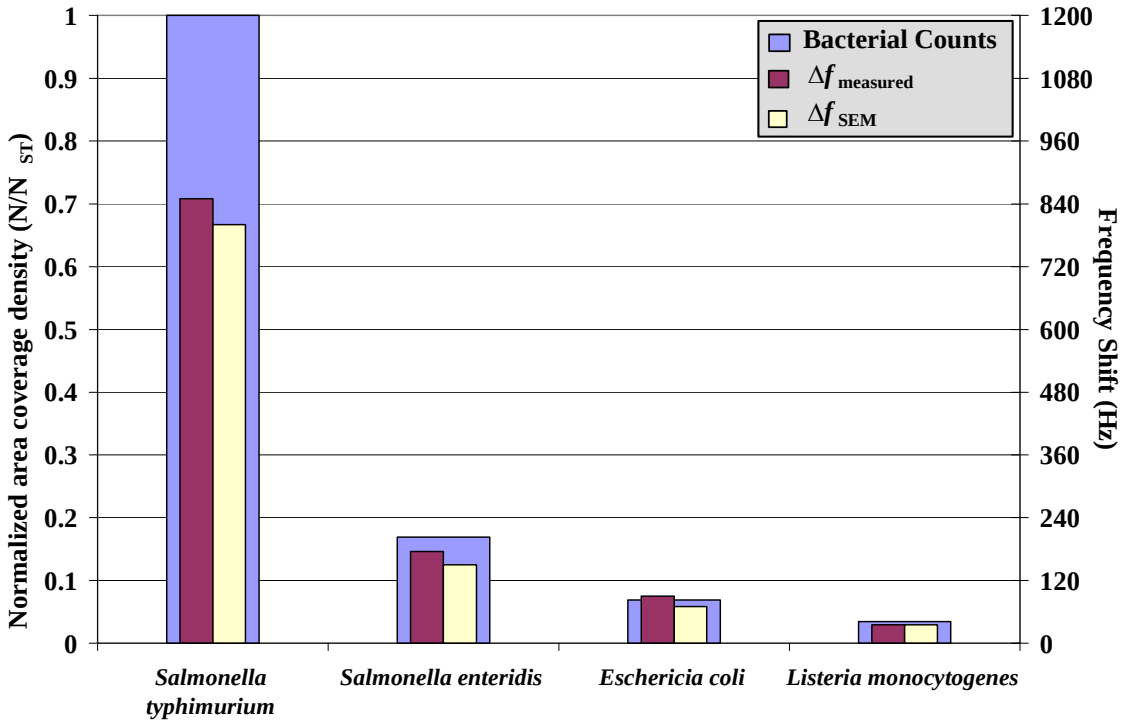

Figure 5-8: Specificity of phage-immobilized sensors exposed to different pathogens (5×10^8 cfu/mL). The normalized area coverage density was calculated from SEM photomicrographs of the sensor surface (an average of 5 sensors each). $\Delta f_{measured}$ and Δf_{SEM} are shown on the right side.

The normalized area coverage density of the biosensors exposed to *S. typhimurium, S. enteritidis*, *E. coli* and *L. monocytogenes* were 1.00, 0.17, 0.06 and 0.03, respectively. Large differences in the distribution density of different pathogens bound to the biosensor's surface can be observed in the SEM micrographs (Figure 5-9). The values of resonance frequency shifts obtained upon exposure to different pathogens followed the same trend as the normalized distribution density. The values of $\Delta f_{measured}$ were slightly higher than the values of Δf_{SEM}. The difference in the values of $\Delta f_{measured}$

and Δf_{SEM} can be attributed to extrapolations used in the calculation of Δf_{SEM}. Figure 5-8 and Figure 5-9 establish that the biosensor had a significantly higher affinity towards *S. typhimurium*.

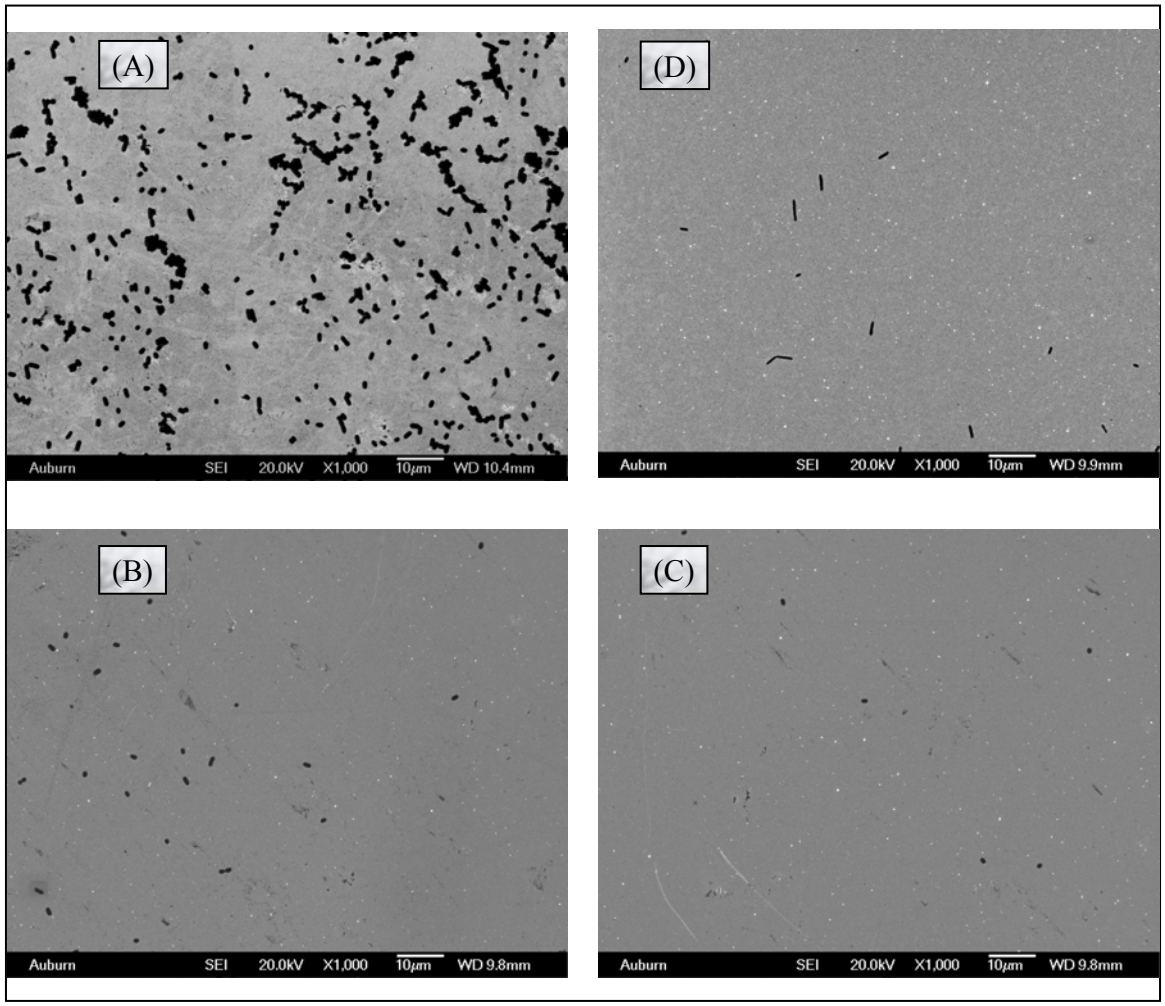

Figure 5-9: Typical SEM images of phage-immobilized sensors exposed to (A) *S. typhimurium*; (B) *S. enteritidis*; (C) *E. coli* and (D) *L. monocytogenes*.

5.3.2 Biosensor dose response

The dose response of magnetoelastic biosensors (Dimensions: 2×0.4×0.015 mm) to various concentrations of *S. typhimurium* suspensions was studied. The dose response

tests were carried out using procedures described in section 3.8.4. Figure 5-10 shows a typical resonance frequency response as a function of time for a biosensor (L=2 mm) exposed to different concentrations of bacterial suspensions. The biosensor's resonance frequency was recorded every 2 minutes. Exactly 1 mL of each concentration was allowed to flow over the sensor at a flow rate of 50 µL/min. At this flow rate, it takes 20 minutes for 1mL of the analyte to flow over the biosensor. As described in section 3.8.4, the resonance frequency at the end of every 20 minutes was used to calculate the resultant frequency shift for that particular concentration.

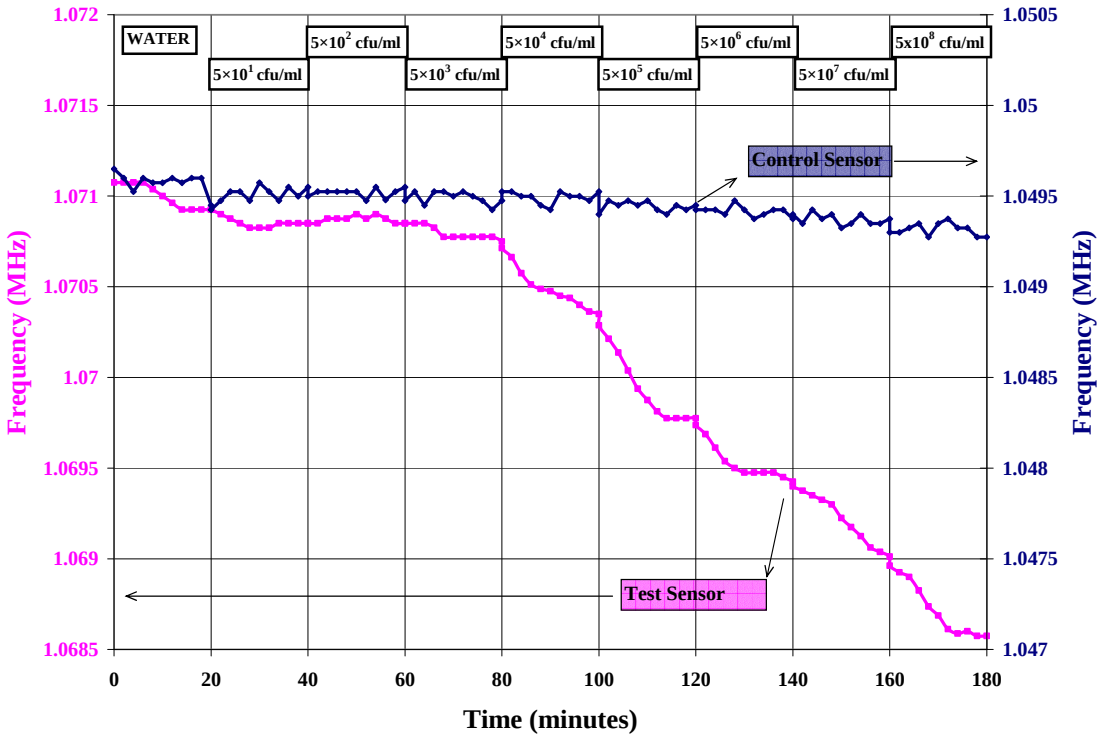

Figure 5-10: Typical dynamic response curve for a sensor with dimensions 2×0.4×0.015 mm. 1 mL of each concentration of bacterial suspension was allowed to flow over the sensor at a flow rate of 50 µL/min. Control sensor response shown is of a sensor devoid of phage.

There was no change in the resonance frequency upon exposure to the lowest concentrations (5×10^1 cfu/mL and 5×10^2 cfu/mL) of *S. typhimurium*. The first measurable decrease in the resonance frequency occured when the biosensor was exposed to a concentration of 5×10^3 cfu/mL of *S. typhimurium*. The resonance frequency decreased with the introduction of each successive concentration (5×10^4 cfu/mL through 5×10^8 cfu/mL) of *S. typhimurium*. The control sensor that was devoid of any phage on the sensor surface had a negligible change in its frequency even upon exposure to very high concentrations (5×10^8 cfu/mL) of bacteria.

In order to confirm the results obtained from frequency shifts (Figure 5-11), pictures were taken of different regions on the assayed biosensors using SEM. Intentionally interrupted tests were performed to visually verify (using SEM) that a lower number of *S. typhimurium* were bound to biosensors after exposure to lower concentration solutions. Interrupted tests were performed by intentionally stopping the dose response tests once the biosensors were exposed to all concentrations up to 5×10^6 cfu/mL in one test and up to 5×10^3 cfu/mL in another test. The SEM micrograph shown in Figure 5-12(a) is of an assayed biosensor that had gone through an uninterrupted dose response test (exposure to 5×10^1 cfu/mL through 5×10^8 cfu/mL). SEM micrographs for the biosensors subjected to the two interrupted dose response tests are shown in Figure 5-12(b) and Figure 5-12(c). Figure 5-12(d) is an SEM micrograph of the control sensor (devoid of bio-recognition element) after a completed dose response test. A lower area coverage density (Figure 5-12 (a-c)) was observed for lower concentrations of *S. typhimurium*. The negligible change in resonance frequency of the control sensor was

further confirmed by the nominal binding observed in the SEM micrograph (Figure 5-12 (d)).

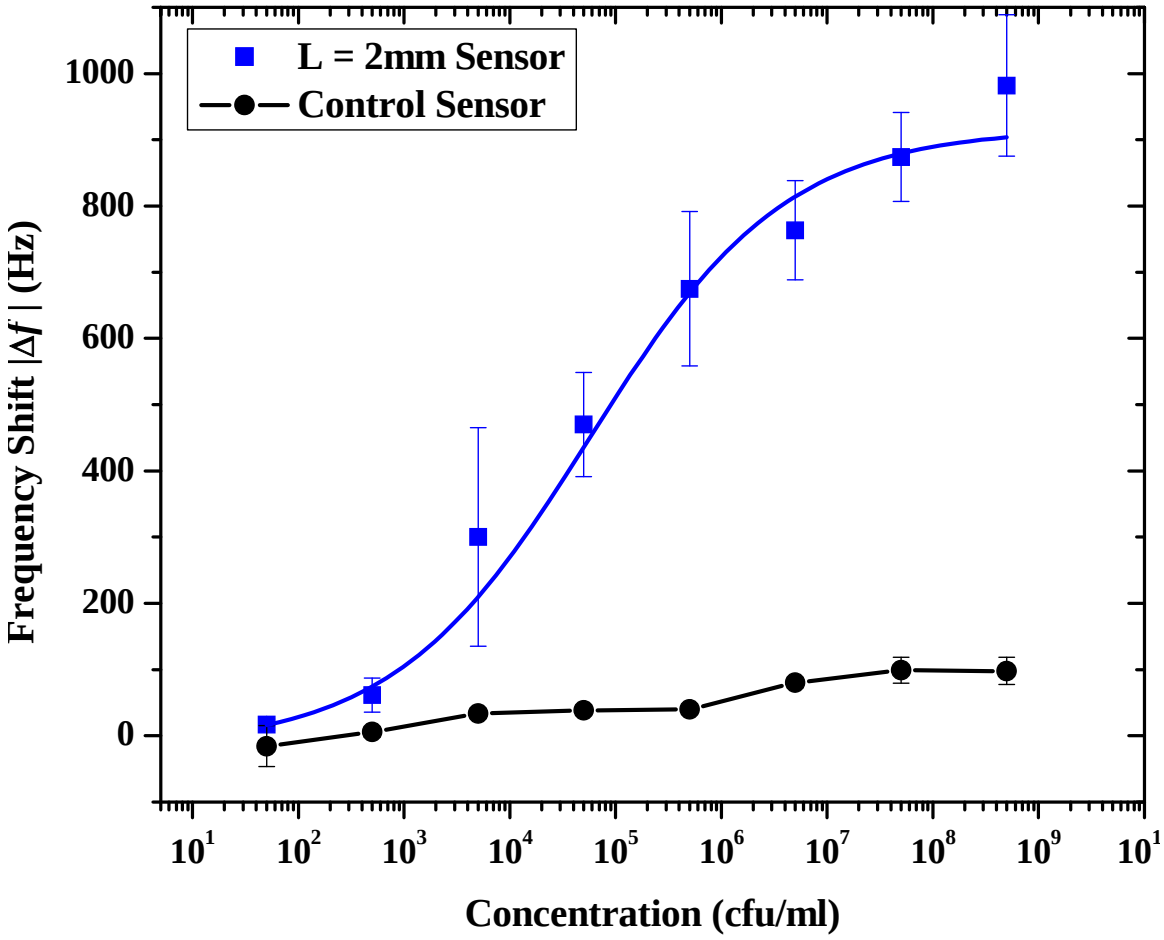

Figure 5-11: Magnetoelastic biosensor's responses, when exposed to increasing concentrations (5×10^1 to 5×10^8 cfu/mL) of *S. typhimurium* suspensions on test sensors (2×0.4×0.015 mm) (■- Test sensor: sigmoidal fit χ^2=0.048, R^2=0.99) and control (2×0.4×0.015 mm) (● - Control sensor). Each data point is the average value obtained from five individual experiments (different sensors) carried out under identical conditions.

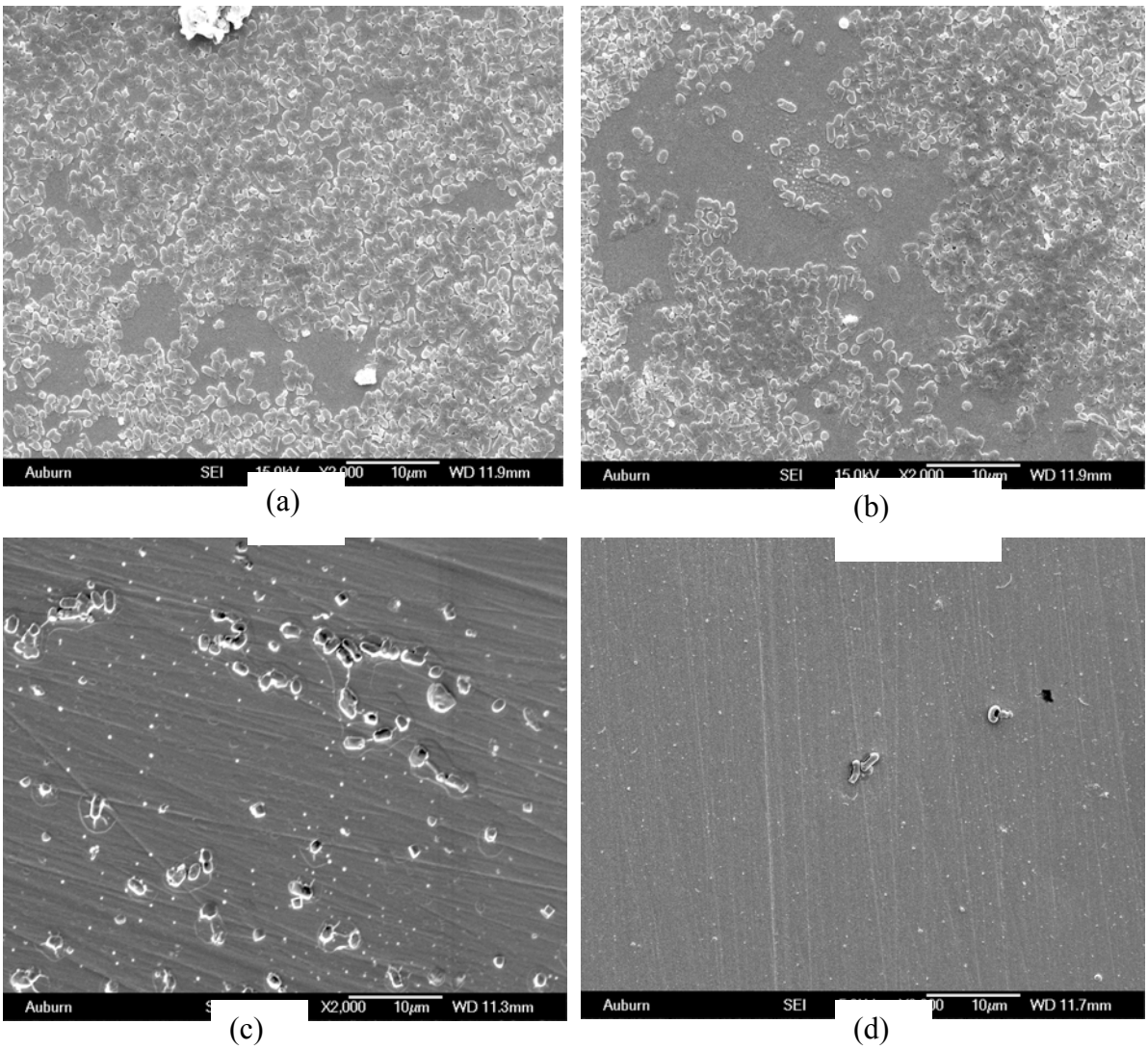

Figure 5-12: Typical SEM images depicting *S. typhimurium* attachment to phage-immobilized magnetoelastic sensor surface. Sensors exposed to *S. typhimurium* at concentrations of (a) 5×10^{8} cfu/mL, (b) 5×10^{6} cfu/mL (c) 5×10^{3} cfu/mL and (d) control (biosensor devoid of phage and treated with 5×10^{1} cfu/mL through 5×10^{8} cfu/mL of bacterial sample).

5.3.3 Biosensor response in real food

The detection of *S. typhimurium* suspended in different media (water, milk and apple juice) was essential to establish the field applicability of magnetoelastic biosensors. The sensors (2×0.4×0.015 mm) were exposed to milk and apple juice spiked with increasing concentrations of *S. typhimurium* (5×10^1 through 5×10^8 cfu/mL). The biosensor's dose responses to spiked samples were evaluated using procedures described in section 3.8.5.

The first detectable shift in resonance frequency occured at a concentration of 5×10^3 cfu/mL. An average of five different sensor responses was used to construct the dose response curves depicted in Figure 5-13. The dose response of the sensors exposed to spiked milk, apple juice and water samples was similar except at higher concentrations. The resonance frequency shifts obtained for spiked milk samples were lower than that of spiked water and spiked apple juice samples. The dose response was linear over five aliquots of concentrations (5×10^3 through 5×10^7 cfu/mL) for the three different media. The sensitivity of the biosensor was calculated as the slope of the linear region of the dose response curve (Hz per decade of concentration change). The sensitivity of biosensors exposed to spiked water, apple juice, and milk was 161 Hz/decade, 155 Hz/decade and 118 Hz/decade, respectively. The control sensor (Figure 5-13) had a negligible change in resonance frequency in response to even high concentrations of *S. typhimurium*. The control sensor showed a maximum resonance frequency shift of 50 Hz, while a maximum resonance frequency shift of 980 Hz was observed for the biosensor. This significant difference in the measured frequency shifts (control versus measurement sensor) indicates negligible, non-specific binding of bacteria to the bare gold surface.

A Hill plot constructed from the dose response data was used to study the kinetics of the *Salmonella*-phage binding reaction. This plot was constructed using methods described in section 3.9. A Hill plot, constructed using the three different dose response curves, is shown in Figure 5-14. A binding valency of 2.4, 2.5 and 2.3 were calculated for the biosensors in response to spiked water, milk and apple juice, respectively. These values indicate that the binding of *S. typhimurium* to immobilized phage was multivalent in nature. More than two phage binding sites participated in the capture of one *S. typhimurium* cell. The values of K_d (apparent) obtained for biosensors exposed to spiked water, milk and apple juice were 1.82×10^5, 2.51×10^5 and 2.16×10^5 cfu/mL, respectively. The higher value for K_d (apparent) obtained for biosensors exposed to milk is also evident from the lower resonance frequency shifts observed. The lower frequency shifts and higher K_d (apparent) values obtained for biosensors exposed to spiked milk samples is hypothesized to result from the milk proteins blocking of some of the available binding sites.

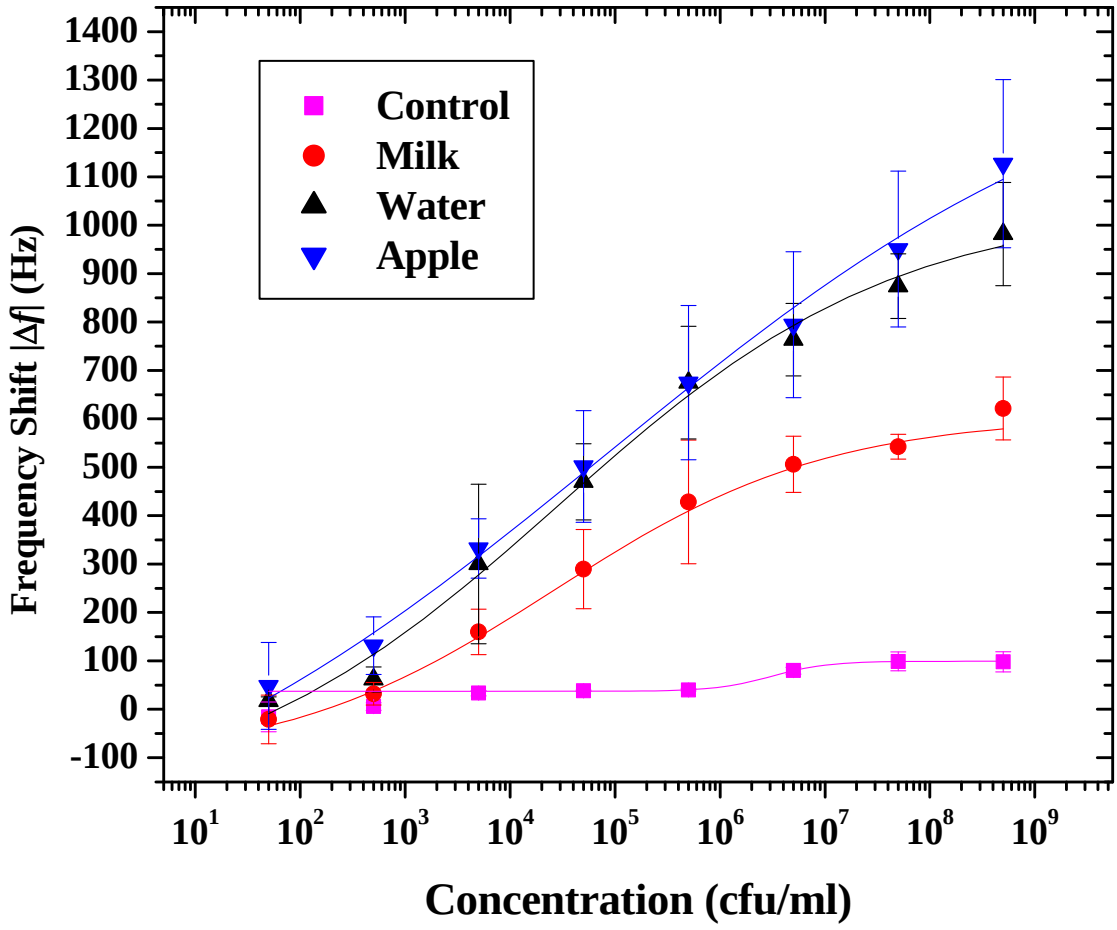

Figure 5-13: Comparison of dose responses of magnetoelastic biosensor (2×0.4×0.015 mm), when exposed to increasing concentrations (5×10^1 to 5×10^8 cfu/mL) of *S. typhimurium* suspensions in water ((▲) χ^2=0.442, R^2=0.99), apple juice ((▼) χ^2 =0.237, R^2=0.99) and fat free milk ((●) χ^2=0.194, R^2=0.99). Control (■) represents the uncoated (devoid of phage) sensor's response. The curves represent the sigmoid fit of signals obtained.

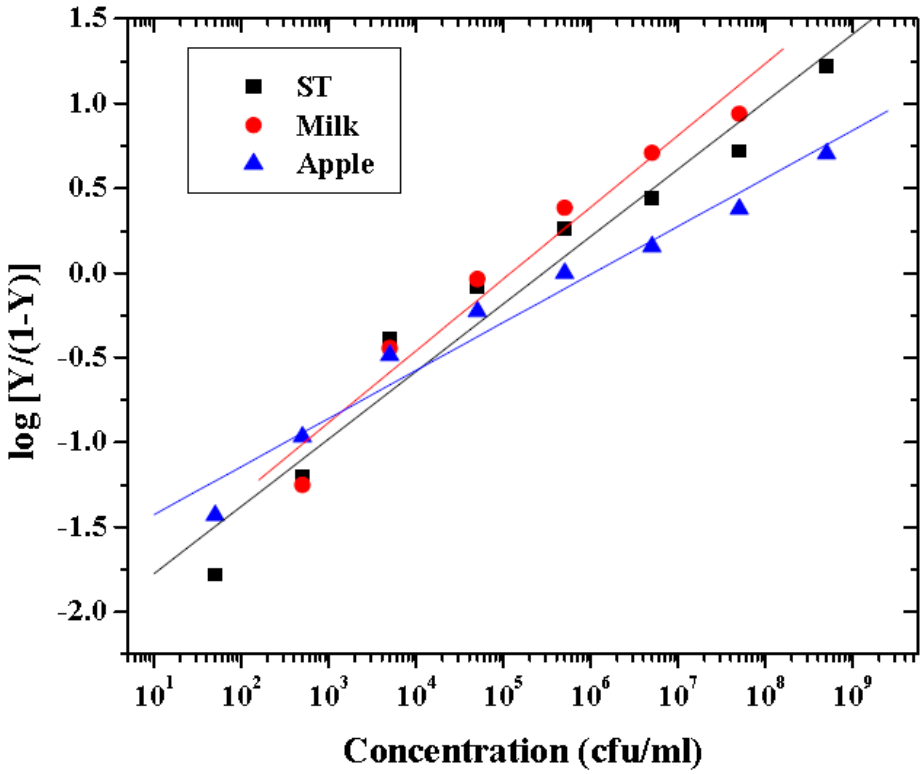

Figure 5-14: Hill plots of binding isotherms showing the ratio of occupied and free phage sites as a function of bacterial concentrations spiked in different food samples. The straight line is the linear least squares fit to the data (water (■): slope=0.40±0.03, R=0.97; fat-free milk (●): slope=0.41±0.04, R=0.98; apple juice (▲) slope=0.36, R=0.96).

SEM micrographs of assayed biosensors were used to provide visual verification of measured experimental data shows SEM micrographs of the biosensor surfaces after dose response testing to *S. typhimurium*. For biosensors exposed to spiked milk samples, the binding appeared lower than that for spiked water or spiked apple juice samples. The smaller number of bound *S. typhimurium* cells explains the lower values of frequency shifts obtained for milk samples. The milk proteins can be seen as white spots in the SEM micrograph for the biosensor exposed to spiked milk (Figure 5-15(a)). In this test,

it was established that the biosensors can detect the concentrations of *S. typhimurium* present in both water and food samples.

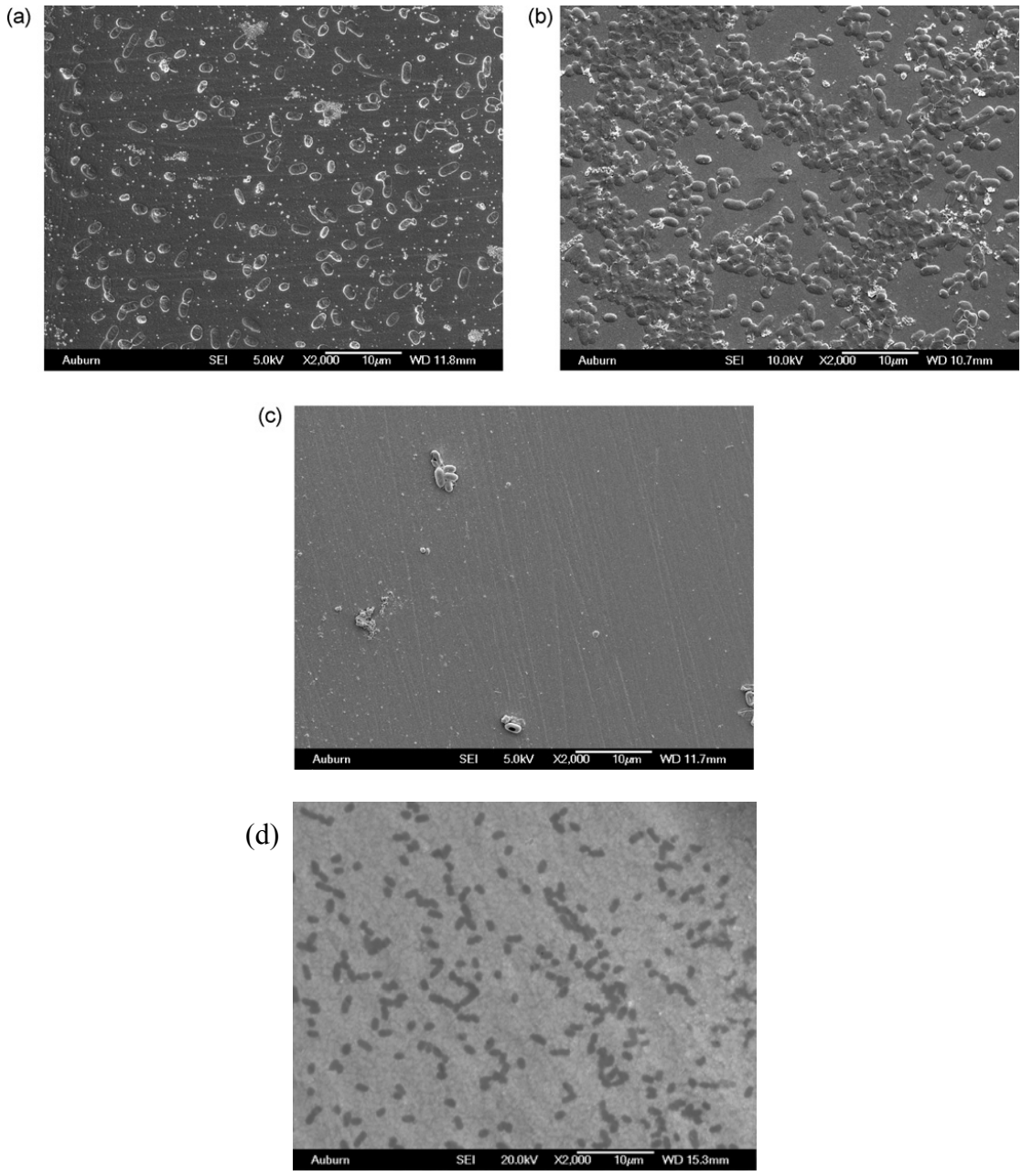

Figure 5-15: Typical SEM images of *S. typhimurium* bound to a magnetoelastic biosensor surface (2×0.4×0.015 mm) in (a) fat-free milk, (b) water (d) apple juice and (c) control (biosensor devoid of phage and treated with 5×10^8 cfu/mL of bacterial sample).

5.3.4 Selectivity in the presence of high concentrations of masking bacteria

The effect that masking bacteria has on the measurement of *S. typhimurium* on the response of the biosensor was studied. This was done by exposing the biosensors to three different sets of prepared suspensions: 1). *S. typhimurium*, 2). *S. typhimurium* + *E. coli and* 3). *S. typhimurium* + *E. coli* + *L. monocytogenes*). The test procedures described in section 3.8.5 were used to obtain the dose response curves. The obtained dose response curve is shown in Figure 5-16. The biosensor's dose response had similar sigmoidal trends. The dose response curves indicated that the frequency shifts for biosensors exposed to the two mixtures (suspensions 2 and 3) were lower than the ones exposed to *S. typhimurium* alone. However, there was no significant difference in response between the mixtures with one or two masking bacteria. The dose responses for biosensors exposed to the three suspensions were linear over the range of 5×10^3 cfu/mL to 5×10^7 cfu/mL. The sensitivity of the biosensor exposed to *S. typhimurium* in the absence of masking bacteria was 161 Hz/decade. In presence of one masking bacteria (*E. coli*) and two masking bacteria (*E. coli* and *L. monocytogenes*) in the mixtures the sensitivity was 131 Hz/decade and 127 Hz/decade (R^2=0.97), respectively.

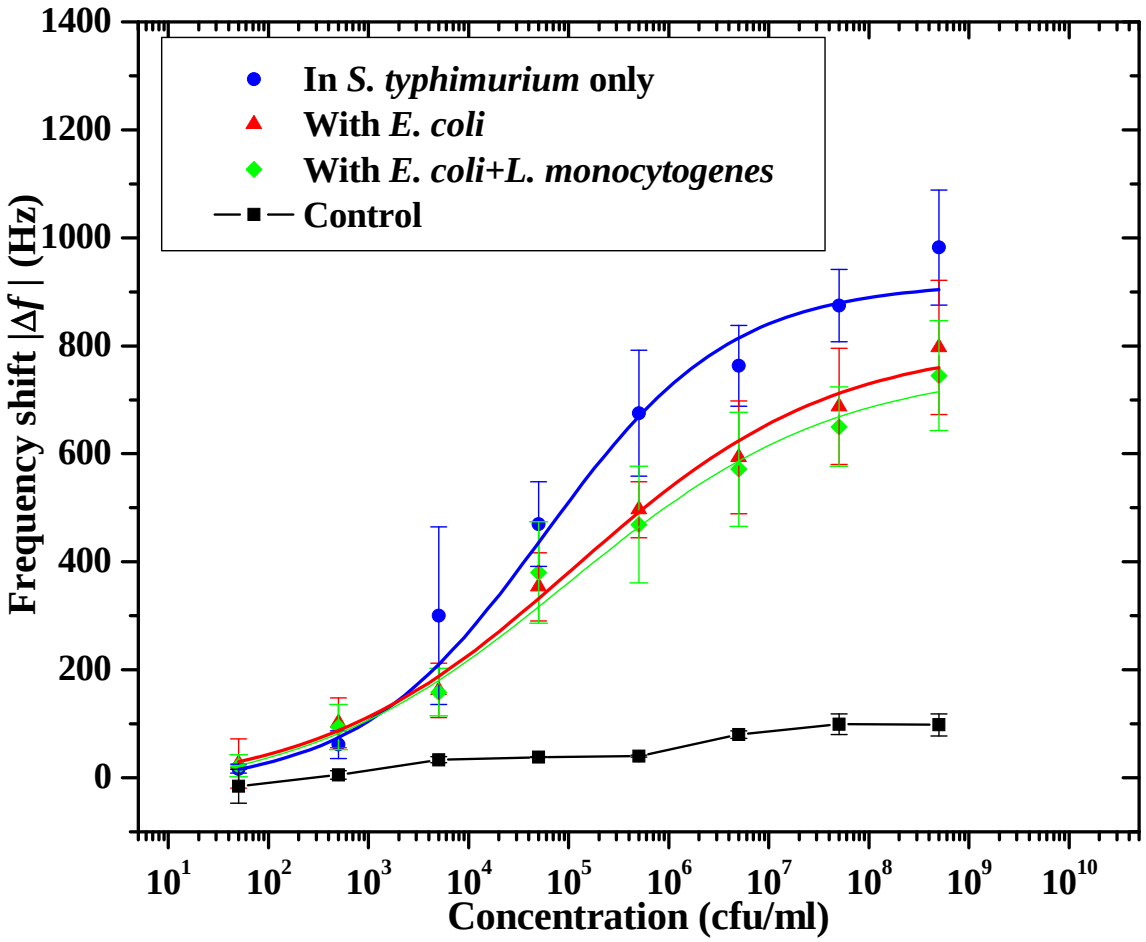

Figure 5-16: Dose response curve of magnetoelastic sensors (2×0.4×0.015 mm) in response to *S. typhimurium* in mixture with other masking bacteria. Sensors (each data point is an average of the response from five sensors) exposed to only *S. typhimurium* (●-χ^2=0.44, R^2=0.99), *S. typhimurium* in mixture with *E. coli* (▲-χ^2=0.18, R^2=0.99), and *S. typhimurium* in mixture with *E. coli* + *L. monocytogenes* (♦-χ^2=0.24, R^2=0.99). The control (■-χ^2=0.048, R^2=0.99), is the response of an uncoated (devoid of phage) sensor. The curves represent the sigmoidal fit of signals obtained.

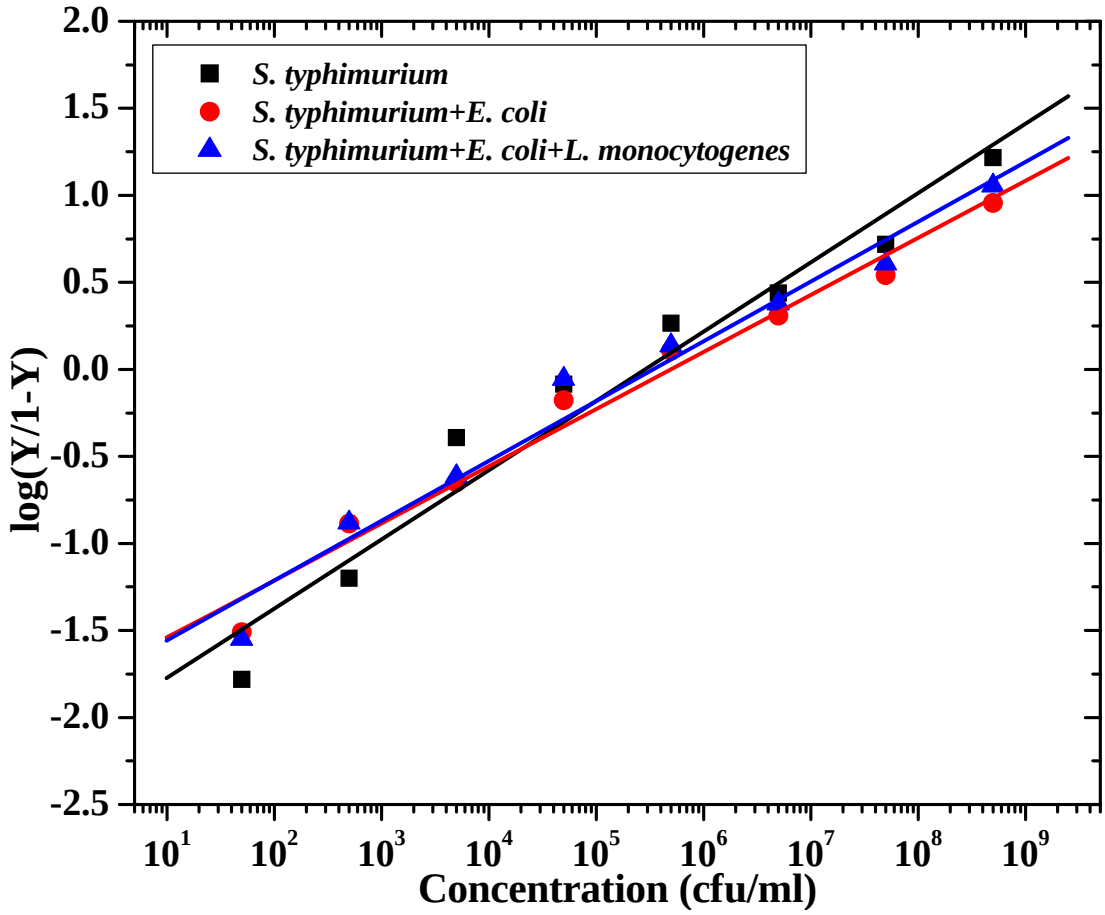

Figure 5-17: Hill plot constructed from the dose response curves, showing the ratio of occupied (Y) and free phage sites (1-Y) as a function of bacterial concentrations in different mixtures. The straight line is the linear least squares fit to the data (*S. typhimurium* (■): slope=0.40±0.03, R^2=0.97; *S. typhimurium* + *E. coli* (●): slope=0.33±0.02, R^2=0.98; and *S. typhimurium* + *E. coli* + *L. monocytogenes* (▲) slope=0.34±0.02, R^2=0.97).

A hill plot (Figure 5-17) was constructed using the dose response curves [1-4] to determine the binding kinetics. The binding valency was similar for all the three prepared suspensions. The binding valencies obtained from the hill plots were 2.42, 2.79 and 2.91 for the suspension 1, suspension 2 and suspension 3, respectively. This reaffirms the multivalent nature of phage-*Salmonella* interaction on the biosensors. The biosensors exposed to *S. typhimurium* in the presence of masking bacteria had a higher value of the apparent dissociation constant. The lower sensitivity and the higher dissociation constants obtained for the mixtures can be attributed to the presence of the masking bacteria. The presence of masking bacteria in the mixtures reduces the probability of interaction between *S. typhimurium* and the binding sites on the biosensor. A summary of results from the calculations for sensitivity, binding valency and apparent dissociation constant for the assayed biosensors discussed in section 5.3.3 and section 5.3.4 are presented in Table 5-2.

Table 5-2: The sensitivity, dissociation constant and binding valency of magnetoelastic sensors in different bacterial mixtures.

Bacterial mixtures	**Sensitivity (**Hz/decade**)**	**Binding valency** (1/n)	$\mathbf{K_d}$ (cfu/mL)	$\mathbf{K_{d(apparent)}=K_d^n}$ (cfu/mL)
S. typhimurium	161	2.42	149	1.82×10^5
S. typhimurium + *E. coli*	131	2.79	82	2.19×10^5
S. typhimurium + *E. coli* + *L. monocytogenes*	127	2.91	87	4.41×10^5
Spiked Apple Juice	155	2.77	89	2.51×10^5
Spiked Milk	118	2.5	136	2.16×10^5

The detection limit of the biosensor (2×0.4×0.015 mm) in all the above described tests was 5×10^3 cfu/mL. The biosensor was capable of detecting small amounts of *S. typhimurium*, even in the presence of high concentrations of masking bacteria. In the preceding sections, it was established that the biosensor could detect *S. typhimurium* with high specificity and selectivity.

5.3.5 Longevity of magnetoelastic biosensors

In this section, the longevity/thermal stability of the magnetoelastic biosensors was studied at three different temperatures (25 °C, 45 °C and 65 °C). The transducer and bio-recognition element of a typical diagnostic biosensor should to be robust to endure the variations in temperatures that they might experience in real applications. Conventionally used antibodies face a major disadvantage, due to their poor performance at higher temperatures. Antibodies are known to lose their activity at 25 °C in less than 20 days [5-8]. However, filamentous phage has been shown to display better stability in adverse conditions of temperature and pH [9-12]. The procedures used for the longevity testing have been described in section 3.8.3. All of the assayed sensors were prepared for SEM (section 3.5) and the area distribution density as a function of time and temperature were evaluated. Figure 5-18, Figure 5-19 and Figure 5-20 show typical SEM images of the assayed biosensors incubated at 65 ºC, 45 ºC and 25 ºC, respectively. The area coverage density was observed to decrease with increasing time and temperature. The number of cells present on the sensor was then counted using the procedures described previously (section 3.7)

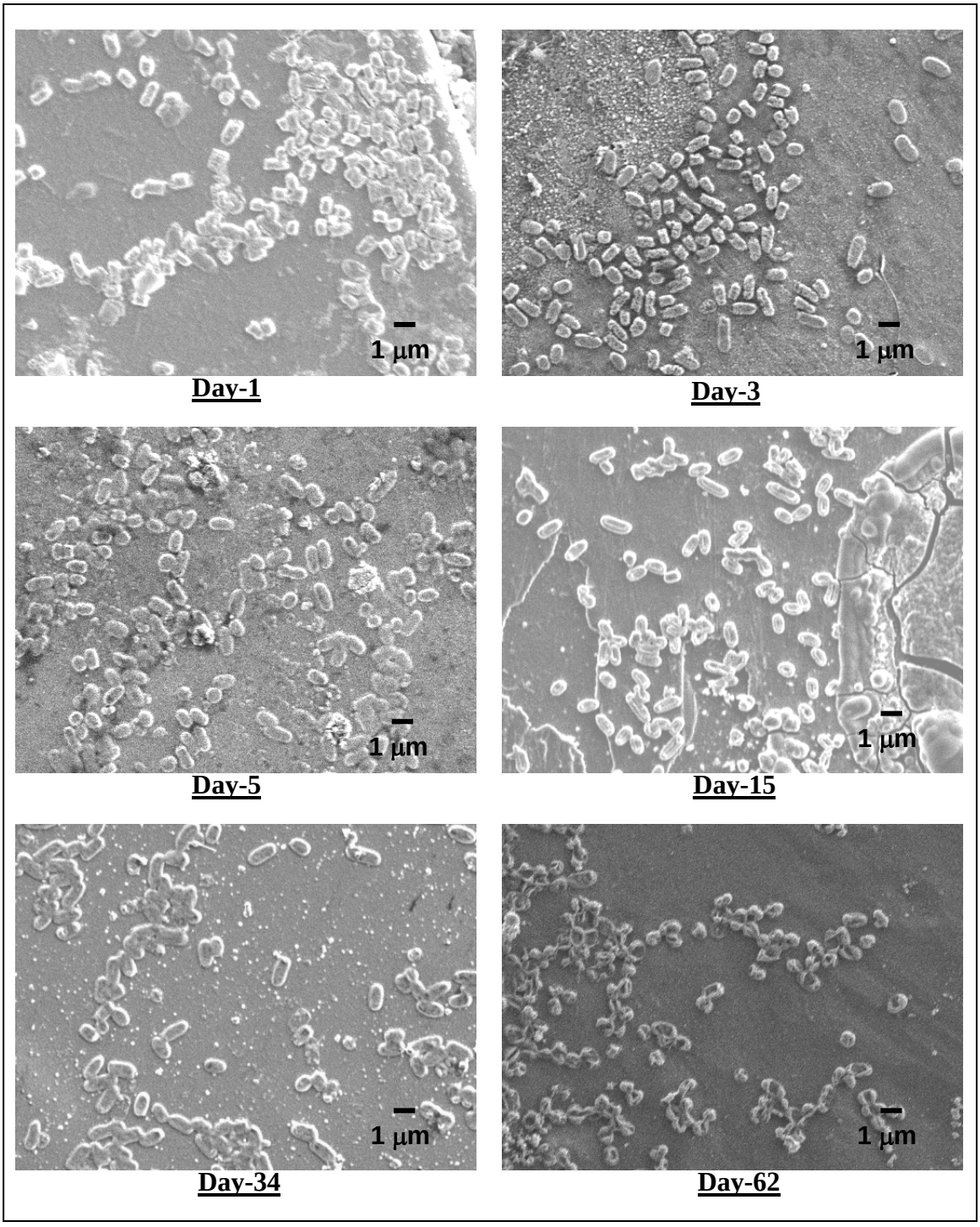

Figure 5-18: Typical SEM images of *S. typhimurium* bound to the phage-immobilized biosensor surface with increasing time (1, 3, 5, 15 34 and 62 days) at 65 ºC.

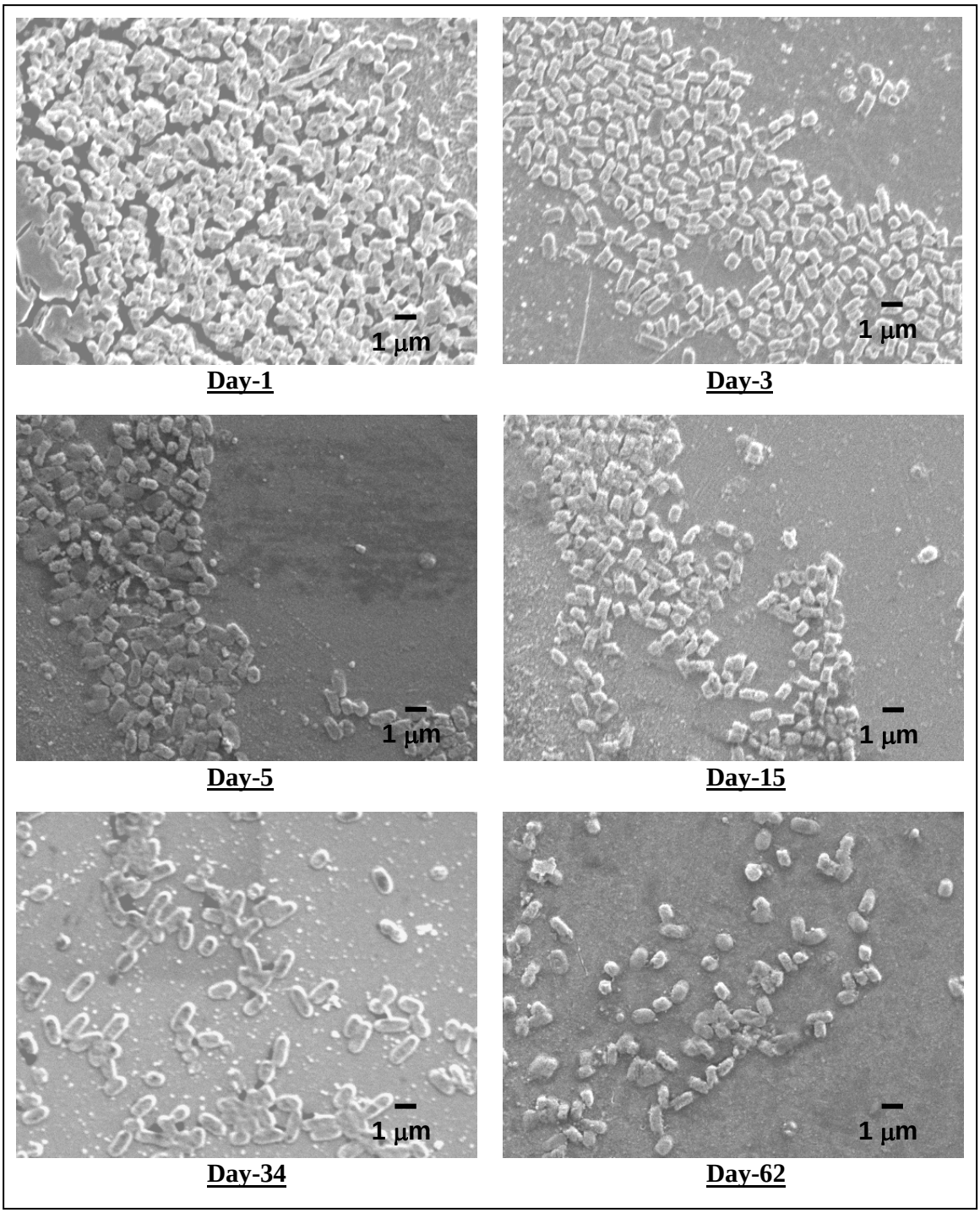

Figure 5-19: Typical SEM images of *S. typhimurium* bound to the phage-immobilized biosensor surface with increasing time (1, 3, 5, 15, 34 and 62 days) at 45 ºC.

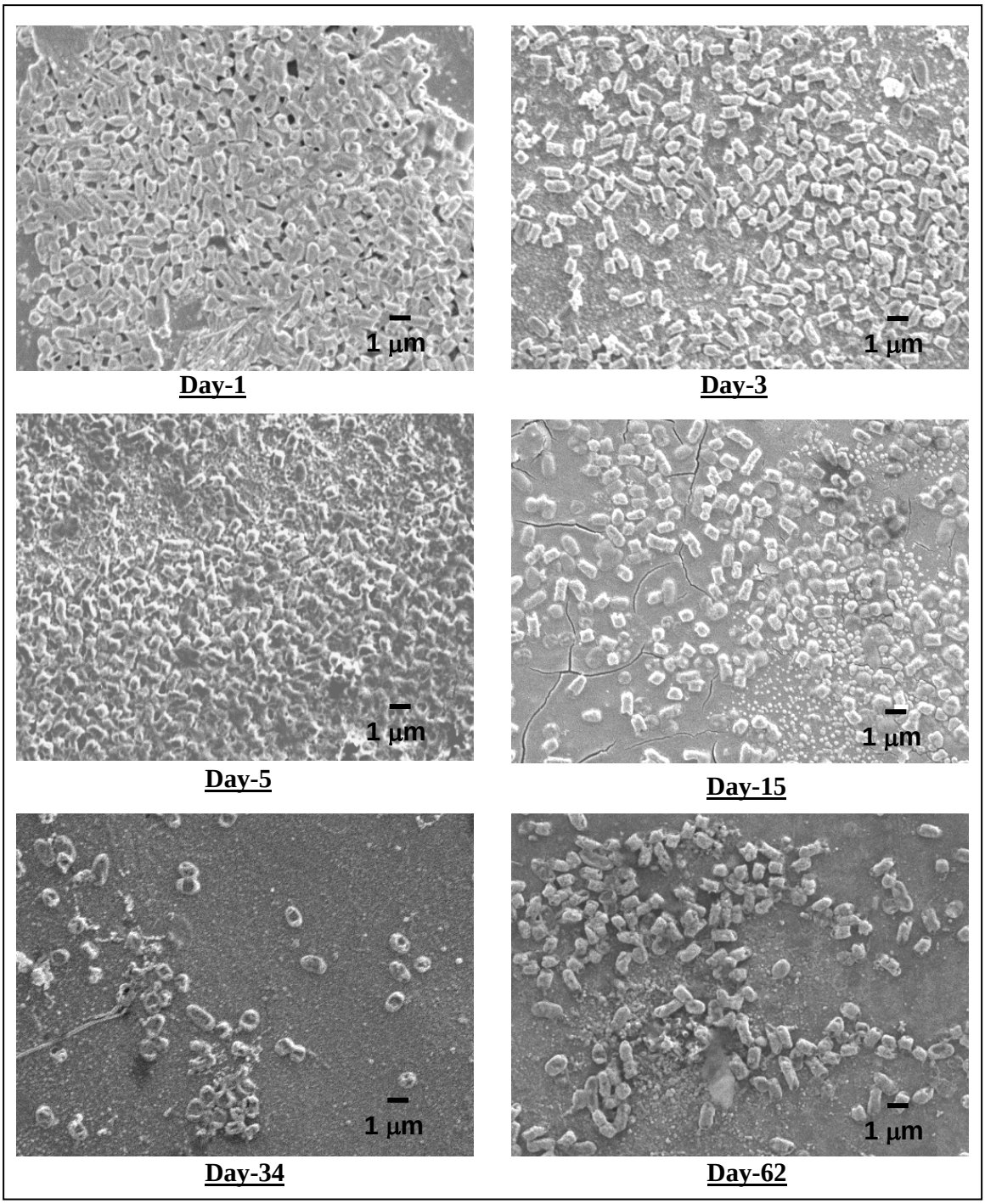

Figure 5-20: Typical SEM images of *S. typhimurium* bound to the phage-immobilized biosensor surface with increasing time (1, 3, 5, 15, 34 and 62 days) at 25 ºC.

The changes in the surface distribution density of the bacteria bound to the biosensor surface as a function of time (in days) for the different incubation temperatures are shown in Figure 5-21. A gradual decrease in the binding affinity with time can be seen for the biosensors incubated at the three temperatures. However, the biosensors retained 59%, 45% and 33% of their binding affinity at 25 °C, 45 °C and 65 °C, respectively after a period of 63 days. Figure 5-21 also shows the result of a similar experiment done with magnetoelastic sensors immobilized with a polyclonal antibody (data kindly provided by Guntupalli et.al. [8]). The initial (day 1) area coverage densities for phage-immobilized biosensors was approximately two times higher than antibody-immobilized biosensors. However, there was a rapid loss in the binding activity of the antibody-based sensors following day 1; losing all binding activity in less than 10 days even at 45 °C. On the other hand, phage-immobilized biosensors had significant binding even at the end of 2 months.

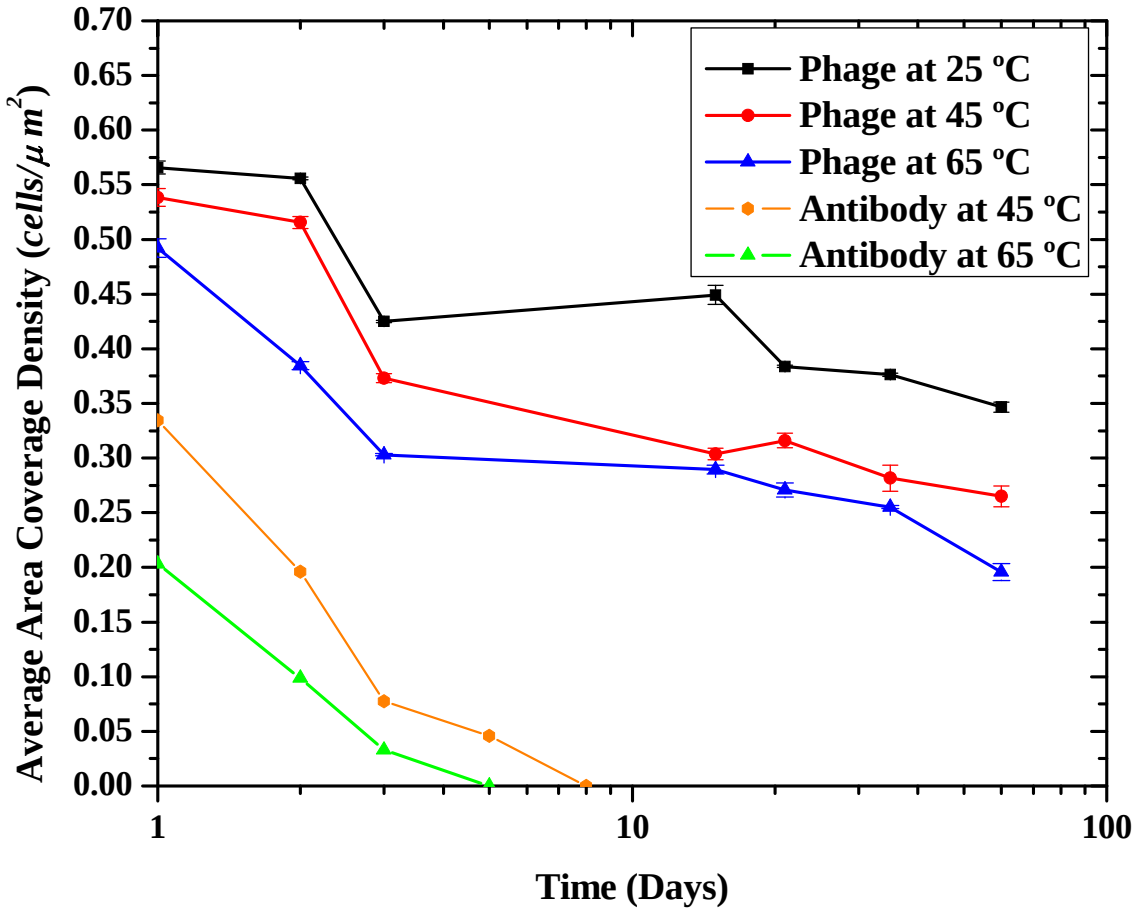

Figure 5-21: Surface coverage densities (average number of cells/μm^2) calculated from SEM micrographs of stored magnetoelastic biosensors (25 ºC, 45 ºC, and 65 ºC) after exposure to *S. typhimurium* (5×10^8 cfu/mL).

5.4. Size dependent Sensitivity

5.4.1 Dose response of biosensors with different lengths

As discussed previously, an enhanced sensitivity of magetoelastic sensors could be achieved by reducing the physical dimensions of the sensor. Hence we studied the dose response of sensors with different dimensions upon exposure to different concentrations of *S. typhimurium*. Since the sensitivity of the sensor depends on the

length of the sensor, biosensors with dimensions of 5×1×0.015 mm, 2×0.4×0.015 mm, 1×0.2×0.015 mm and 0.5×0.1×0.015 mm were prepared. The dose response tests were conducted (section 3.8.4) for biosensors with the four different dimensions. Typical curves comparing dose responses (each curve represents an average of 5 different biosensors) obtained for 5 mm and 2 mm is shown in Figure 5-22. It can clearly be seen that higher frequency shifts were obtained for a smaller sensor. The detection limit for a 5 mm sensor was 5×10^4 cfu/mL and for a 2 mm sensor was 5×10^3 cfu/mL. The sensitivity of the biosensor in the linear region of the dose response curve increased from 98 Hz/decade to 161 Hz/decade. Similar comparisons of dose response for a reduction in length from 2 mm to 1 mm and from 1 mm to 500 μm are shown in Figure 5-23 and Figure 5-24, respectively. An increase in sensitivity and reduction in detection limits were obtained for sensors with smaller dimensions. The detection limits went from 5×10^4 cfu/mL for a 5 mm sensor down to 5×10^2 cfu/mL for a 500 μm sensor. The sensitivity of the response in the linear region was measured to be 770 Hz/decade for a 1mm sensor and 1152 Hz/decade for a 500 μm sensor respectively.

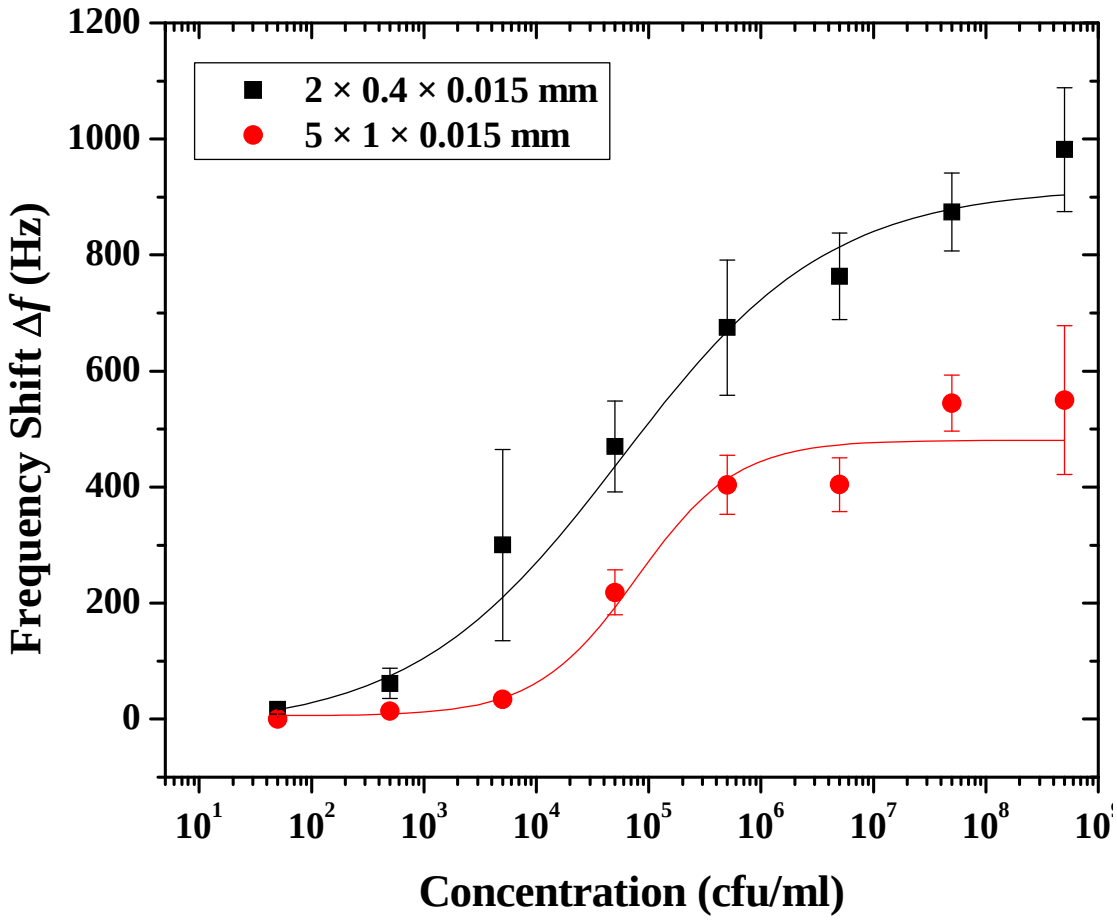

Figure 5-22: Comparison of magnetoelastic biosensor's dose responses, when exposed to increasing concentrations (5×10^1 to 5×10^8 cfu/mL) of *S. typhimurium* suspensions on two different sizes of sensors 2×0.4×0.015 mm (■- χ^2=0.048, R^2=0.99) and 5×1×0.015 mm (●- χ^2=0.32, R^2=0.99). The curves represent the sigmoidal fit of signals obtained.

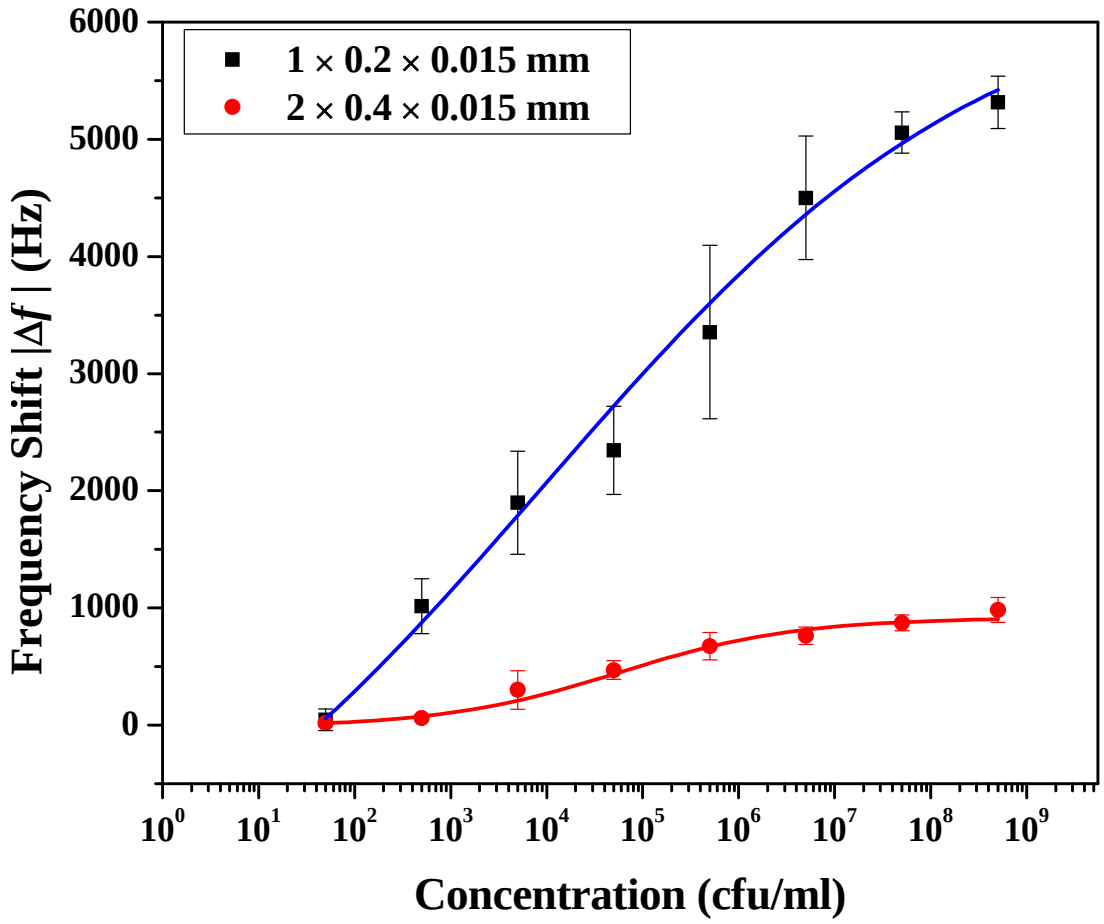

Figure 5-23: Comparison of magnetoelastic biosensor's dose responses, when exposed to increasing concentrations (5×10^{1} to 5×10^{8} cfu/mL) of *S. typhimurium* suspensions on two different sizes of sensors ($1\times0.2\times0.015$ mm (■- χ^2=0.048, R^2=0.99) and $2\times0.4\times0.015$ mm (●- χ^2=0.32, R^2=0.99)). The curves represent the sigmoidal fit of signals obtained. Each data point is the average value obtained from five individual experiments (different sensors) carried out under identical conditions.

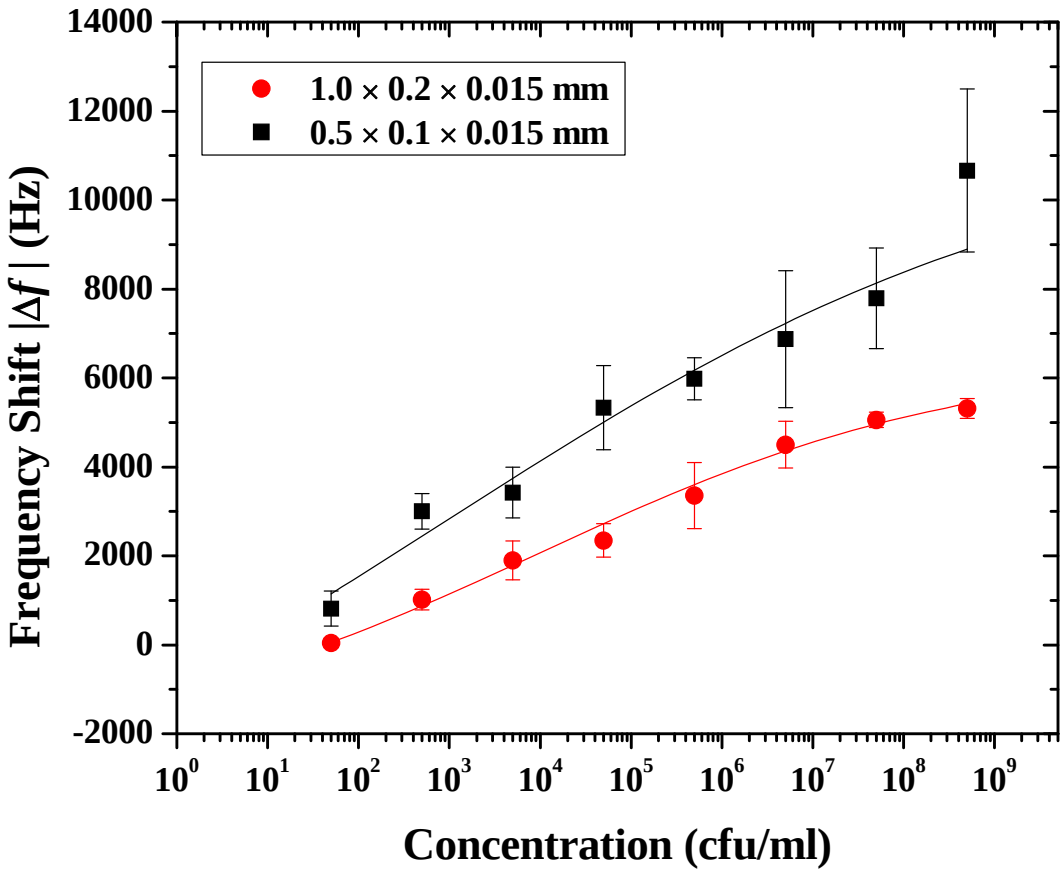

Figure 5-24: Comparison of magnetoelastic biosensor's dose responses, when exposed to increasing concentrations (5×10^1 to 5×10^8 cfu/mL) of *S. typhimurium* suspensions on two different sizes of sensors ($0.5\times0.1\times0.015$ mm (■- χ^2=0.048, R^2=0.99) and $1\times0.2\times0.015$ mm (●- χ^2=0.7231, R^2=0.91) The curves represent the sigmoidal fit of signals obtained.

Due to the small size of a 500×100×15 μm biosensor, the entire surface of the biosensor could be imaged using SEM. Five pictures were taken and attached to view the entire surface. SEM micrographs of the assayed biosensors are shown in Figure 5-25.

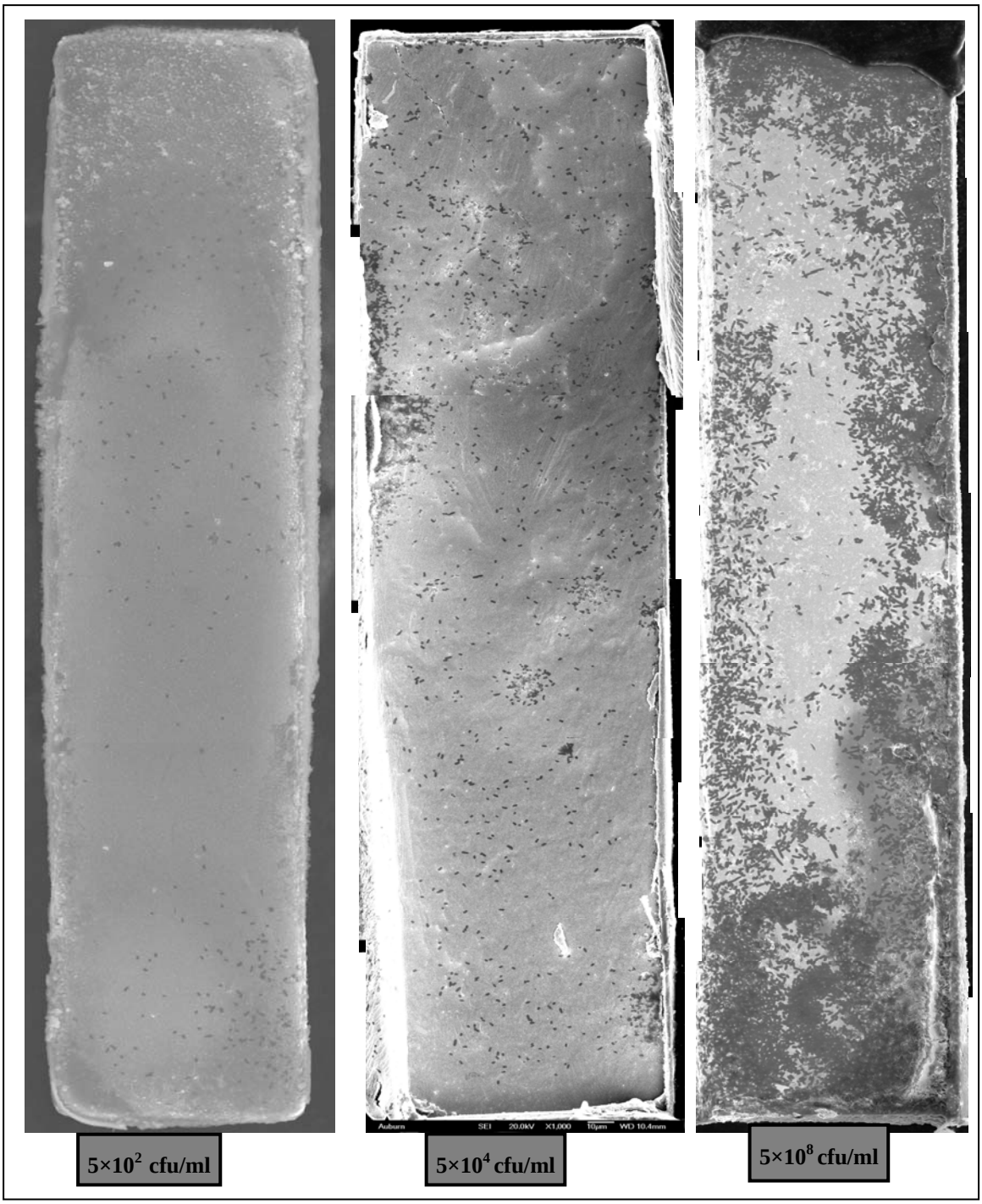

Figure 5-25: Typical SEM images of the entire surfaces of assayed 500μm sensors at three different concentrations (5×10^2 cfu/mL, 5×10^4 cfu/mL and 5×10^8 cfu/mL). Bound *S. typhimurium* can be seen as black spots on the pictures.

A clear decrease in the number of bacteria bound to the sensor can be observed for the biosensors exposed to the three different concentrations (5×10^2 cfu/mL, 5×10^4 cfu/mL and 5×10^8 cfu/mL). The number of bacteria attached to the entire biosensor surface (one side) was counted manually. The total number of attached *S. typhimurium* cells were 14278, 3286 and 157 for the three different biosensors exposed to concentrations of 5×10^8, 5×10^4 and 5×10^2 cfu/mL, respectively. An attachment of 14278 cells on the sensor surface theoretically corresponds to a frequency shift of 9.5 kHz. This number is very similar to the measured resonance frequency shift of 10 kHz for the biosensor.

A summary of the observations for sensors with different dimensions is shown in Table 5-3. This table lists the sensitivity and detection limits achieved for sensors of each of these dimensions. An average increase in sensitivity by 400% was achieved by reducing the dimension of the biosensor by 50%. It can clearly be inferred that better sensitivity can be achieved by reducing the dimensions of the biosensor.

Table 5-3: Table summarizing the sensitivity and detection limits achieved for sensors with different dimensions.

Sensor Dimensions	Sensitivity (Hz/decade)	Order of detection Limit
5.0×1.0×0.015 mm	98	10^5 cfu/mL
2.0×0.4×0.015 mm	161	10^4 cfu/mL
1.0×0.2×0.015 mm	770	10^3 cfu/mL
0.5×0.1×0.015 mm	1150	10^2 cfu/mL

5.5. Phage immobilization

An understanding of the distribution characteristics of the immobilized phage is essential in achieving better sensitivity and stability of biosensor responses. Olsen et. al. [13] had discussed two possible distributions of phage (assuming no bundle formation) on the sensor surface and calculated an optimum concentration of phage needed for immobilization. In this dissertation, the concentration of phage (5×10^{11} vir/mL), suggested by Olsen et. al. [13], was used for immobilization. They also hypothesized that the phage aggregates would be more prevalent rather than individual phage filaments on sensor surfaces.

The aggregation of like charged polyelectrolytes (such as phage) to form 'bundles' caused due to the presence of counterions, has been studied extensively [14-16]. However, the application of phage as a bio-recognition element is limited in the literature. There is very little understanding of whether a uniform distribution of phage filaments or a uniform distribution of phage 'bundles' on the surface would be better for a typical sensor application. Also there is limited understanding [17] of the binding interaction between the gold surface and phage filaments.

Electron Microscopy was used to study the distribution of phage on the sensor surface. For SEM studies, phage immobilization was carried out using procedures described in section 3.2. The immobilization step was followed by an exposure of the biosensor to 5×10^{8} cfu/mL of *S. typhimurium* for 45 minutes. The assayed sensors were then mounted on aluminum stubs with the help of a double-sided carbon tape and exposed to OsO_4 vapors for 15 minutes. The main challenge in imaging immobilized phage on the biosensor surface was to resolve the nanometer sized phage filaments on the

sensor surface. In our earlier experiments, the assayed sensors were prepared for SEM by sputtering a very thin layer of gold (≈30 nm) on the sensor surface. However, sputtering of gold films on the sensor surface covered the phage filaments completely. After trying several different thicknesses of the gold film, we discovered that assayed biosensors prepared without a gold film allowed imaging of immobilized phage on the sensor surfaces. The presence of Os diffused into the bacterial cells, the smaller size of the sensors and the use of a low probe current, minimized the charge accumulation on the samples in the SEM chamber. A lower probe current also resulted in a better resolution for the SEM micrographs. Figure 5-26 shows an SEM picture of a sensor surface before and after immobilization of phage.

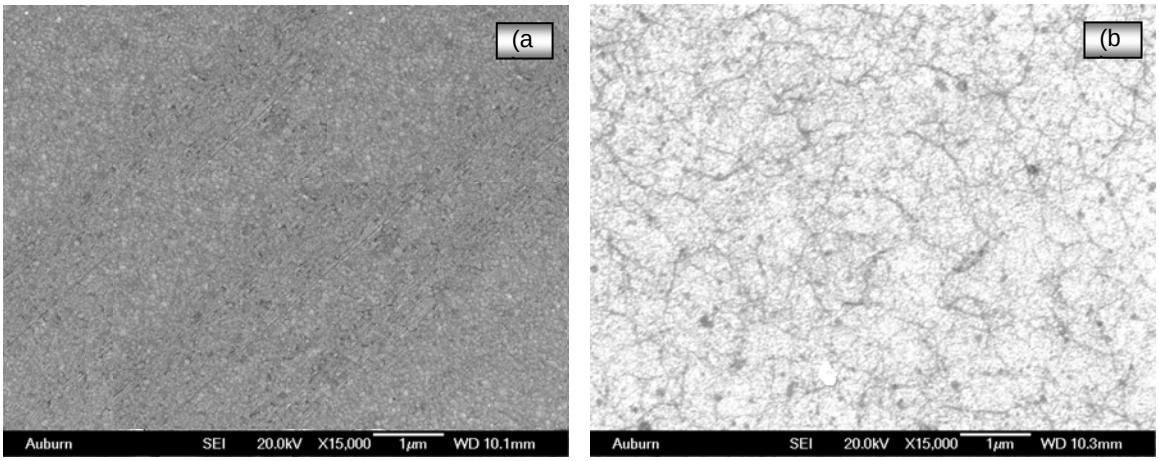

Figure 5-26: High magnification (15000X) SEM images of sensor surface (a) before and (b) after immobilization of phage.

Upon immobilization of phage (5×10^{11} vir/mL suspended in 1X TBS) using physical adsorption on the sensor surface, it was observed (Figure 5-26 (b)) that randomly oriented phage filaments saturated the entire surface. Phage was visible as

thread like features observed in the SEM micrograph shown in Figure 5-26. The as-received phage was suspended in 1XTBS solution containing 140 mM of NaCl. To study the effect of the concentration of counterions we varied the concentration of the NaCl (280 mM, 420 mM, 560 mM and 840 mM) in the TBS solution. The different Na^+ ion concentrations were used in order to facilitate formation of phage 'bundles.' Typical high magnification (15000X) SEM micrographs for each of the sensor surfaces at these concentrations are shown in Figure 5-27 (a) through (d).

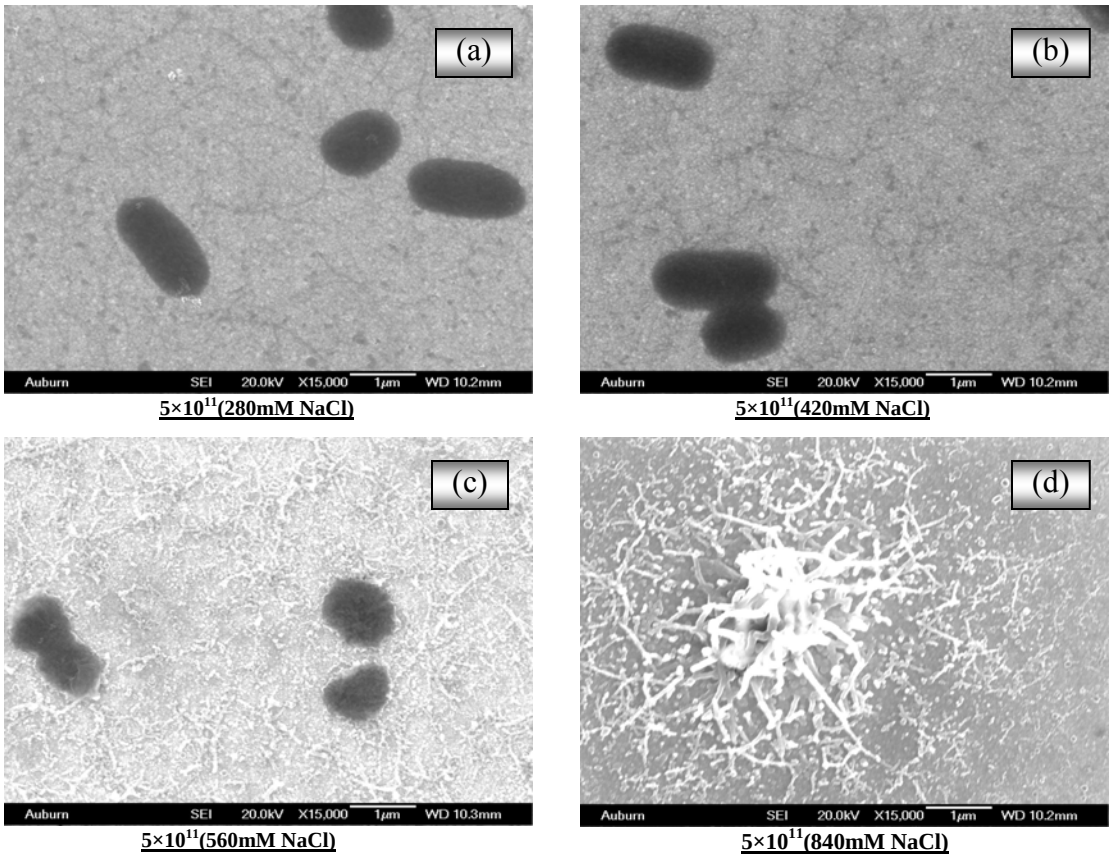

Figure 5-27: SEM images showing the nature of phage distribution in presence of different Na^+ ion concentrations (a) 280 mM; (b) 420 mM; (c) 560 mM; (d) 840 mM.

At lower concentrations of the counterion (280 mM and 420 mM of NaCl) a uniform distribution of individual phage filaments was observed (Figure 5-27(a), (b)). However, an increase in the counterion concentration resulted in the formation of phage "bundles." The phage "bundles" formed can be seen in Figure 5-27 (c) and Figure 5-27 (d).

The typical distribution of the binding of *S. typhimurium* on the biosensor surface for the different concentrations of the counterion (Na^+) is shown in Figure 5-28. A uniform distribution of individual filaments on the entire surface enabled a uniform distribution of bound *S. typhimurium* (Figure 5-28 (a) through (d)) for low counterion concentrations (≤ 420 mM). SEM micrographs of the sensor surface at a lower magnification indicated that the "bundles", unlike the individual phage filaments, were not uniformly distributed over the entire surface. At higher counterion concentrations (> 420 mM), due to localized accumulation of bundles (seen as bright white spots in Figure 5-28 (e) through (h)) the binding of *S. typhimurium* was also localized. This resulted in an overall reduction of the number of *S. typhimurium* attached to the sensor surface (Figure 5-28).

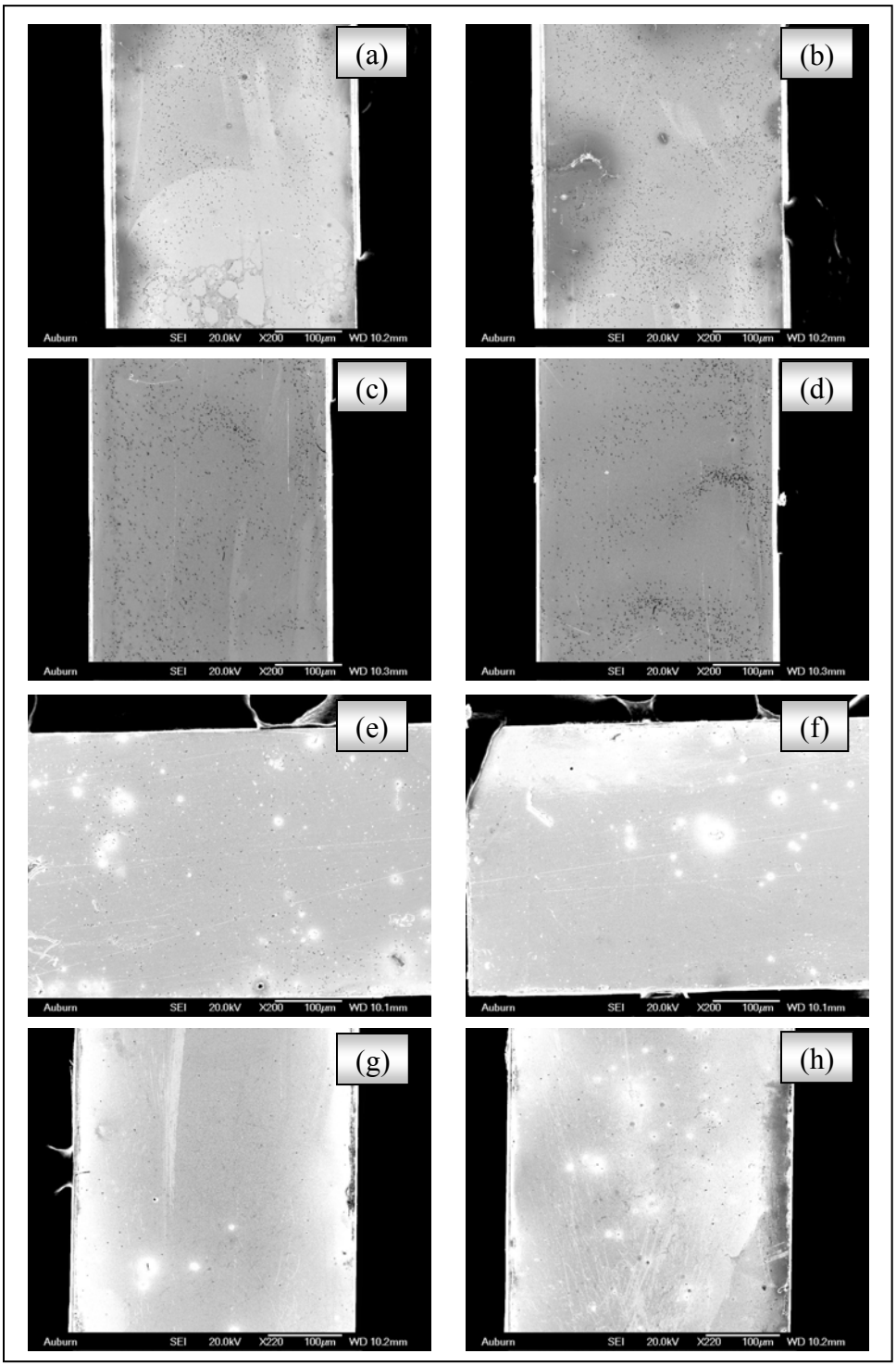

Figure 5-28: SEM images showing binding distribution on sensors immobilized with phage with varying counterion (Na^+) concentrations (a, b) 240 mM; (c, d) 420 mM; (e, f) 560mM; and (g, h) 840mM.

From the studies done so far we can conclude that formation of phage "bundles" can be achieved by altering the counterion concentration. The SEM observations could mislead to a conclusion that the presence and formation of phage "bundles" would be detrimental for typical sensor applications. A phage "bundle" consists of more than thousand individual phage filaments. This would result in large number of binding receptors to be concentrated on each phage "bundle". However the localized accumulation of these "bundles" resulted in a decrease in the number of attached *S. typhimurium* cells.

A hypothesis for the significant difference in the nature of distribution of phage is the difference in effective concentration of the bio-recognition probe. When individual phage filaments are present, each filament is a bio-recognition probe. Each phage "bundle" would consist of several thousands of individual phage filaments hence the effective number of these "bundles" available for binding would be lower than that for individual phage filaments. Additionally, these "bundles" have a tendency to accumulate at certain regions on the sensor surface rather than a uniform distribution. Additional work is required to achieve a uniform distribution of the bundles and to ascertain the nature and conditions that would optimize the performance of phage as a bio-recognition probe for sensor applications.

REFERENCES

1. Guntupalli, R., Lakshmanan, R.S., Johnson, M.L., Hu, J., Huang, T.S., Barbaree, J.M., Vodyanoy, V.J., and Chin, B.A., *Magnetoelastic biosensor for the detection of Salmonella typhimurium in food products.* Sensing and Instrumentation for Food Quality and Safety, 2007. **1** (1): 3-10.

2. Nanduri, V., Sorokulova, Iryna B., Samoylov, Alexandre M., Simonian, Aleksandr L., Petrenko, Valery A., Vodyanoy, Vitaly., *Phage as a molecular recognition element in biosensors immobilized by physical adsorption.* Biosensors and Bioelectronics, 2007. **22**(6): 986-992.

3. Nanduri, V., Kim., G., Morgan, M.T., Ess, D., Hahm, B.-K., Kothapalli, A., Valadez, A., Geng, T., and Bhunia, A.K., *Antibody Immobilization on Waveguides Using a Flow–Through System Shows Improved Listeria monocytogenes Detection in an Automated Fiber Optic Biosensor: RAPTOR™.* Sensors, 2006. **6**: 808-822.

4. Petrenko, V.A. and Vodyanoy, V.J., *Phage display for detection of biological threat agents.* Journal of Microbiological Methods, 2003. **53**(2): 253-262.

5. Van der Linden, R.H., L.G.F., de Geus, B., Harmsen, M.M., Ruuls, R.C., Stok, W., de Ron, L., Wilson, S., Davis, P., and Verrips, C.T., *Comparison of physical chemical properties llamma VHH antibody fragments and mouse monoclonal antibodies.* Biochimica Biophysica Acta, 1999. **1431**: 37-46.

6. Usami, A., A.O., Takahama, S., and Fujii, T., *The effect of pH, hydrogen peroxide and temparature on the stability of human monoclonal antibody.* J. Pharm. Biomed. Anal, 1996. **14**: 1133-1140.

7. Dooley, H., S.D.G., Harris, W.J., and Porter, A.J., *Stabilization of antibody fragments in adverse environments.* Biotechnol. Appl. Biochem, 1998. **28**: 77-83.

8. Guntupalli, R., Lakshmanan, R., Wan, J., Kim, D.J., Huang, T., Vodyanoy, V., and Chin, B., *Analytical performance and characterization of antibody immobilized magnetoelastic biosensors.* Sensing and Instrumentation for Food Quality and Safety, 2007. **DOI: 10.1007/s11694-007-9025-x**: Accepted/ Online First.

9. Goldman, E.R., Pazirandeh, M.P., Mauro, J.M., King, K.D., Frey, J.C., and Anderson, G.P., *Phage-displayed peptides as biosensor reagents.* Journal of Molecular Recognition, 2000. **13**(6): 382-387.

10. Brigati, J.R. and Petrenko, V.A., *Thermostability of landscape phage probes.* Analytical and Bioanalytical Chemistry, 2005. **382**(6): 1346-1350.

11. Petrenko, V.A. and Sorokulova, I.B., *Detection of biological threats. A challenge for directed molecular evolution.* Journal of Microbiological Methods, 2004. **58**(2): 147-168.

12. Sorokulova, I.B., Olsen, E.V., Chen, I.H., Fiebor, B., Barbaree, J.M., Vodyanoy, V.J., Chin, B.A., and Petrenko, V.A., *Landscape phage probes for Salmonella typhimurium.* Journal of Microbiological Methods, 2005. **63**(1): 55-72.

13. Olsen, E.V., Sorokulova, I.B., Petrenko, V.A., Chen, I.H., Barbaree, J.M., and Vodyanoy, V.J., *Affinity-selected filamentous bacteriophage as a probe for acoustic wave biodetectors of Salmonella typhimurium.* 2006. **21**(8): 1434.

14. Angelini, T.E., Liang, H., Wriggers, W., and Wong, G.C.L., *Direct observation of counterion organization in F-actin polyelectrolyte bundles.* The European Physical Journal E - Soft Matter, 2005. **16**(4): 389.

15. Lyubartsev, A.P., Tang, J.X., Janmey, P.A., Nordenskiold, L., *Electrostatically induced polyelectrolyte association of rodlike virus particles.* Physical Review Letters, 1998. **81**(24): 5465-5468.

16. Tang, J.X., Janmey, P.A., Lyubartsev, A., and Nordenskiold, L., *Metal Ion-Induced Lateral Aggregation of Filamentous Viruses fd and M13.* Biophysical Journal, 2002. **83**(1): 566.

17. Souza, G.R., Christianson, D.R., Staquicini, F.I., Ozawa, M.G., Snyder, E.Y., Sidman, R.L., Miller, J.H., Arap, W., and Pasqualini, R., *Networks of gold nanoparticles and bacteriophage as biological sensors and cell-targeting agents.* Proceedings of the National Academy of Science USA, 2006. **103** (5): 1215-1220.

6. CONCLUSIONS

In this dissertation, it was established that a phage-based magnetoelastic biosensor can be used for the specific and selective detection of *S. typhimurium*. The biosensor's performance was characterized for longevity, specificity, selectivity, and size dependent sensitivity.

The dose response curves obtained for the magnetoelastic biosensor show that different concentrations of *S. typhimurium* can be detected. The biosensor is capable of detecting *S. typhimurium* present in water and food matrices (milk and apple juice). The biosensor was also able to detect *S. typhimurium* in the presence of high concentrations of one and two masking bacteria. It was demonstrated that a minimum concentration of 5×10^3 cfu/mL could be detected by a biosensor with dimensions of 2×0.4×0.015 mm. The results obtained from the study of binding kinetics using Hill plots indicated a strong binding of *S. typhimurium* to the biosensor. It was also established that phage and *S. typhimurium* had a multivalent interaction.

It was demonstrated that the sensitivity of the magnetoelastic biosensors could be increased by decreasing the dimensions of the sensor. A biosensor with dimensions of 5×1×0.015 mm showed a minimum detection limit of 5×10^4 cfu/mL and a sensitivity of 98 Hz/decade. However, a 0.5×0.1×0.015 mm showed a minimum detection limit of 5×10^2 cfu/mL and a sensitivity of 1150 Hz/decade.

For real-time field applications it was essential to establish the thermal stability of magnetoelastic biosensors. Biosensors stored at elevated temperatures (65 ºC) had significant binding activity even after 60 days. A high specificity of the biosensor to *S. typhimurium* was demonstrated. The normalized area coverage densities observed for the biosensor exposed to *S. typhimurium*, *S. enteritidis*, *E. coli* and *L. monocytogenes* were 1.00, 0.17, 0.06 and 0.03, respectively. These values indicated that the immobilized phage had negligible affinity for pathogens other than *S. typhimurium*.

Scanning Electron Microscopy provided a visual verification of bacterial attachment to biosensor surfaces. High magnification (15000X) imaging of biosensor surfaces also provided an insight into the nature of phage binding characteristics (present in the form individual filaments or phage bundles). By increasing the concentration of counterions (Na^+) in the phage solutions, it was demonstrated that the formation of phage bundles could be achieved. It was established that phage stored in suspensions containing less than 420mM of the monovalent ion will have a uniform distribution of phage filaments on the sensor surface. It was observed that the formed "bundles," upon immobilization, had a tendency to accumulate at certain regions on the biosensor. However, further studies need to be performed to achieve a uniform distribution of the phage "bundles."

In summary, a magnetoelastic transducer immobilized with filamentous phage as a sensitive, specific, selective and robust diagnostic biosensor platform for the detection of *S. typhimurium* was demonstrated. Such a biosensor system presents several advantages over the existing detection methodologies including low cost, wireless nature, environmental robustness, ease of operation and the possibility of miniaturization.